Alberto Hernando Sanz

Characterization of the Autonomic Nervous System Response in Hyperbaric Environments.

Director/es

Peláez Coca, María Dolores
Gil Herrando, Eduardo

Universidad Zaragoza
1542

Tesis Doctoral

CHARACTERIZATION OF THE AUTONOMIC NERVOUS SYSTEM RESPONSE IN HYPERBARIC ENVIRONMENTS.

Autor

Alberto Hernando Sanz

Director/es

Peláez Coca, María Dolores
Gil Herrando, Eduardo

UNIVERSIDAD DE ZARAGOZA
Escuela de Doctorado

Programa de Doctorado en Ingeniería Biomédica

2021

Characterization of the Autonomic Nervous System Response in Hyperbaric Environments

Alberto Hernando Sanz

Supervisors:

Eduardo Gil Herrando

María Dolores Peláez Coca

Ph.D in Biomedical Engineering

Zaragoza, May 2021

Characterization of the Autonomic Nervous System Response in Hyperbaric Environments

Acknowledgements

Now that the Ph.D is coming to its end, it is time to do a review of this 5 years of my life and thank for all the help and affection that I have received during this stage.

First of all, I have to thank to my supervisors, Mariola and Eduardo. Thank you for support me and give me the chance to grow up as an investigator and as a person. Thank you for all your understanding, patience, and wisdom during all this time, that allow us to come to this end, despite all the bumps in the roads. I own you a lot and I hope having corresponded you at least the half that you deserve. I would like to thank to Rute and Carolina, for reading this thesis in such a short amount of time.

I also have to thank to the BSICoS group, for welcoming me. Thank you for the coffees, seminars, conferences and all good moments. You/we are too much to be named one by one, but I want to specially mention the NIP group, for all the advises and laughs. I want to mention too the CUD staff, thank you for the coffees, paddle games, ceremonies, diving trips and for being volunteers in all imaginable recordings. Please, don't let the bad executive decisions cause you to lose the good feeling that makes you so special.

I never have reached this point without the help of Professor Ki Chon, who welcomed me in his lab in University of Connecticut during three months. Thank you very much for allowing me to have this experience that change my mind in a lot of aspects. A special mention for Hugo, who helps me like he was my big brother, advising me about life in Uconn and helping me with language issues, and for Jesús, whose help was vital and he was the perfect host during my first weeks there. I also have to mentioned Susan, the best possible landlord and of course all the members

in the lab, I never going to forget our all-you-can-eat buffet sessions and our real football games.

I also want to thank to all my friends, the ones that I have from the beginning and the others that I have been made, for cheer me up, supporting me and enjoying our free time. To Rodrigo, Alex, Azcona, Cartiel and Tomás, thank for being there day after day, for our dinners, our parties and our special sense of humor; to Antonio, Miguel and Adrián, do not hesitate that Marcos Llorente spirit guide me to finish the Ph.D; to the gang, Badías, Gonzalo and Sampedro, I hope you to keep the tradition and celebrate my thesis without (or with) me.

Finally, I want to specially thank to my family, who give me strength to face everything it comes, because I face it with them at my side. To my grandmothers, aunts and uncles, those who are still around, and those who have left us. To my cousin, who teach me that seeing us from time to time is not related with loving us few. To Nico, for bring us happiness. To the little child to come, who comes with this thesis. To my father, to teach me the value of work. To my mother, for being the main support of everyone at home. And, above all, to my sister, for being with us and teach us how lucky we are to having you each day.

Alberto

Agradecimientos

Ahora que el doctorado llega a su fin, toca hacer un repaso de estos 5 años de mi vida y agradecer toda la ayuda y el cariño que he recibido durante esta etapa.

Lo primero de todo, debo acordarme de mis directores de tesis, Mariola y Eduardo. Gracias por apostar por mí y darme la oportunidad de crecer como investigador y como persona. Gracias también por vuestra comprensión, paciencia y sabiduría durante todo este tiempo, que nos ha permitido llegar al final a pesar de todas las piedras en el camino. Os debo mucho a los dos y espero haberos correspondido al menos la mitad de lo que os merecéis. También me gustaría agradecérselo a Rute y Carolina, por leerse esta tesis en tan poco tiempo.

También tengo que dar las gracias al grupo BSICoS, por acogerme como uno más. Gracias a todos por los cafés, seminarios, congresos y demás buenos momentos. Sois/somos demasiados para nombraros a todos, pero si que quiero hacer una especial mención al grupo NIP, por los consejos y las risas. También quiero acordarme de la gente del CUD, gracias por los cafés, el pádel, los actos, las excursiones de buceo y por ser voluntarios en todos los registros inimaginables. No dejéis que las malas decisiones de los que mandan os hagan perder ese buen ambiente que os hace tan especiales.

No podría haber llegado hasta aquí sin la ayuda de Ki, que me acogió como uno más en su laboratorio de la Universidad de Connecticut durante tres meses. Muchas gracias por esa estancia que me hizo cambiar mi manera de pensar en muchos aspectos de mi vida. Especial mención se merecen Hugo, que me ayudo como si fuera mi hermano mayor, aconsejándome sobre la vida allí y ayudándome con lo problemas del idioma, y Jesús, que fue de vital ayuda y el perfecto anfitrión durante las primeras semanas. También debo acordarme de Susan, por ser la mejor casera posible y de

todos los miembros del laboratorio, no voy a olvidar nuestras comidas en el buffet y nuestros partidos de futbol de verdad.

También quiero agradecérselo a todos mis amigos, los que tenía desde el principio y los que he ido haciendo, por animarme y hacerme desconectar cuando lo necesitaba. A Rodrigo, Alex, Azcona, Cartiel y Tomas, gracias por estar ahí día si día también, por nuestras cenas, nuestras salidas y nuestro especial sentido del humor; a Antonio, Adrián y Miguel, no dudéis que el espíritu de Marcos Llorente me ha ayudado a acabar esta tesis; y a la banda, Badías, Gonzalo y Sampedro, espero que cumpláis con la tradición y celebréis mi tesis, conmigo o sin mí.

Por último, quiero agradecérselo en especial a mi familia. Gracias a esas personas que me dan fuerzas para afrontar todo lo que venga, porque lo afronto con ellos de mi lado. A mis abuelas, tías tios, tanto los que están como los que ya se han ido. A mi prima, que me enseño que verse poco no implica quererse igual. A Nico, por traer alegría en tiempos duros. Al peque que está por llegar, por venir con mi tesis debajo del brazo. A mi padre, por enseñarme el valor del trabajo. A mi madre, por ser el soporte principal de todos de la casa. Y sobre todo a mi hermana, por quedarte con nosotros y enseñarnos la suerte que es tenerte cada día.

Alberto

Abstract

This dissertation focuses on the study of the Autonomic Nervous System (ANS) response in hyperbaric environments. Hyperbaric environments are those scenarios in which atmospheric pressure increases and this increase in pressure produces changes in the cardio-respiratory system of the subject to maintain the homeostasis. These changes are reflected in the ANS, whose response can be measured in a non-invasive way with the Heart Rate Variability (HRV), extracted from the electrocardiogram (ECG) or with the Pulse Rate Variability (PRV), extracted from the photoplethysmogram (PPG). The description of the hyperbaric environments, the ANS activity, the relationship between them and how the ANS response can be measured through ECG and PPG signals can be found in Chapter 1.

In Chapter 2, to corroborate if PPG signal provides the same information in terms of ANS response than ECG signal, both signals were recorded for subjects inside a hyperbaric chamber when the atmospheric pressure varied from 1 atm to 3 atm and 5 atm and the coming back to 3 and 1 atm. The correlation and statistical analysis between time and frequency domain parameters extracted from both signals demonstrates that PRV can be considered as a surrogate measurement of HRV inside a hyperbaric chamber. This makes PPG a signal to be considered in hyperbaric environments, since its sensor is cheaper and easier to place than ECG electrodes (especially under the water), and PPG can estimate some parameters, as the oxygen saturation, than ECG cannot. Also a characterization of how the ANS reacts to pressure changes and the time spent in the hyperbaric environment is done with ECG and PPG parameters, increasing those related with the parasympathetic system when the pressure is high and decreasing the heart rate and the parameters related with the sympathetic system when more time is spent inside the chamber.

Respiration plays an important role in hyperbaric environments, so it is important to include respiratory information in the HRV/PRV analysis, since it has been shown that changes in the respiratory pattern could alter the interpretation of the ANS response. Therefore, once that PPG signal has been proved as an interesting signal to consider in hyperbaric environments, in Chapter 3 a study about the respiratory rate estimation from different locations of the PPG sensor is performed. To do that, the respiratory signal together with finger and forehead PPG were recorded from 35 subjects while breathing spontaneously, and during controlled respiration experiments at a constant rate from 0.1 Hz to 0.6 Hz, in 0.1 Hz steps. Four PPG derived respiratory (PDR) signals were extracted from each one of the recorded PPG signals: pulse rate variability (PRV), pulse width variability (PWV), pulse amplitude variability (PAV) and the respiratory-induced intensity variability (RIIV). Respiratory rate was estimated from each one of the 4 PDR signals for both PPG sensor locations. Results suggest that: i) respiratory rate estimation is better at lower rates (0.4 Hz and below); ii) the signals recorded at the finger are better than those at the forehead to estimate respiratory rate; iii) it is better not to include RIIV signal to estimate the respiratory rate.

Following with the PPG signal, not only PRV contains information about the ANS response. Also, PPG morphology can provide a great amount of information about vascular assessment or arterial compliance, since pulse pressure propagation in arteries causes alterations in blood volume and therefore changes in the PPG pulse shape. That is the reason why, in Chapter 4, a new algorithm to decompose the PPG pulse into two waves related with the systolic and the diastolic peaks is presented. The first wave is obtained concatenating the up-slope from the beginning to the first maximum with itself flipped horizontally. The second wave is modelled by a lognormal curve, adjusting its maximum to the diastolic peak. From these two waves, the amplitude, the time instant, the width, the area and some ratios are extracted. This method is applied in a hyperbaric chamber dataset to identify alterations in the morphology of the PPG pulse due to the exposure of the subjects to different pressures. Results of the time and width of the wave related with the systolic peak point out to a vasoconstriction when the pressure increases, probably due to an activation of the sympathetic system on the blood vessels. Results of the

time and width of the wave related with the diastolic peak reflect the vasoconstriction but also a dependency with the pulse-to-pulse interval. Therefore this methodology allows to extract a great set of parameters related with the PPG morphology that are affected by the change of pressure in hyperbaric environments.

In Chapters 2 and 4, the ANS response is studied inside a hyperbaric chamber, where the pressure varies. However, there are many variables that could affect the body's cardiovascular response during diving, such as diver body position, physical activity, water temperature, breathing with a scuba mouthpieces and more. This is the reason why in Chapter 5 the ANS response is studied in three different hyperbaric environments: inside a hyperbaric chamber, where only the pressure varied; during a controlled dive in the sea, where the pressure changed but the effects of other factors were minimized; and during an uncontrolled dive in a reservoir, where more factors differed from baseline to immersion stage. A comparison of the HRV features between the two stages (baseline and immersion) in each dataset is carried out to study how these factors related to scuba diving activity affect the ANS response. To do this comparison, instead of the classic frequency methods, the Principal Dynamic Mode (PDM) and the Orthogonal Subspace Projection (OSP) methods are used to account for linear and non-linear interactions and to deal with the respiratory component that could affect the ANS response, respectively. OSP results indicate that most of the variation in the heart rate variability cannot be described by changes in the respiration, so changes in ANS response can be assigned to other factors. Time domain parameters reflect vagal activation in the hyperbaric chamber and in the controlled dive because of the effect of pressure. In the uncontrolled dive, sympathetic activity seems to be dominant, due to the effects of other factors such as physical activity, the challenging environment, and the influence of breathing through the scuba mask during immersion. In summary, a careful description of the changes in all the possible factors that could affect the ANS response between baseline and immersion stages in hyperbaric environments is performed for better explanation of the results.

Resumen y conclusiones

Esta tesis se centra en el estudio de la respuesta del Sistema Nervioso Autónomo (ANS) en entornos hiperbáricos. Los entornos hiperbáricos son aquellos escenarios en los cuales la presión atmosférica aumenta y ese aumento en la presión produce cambios en el sistema cardio-respiratorio del sujeto para mantener la homeostasis. Estos cambios se ven reflejados en el ANS, cuya respuesta puede ser medida de manera no invasiva a través de la Variabilidad del Ritmo Cardiaco (HRV), extraída del electrocardiograma (ECG), o a través de la Variabilidad del Ritmo del Pulso (PRV), extraída de la señal de pulso pletismográfico (PPG). La descripción de los entornos hiperbáricos, de la actividad del ANS, de la relación entre ellos y de cómo la respuesta del ANS puede ser medida a través de las señales ECG y PPG, puede encontrarse en el Capítulo 1.

En el Capítulo 2, para corroborar si la señal PPG proporciona la misma información en términos de respuesta del ANS que la señal ECG, ambas señales fueron registradas en sujetos en el interior de una cámara hiperbárica, con la presión atmosférica aumentando desde 1 atm a 3 y 5 atm y luego volviendo a 3 y 1 atm. La correlación y el análisis estadístico entre los parámetros en el dominio temporal y frecuencial extraídos de ambas señales demuestran que la PRV puede ser considerada una medida sustituta de la HRV para los sujetos en el interior de la cámara hiperbárica. Esto hace de la PPG una señal a ser considerada en los entornos hiperbáricos, dado que su sensor es más barato y fácil de colocar que los electrodos del ECG (especialmente debajo del agua), y además la PPG puede estimar otros parámetros, como la saturación de oxígeno, que no se pueden estimar con el ECG. También se ha realizado una caracterización de cómo el ANS reacciona ante los cambios de presión y ante el tiempo pasado en el entorno hiperbárico mediante

los parámetros extraídos del ECG y la PPG, aumentando aquellos relacionados con el sistema parasimpático cuando la presión es alta y disminuyendo los parámetros relacionados con el sistema simpático conforme más tiempo se pasa dentro de la cámara.

La respiración juega un papel importante en los entornos hiperbáricos por lo que se debe incluir la información respiratoria en el análisis del HRV/PRV, dado que se ha demostrado que los cambios en el patrón respiratorio pueden alterar la interpretación de la respuesta del ANS. Por lo tanto, una vez que se ha probado que la señal PPG debe ser tenida en cuenta en los entornos hiperbáricos, en el Capítulo 3 se ha realizado un estudio sobre la estimación de la frecuencia respiratoria colocando el sensor de la PPG en distintas localizaciones. Para hacer esto, se ha registrado la señal respiratoria junto con la señal PPG en el dedo y en la frente en 35 sujetos mientras respiraban espontáneamente y de forma controlada a un ritmo constante, desde 0,1 Hz a 0,6 Hz en pasos de 0,1 Hz. Cuatro señales respiratorias derivadas de la PPG (PDR) fueron extraídas de cada una de las señales PPG registradas. Éstas son: la variabilidad del ritmo del pulso (PRV), la variabilidad de la anchura del pulso (PWV), la variabilidad de la amplitud del pulso (PAV) y la variabilidad de la intensidad inducida de la respiración (RIIV). La frecuencia respiratoria fue estimada para cada una de las 4 señales PDR en ambas localizaciones del sensor PPG. Los resultados sugieren que: i) la estimación de la frecuencia respiratoria es mejor en frecuencias bajas (por debajo de 0,4 Hz); ii) las señales registradas en el dedo son mejores para la estimación que las registradas en la frente; iii) es mejor no incluir la señal RIIV para estimar la frecuencia respiratoria.

Siguiendo con la señal PPG, no sólo la PRV contiene información sobre la respuesta del ANS. También la morfología de la PPG puede proporcionar una gran cantidad de información sobre el estado vascular o sobre la distensibilidad arterial, dado que la propagación de la presión del pulso en las arterias causa alteraciones en el volumen de la sangre y por lo tanto cambios en la forma de onda de la PPG. Esta es la razón por la que, en el Capítulo 4, se presenta un nuevo algoritmo para descomponer el pulso de la PPG en dos ondas relacionadas con los picos sistólico y diastólico. La primera onda es obtenida concatenando la pendiente de subida del pulso, desde el principio hasta el primer máximo, con ella misma girada hori-

zontalmente. La segunda onda se modela como una curva lognormal, ajustando su máximo al pico diastólico. De estas dos ondas, se extraen la amplitud, el instante temporal, la anchura, el área y algunos ratios. Este método se aplica en el conjunto de datos de la cámara hiperbárica para identificar alteraciones en la morfología del pulso PPG debido a la exposición de los sujetos a diferentes presiones atmosféricas. Los resultados del instante temporal y la anchura de la onda relacionada con el pico sistólico apuntan a una vasoconstricción cuando aumenta la presión, probablemente debida a una activación del sistema simpático sobre los vasos sanguíneos. Los resultados del instante temporal y de la anchura de la onda relacionada con el pico diastólico reflejan esta vasoconstricción y también una dependencia con el intervalo entre los pulsos. Por lo tanto, esta metodología permite extraer una gran cantidad de parámetros relacionados con la morfología de la PPG que se ven afectados por los cambios de presión en los entornos hiperbáricos.

En los Capítulos 2 y 4, la respuesta del ANS se ha estudiado dentro de una cámara hiperbárica, donde la presión varía. Sin embargo, hay muchas variables que pueden afectar la respuesta cardiovascular del cuerpo durante el buceo, como son la posición del cuerpo del buceador, la actividad física, la temperatura del agua, respirar por el regulador de presión, y algunas más. Por esta razón, en el Capítulo 5 se estudia la respuesta del ANS en tres entornos hiperbáricos distintos: dentro de la cámara hiperbárica, donde sólo la presión varió; durante una actividad de buceo controlado en el mar, donde la presión cambió, pero los efectos de otras variables se minimizaron lo máximo posible; y durante una actividad de buceo no controlado en un pantano, donde más factores cambiaron entre las etapas basal y de inmersión. Se realiza una comparación de los parámetros extraídos de la HRV entre dos etapas (basal e inmersión) en cada conjunto de datos para estudiar como estos factores relacionados con la actividad de buceo afectan a la respuesta del ANS. Para hacer esta comparación, en lugar de los parámetros frecuenciales clásicos, los métodos Principal Dynamic Mode (PDM) y Orthogonal Subspace Projection (OSP) se usan para tener en cuenta las interacciones lineales y no lineales y para tratar con la componente respiratoria que puede afectar a la respuesta del ANS, respectivamente. Los resultados del método OSP indican que la mayoría de la variación de la HRV no puede ser descrita por los cambios en la respiración, por lo que los cambios en la

respuesta del ANS pueden aparecer por otros factores. Los parámetros temporales reflejan la activación vagal en la cámara hiperbárica y en el buceo controlado debido al efecto de la presión. En el buceo no controlado, sin embargo, la actividad simpática parece ser la dominante, debido a los efectos de otros factores como la actividad física, el entorno estimulante y el hecho de respirar a través del regulador durante la inmersión. Como resumen, se ha realizado una descripción detallada de los cambios en todos los posibles factores que pueden afectar a la respuesta del ANS entre las etapas basal y de inmersión en los distintos entornos hiperbáricos para una mejor explicación de los resultados.

Contents

Chapter 1

Introduction

1.1   Motivation

It is called hyperbaric environment that scenario in which atmospheric pressure is
increased, so the pressure is greater than 1 atmosphere (atm). The most common
exposure to hyperbaric pressures is during underwater diving, which became practical
with the development of the self-contained underwater breathing apparatus (scuba).
However, as the human body is not adapted to these environments, their biological
and physiological effects must be studied. During a dive, a descent of 10 meters
implies a pressure increase of 1 atm (meaning the ambient pressure is 2 atm), because
water is almost 800 times denser than air. Therefore, the maximum descent for
recreational diving is fixed at 40 meters (5 atm), although some professionals, such
as scientists or the military, go deeper.

These pressure changes have profound effects on the behaviour of diver's body.
During immersion, the increase of the hydrostatic pressure of the surrounding water
balances the systemic circulation, and shifts the blood from the lower part of the
body to the central circulation, thereby contributing to bradycardia. Breathing air
under increased pressure supposes an increase of the partial pressure of oxygen, that
originates an increase in peripheral arteriolar vasoconstriction. To compensate this
increment, the body response consists of an increase in the parasympathetic activity
over the heart, consequently reducing the heart rate and the cardiac output [1]. The
increase of the partial pressure of the gases also supposes a great amount of gases

being dissolved in body's tissues, which could lead to biochemical intoxication, as narcosis (increase of the partial pressure of carbon dioxide, CO_2, or nitrogen ,N_2) or hyperoxia (increase of the partial pressure of oxygen, O_2). These gases can form bubbles in the tissues or blood vessels during the ascent too, since gas spaces will expand when the pressure decreases [2].

To avoid all these possible complications and to deal with the increase of pressure, the diver's body must produce a response to maintain intern homeostasis. This response is reflected in the Autonomic Nervous System (ANS) through the balance between its two branches (sympathetic and parasympathetic or vagal), which reflects the efforts of the body to adapt to new environments. Hence, monitoring ANS response may lead to a better understanding of diving physiology and could become a potential diagnostic marker of hazards associated with diving.

Non-invasive techniques can be used to measure ANS activity, being the most common the Heart Rate Variability (HRV) signal, which is extracted from the electrocardiogram (ECG). ECG provides a robust signal that allows us to study the electrical activity of the heart, being ANS the primary regulator of cardiac activity [3]. However, as this technique requires electrodes to be placed at several locations on the subject's chest, maybe it is not the most appropriate method in hyperbaric environments in terms of subject's comfort or signal quality.

Another non-invasive way to measure ANS activity is the Pulse Rate Variability (PRV) signal, which is extracted from the pulse-photoplethysmography (PPG). Numerous studies carried out at 1 atm suggest that HRV and PRV signals give the same information about the ANS response [4, 5, 6, 7], although some controversy still exists [8]. Among PPG advantages, PPG measurement requires only one low-cost device that is widely used in routine clinical practice and can be located on several parts of the body. The PPG signal also allows the measurement of oxygen saturation in the subject. Besides, PPG morphology could be used as another marker of ANS activity since distortions in the morphology of the pulse waveform have been related to physiological changes in the subjects [9]. On the other hand, PPG signal is more affected by noise and signal artifacts than ECG, resulting in a higher (potential) loss of information.

There are only a few studies analyzing the ANS response during a dive, either inside a pool [10, 11] or in open waters [12, 13, 14]. It is easier to study the ANS response inside a hyperbaric chamber, simulating the atmospheric pressure conditions but without the needing to go under water [1, 15, 16, 17, 18]. All the cited studies inside a hyperbaric chamber are characterised by: the use of only the HRV to characterise the ANS behaviour; a low number of subjects (between 8 and 12); and the measurement of only one hyperbaric stage between 2.5 and 3 atm. That is the reason why, in Chapter 2, a demonstration that PRV and HRV signals provide similar information inside a hyperbaric chamber is presented. In this Chapter, also a characterization of the ANS response with more subjects than in the rest of the bibliography and more than one stage of pressure is performed. Then, in Chapter 3, since respiration is a physiological parameter of great interest in hyperbaric environments and respiratory information affects the ANS response, an evaluation of the location of the PPG sensor for respiratory rate estimation is also proposed. Later, in Chapter 4, a new algorithm to decompose the PPG pulse into two waves is presented, to identify alterations in the morphology of the PPG pulse due to the exposure of the subjects to the hyperbaric environment. Finally, an evaluation of the ANS response in three different hyperbaric environments is carried out, including two real dives and taking into account how different factors as the pressure, the cold water or the activity during the dive affects the ANS response. To do that, the Principal Dynamic Mode (PDM) method to account for linear and non-linear interactions and the Orthogonal Subspace Projection (OSP) method to extract the respiratory component, are used. Therefore, monitoring subjects in these environments may lead to a better understanding of physiology when the pressure is high and could increase the safety of the subject by detecting abnormal ANS responses.

1.2 Hyperbaric environments

The hyperbaric environments are those scenarios where the atmospheric pressure increases. In this thesis, two main hyperbaric environments are considered: a hyperbaric chamber, that allows us to simulate atmospheric pressure conditions, without needing to go under water or affecting other conditions; and an underwater div-

ing, that supposes a real immersion, with more variables affecting the diver status. Figure 1.1 shows an example of a hyperbaric chamber and a real dive.

Figure 1.1: An example of a hyperbaric chamber (left) and a real dive (right).

There are several factors that affect subjects in the hyperbaric environment [15]. One is the increased ambient pressure, since during immersion, the hydrostatic pressure of the surrounding water balances the systemic circulation, and shifts the blood from the lower part of the body to the central circulation. This contributes to bradycardia, increased stroke volume and cardiac output, reduced muscle sympathetic nerve activity and unaltered blood pressure [19].

Another factor is temperature changes. Water immersion at neutral temperatures would stimulate mainly baroreceptors, but immersion in cold water would stimulate also thermoreceptors, activating different regulatory systems. It has been proved than neutral water immersion decreases heart rate and blood pressure, while cold stimuli increase both of them [20].

Other factor is the presence of gases inside the body. According to Dalton's law, the partial pressures of the gases that divers are breathing increase proportionally with the ambient pressure, and this exposure to supranormal pressures of gases results in a big quantifies of gases being dissolved in the body's tissues (Henry's law). This could lead to biochemical intoxication, as narcosis (increase of CO_2, N_2 partial pressure) or hyperoxia (increase of O_2), being one of their symptoms a dysfunction of the central nervous system. The increased density of the breathing gas results in a reduced heart rate, reduced pulmonary compliance, increased airways resistance and an increase in the work of breathing. These factors limit the maximum of recre-

ational diving depth to 40 meters [1, 2]. Still with the gases, as pressure and volume are inversely related (Boyle's law), gases inside the body will expand during the ascent and they could form bubbles in the tissues and blood vessels, which is known as decompression sickness (DCS). Its symptoms are variable, ranging from minor skin alterations to neurological and cardiopulmonary disorders. They can occur immediately or be delayed up to 48 hours, and they can remit or be permanent [2]. Epidemiological studies have shown an increase in DCS manifestation in the inner ear over the past two decades [21]. Most cases were developed after multiple deep dives or after dives in which an inadequate decompression occurs [22]. To prevent this type of accidents, there are dive tables that inform about the maximum time the diver can spend inside the water, about the maximum depth the diver can reach and about the decompression stops the diver must complete at a specified depth for a specified time during ascent before continuing to the surface (see Figure 1.2). Another possible option to increase the security of the divers lies in the study of the ANS response in hyperbaric environments for a better understanding of the physiology under the water, that together with the monitoring of the divers,could prevent possible accidents.
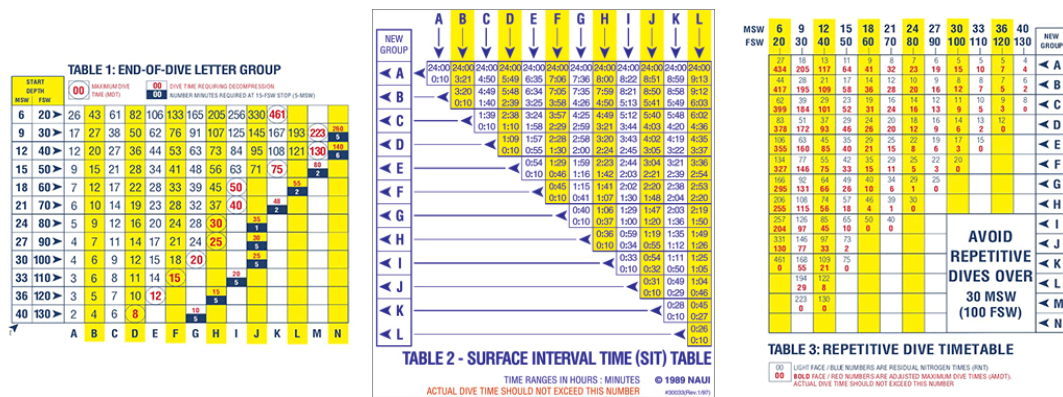

Figure 1.2: Dive tables that inform about the maximum time the diver can spent inside the water, the maximum depth the diver can reach and the decompression stops the diver must complete at a specified depth for a specified time during ascent, provided by National Association of Underwater Instructors (NAUI).

1.3 Autonomic Nervous System

All these factors linked to hyperbaric environments presented in the previous Section produce a response in the diver's body to maintain homeostasis that is reflected in the ANS. This is a control system that regulates bodily functions, such as heart rate, digestion, respiratory rate or urination in order to supply the body's needs [23]. To do that, subconscious sensory signals from an organ are transmitted to homeostatic control centers, the brainstem and hypothalamus, where they are processed and integrated. Then, these brain structures exert their control and subconscious reflex responses are returned directly back to the visceral organ to regulate its activities [23, 24].

The efferent autonomic signals are transmitted through two major subdivisions called the sympathetic nervous system and the parasympathetic (or vagal) nervous system. The sympathetic nervous system is considered the "fight or flight" system. Its main function is to prepare the body for dealing with a threat or for actions requiring quick responses. Some of the effects of a sympathetic activation are, among others, an increase in the heart rate and in the respiratory rate, vasoconstriction and bronchodilation. On the other hand, the parasympathetic nervous system is considered the "rest and digest" system. Its main function is to relax the body, with actions that do not require immediate reaction. Some of the effects of a parasympathetic activation are a decrease in the heart rate and respiratory rate, vasodilation and bronchoconstriction. As it can be shown with those examples, in many cases, both of these systems have opposite actions over the same tissue or organ, where one system activates a physiological response and the other inhibits it. The result is a rapid and precise control of a tissue's function. Other tissues, however, are only innervated by one system, for example, arteries constriction is controlled by only the sympathetic branch. Figure 1.3 shows both systems and the tissues and organs related to each of them. Therefore, the overall status of the organism depends on which ANS branch is predominating and how big this predominance is at each moment. This sympathetic-parasympathetic balance is commonly referred to sympathovagal balance.
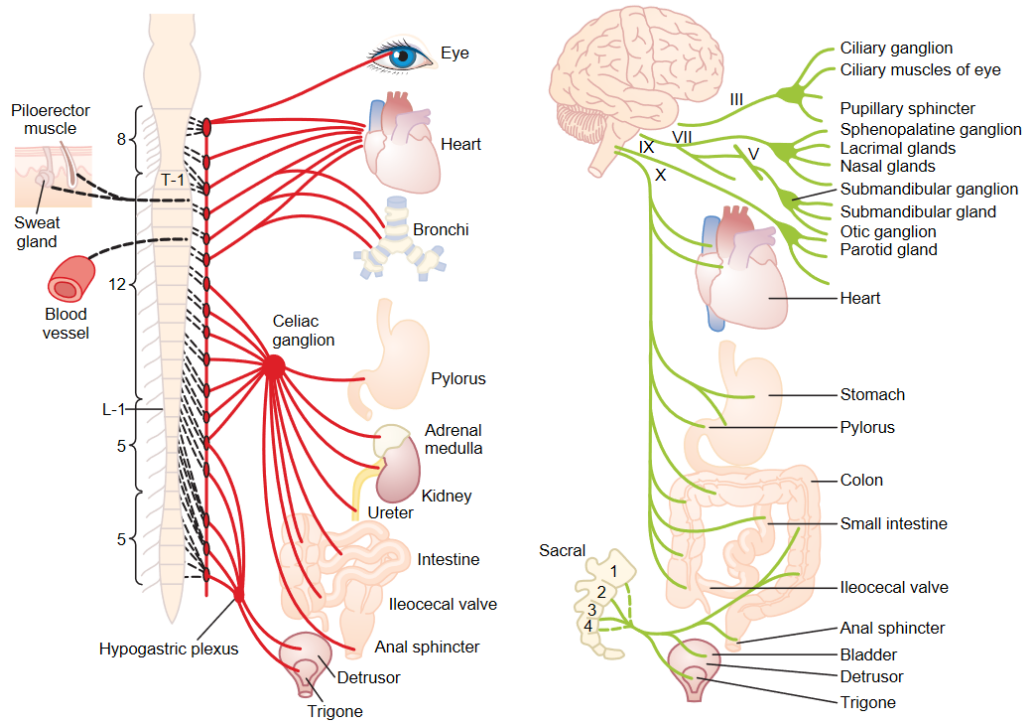
Figure 1.3: Effects of sympathetic nervous system (left) and parasympathetic nervous system (right) over the different organs of the body, from [23].

In this thesis, we focus our attention on the regulation of ANS on the cardiovascular and respiratory system. Sympathetic and parasympathetic systems could alter the heart rate at the same time. In absence of ANS influence, the intrinsic heart rate is about 100 to 120 beats per minute [25]. Therefore, parasympathetic tone is more predominant at rest, lowering the heart rate. This leads to a lower cardiac output, that is the volume of blood the heart pumps per minute. Cardiac output is calculated by multiplying the stroke volume by the heart rate. The decrease of the cardiac output originated by the increase in the vagal tone leads to a decrease in the blood pressure. However, there is no effect of parasympathetic activity on blood vessels. On the other hand, when the sympathetic activity is the one that dominates, there is an increase in the heart rate due to an innervation of the sinoatrial node of the heart. Additionally, sympathetic innervation causes vasoconstriction on blood vessels, leading to a higher stroke volume. Therefore, with the increase in the heart rate and the increase in the stroke volume, there is an increase in the cardiac

output, that originates an increase in blood pressure. Effect of ANS system can also be seen in the respiratory system. Sympathetic activity results on an increase in the respiratory rate and bronchial tubes dilatation and parasympathetic activity has the opposite results, with a decrease in the respiratory rate and bronchial tubes constriction.

The ANS regulation when a subject is exposed to a hyperbaric environment is manifested through an activation of the parasympathetic system and consequently a reduction in the heart rate. This phenomena occurs because breathing air under increased pressure supposes an increase of the partial pressure of oxygen, that originates an increase in peripheral arteriolar vasoconstriction, that has to be compensated with a reduction in the heart rate to maintain the homeostasis inside the body [1]. Even more, during immersion, the increase of the hydrostatic pressure of the surrounding water balances the systemic circulation, and shifts the blood from the lower part of the body to the central circulation, thereby contributing to the heart rate decrease.

1.4   Biological signals

Changes in the ANS response can be assessed in a non-invasive way through biological signals that vary with these changes. In this dissertation, electrocardiogram and photoplethysmography signals are selected since they allow to measure changes in the cardiovascular system due to the ANS response, together with the respiratory signal that reflects changes in the thoracic cavity and it also contains information about the ANS response, complementing the other two biological signals.

1.4.1   Electrocardiogram

The ECG signal describes the electrical activity of the heart and provides, in a non-invasive way, information about the cardiac muscle activity. ECG is composed of the spatio-temporal sum of the action potentials generated by all the cells in the cardiac tissue. The cardiac cycle of a normal beat starts with the spontaneous excitation of the electrical cells (depolarization stage) in the sinoatrial node, located in the upper part of the right atrium. This electrical impulse is propagated through both

atria, producing a mechanical contraction of the heart. This depolarization of the atrial cells is reflected in the ECG by the P wave. Then, the electrical impulse is transmitted to the ventricles through the atrioventricular node allowing the blood to get into ventricles before their contraction. The atrioventricular node transmits the electrical impulse to the bundle of His, which in conjunction with the Purkinje fibers rapidly gets the electrical impulse to all parts of the ventricles, leading to their depolarization associated to their contraction. When ventricles are contracted, the heart pumps out the blood. The depolarization of the ventricles is reflected in the ECG as the QRS complex, composed by a negative deflection (Q wave), followed by a positive deflection (R wave) and another negative one (S wave). To finish the cardiac cycle, the T wave appears in the ECG, and it reflects the ventricular repolarization which occurs during the ventricular relaxation, preparing the ventricles for the next beat [26]. Figure 1.4 shows all this process, the depolarization and repolarization of the different cells of the heart and how this create a sum of action potentials that construct a normal beat in the ECG.

There are also some important time intervals in the ECG. The PQ interval represents the time required for the transmission of the electrical impulse from the sinoatrial node to the ventricles. The QT interval represents the time that passes from the beginning of ventricular depolarization until the end of ventricular repolarization. The ST segment reflects the time that the ventricles remain in a depolarized state. Finally, the distance between two consecutive beats is usually measured as the distance between two consecutive R waves, hence called RR interval. Figure 1.5 represents a normal ECG with the P, Q, R, S and T waves and all the time intervals.

The ECG is usually measured using several electrodes over the skin. There is called lead the voltage difference between two electrodes (bipolar lead) or between a single electrode and a reference electrode (unipolar lead). The most employed recording configuration in the clinical routine is the standard 12 lead ECG, which is composed of 3 bipolar leads and 9 unipolar leads. This configuration accounts for the electrical activity in the frontal plane, through the standard bipolar limb leads (I, II and III) and the augmented unipolar limb leads (aVF,aVL and aVR), and in the horizontal plane, through the six unipolar precordial leads (V1 to V6), as shown in Figure 1.6.
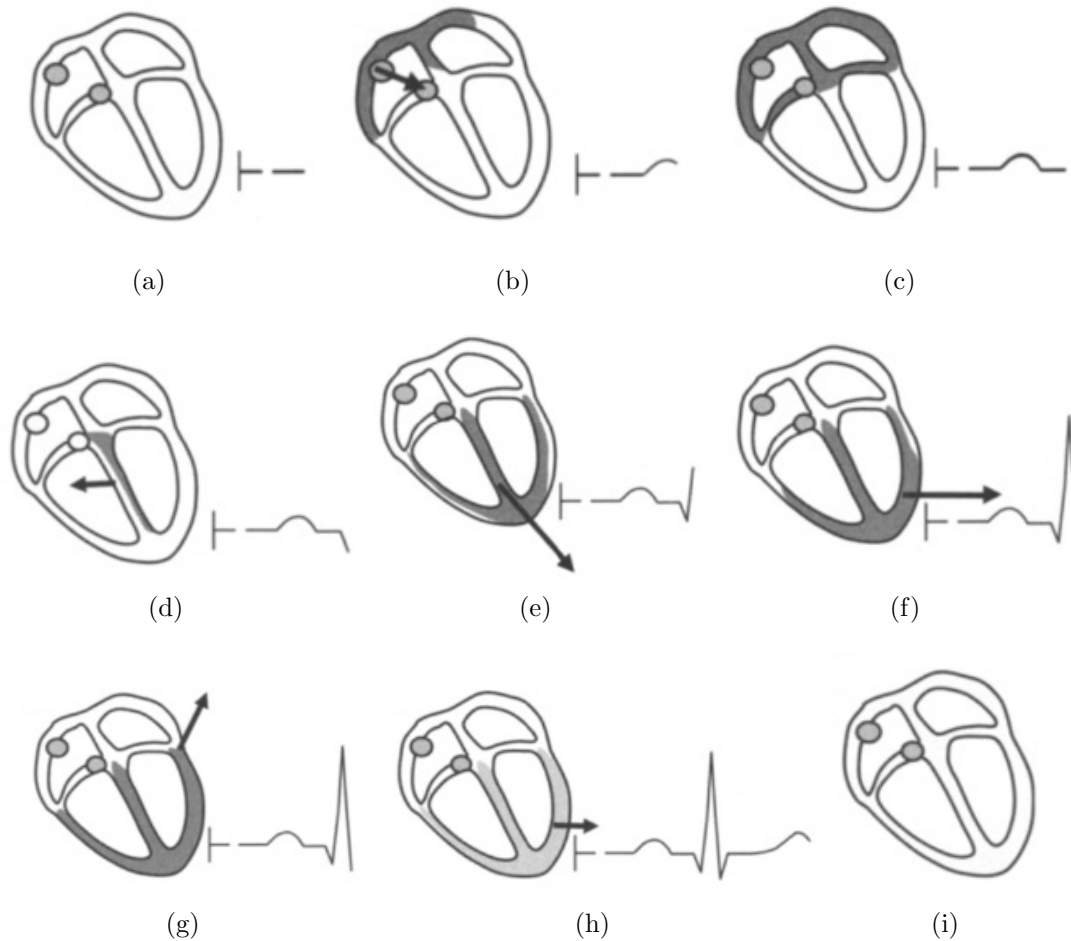
Figure 1.4: ECG recorded during the different cardiac phases: (a) All cardiac cells at rest; (b) Atrial depolarization; (c) the electrical impulse passing through the atrioventricular node; (d)-(g) ventricular depolarization; (h) ventricular repolarization and (i) all cardiac cells at rest again. Figure obtained from [26].

Autonomic information in the ECG

Figure 1.7 shows the effects of ANS activity on the sinus node cells, increasing or decreasing the heart rate. Heart rate varies along the time but also varies beat-to-beat with small variations around the mean. These short-term variations in heart rate are known as HRV, which remains as the most extended tool for ECG-based ANS assessment [27]. The use of RR intervals is generally accepted to measure this slightly variation, since QRS complex has large energy and its detection is reliable [26].
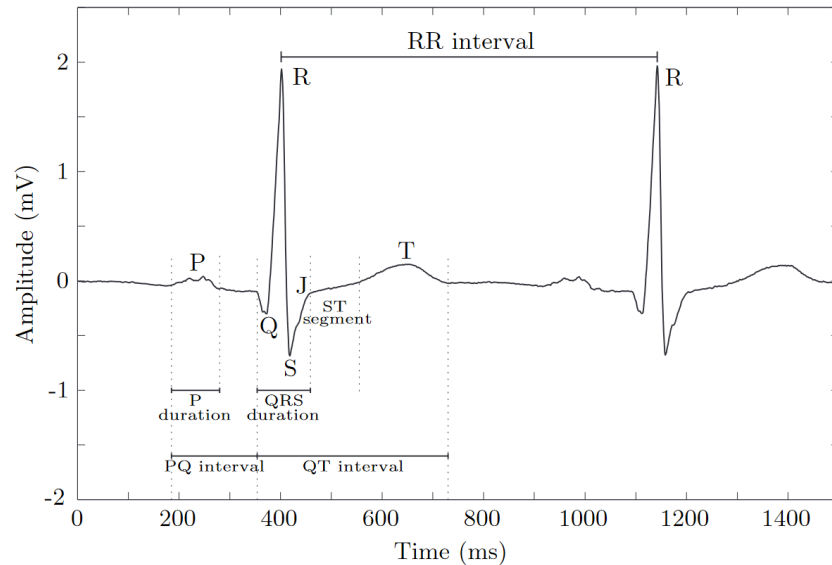
Figure 1.5: ECG waves definitions and time intervals, from [26].

However, sometimes a mass of heart cells not located in the sinus node may generate an electrical impulse. This phenomenon is known as ectopic beat, and since it does not reflect the activity of the sinus node, all of them must be excluded in HRV analysis, creating a new interval series denoted normal-to-normal (NN) intervals.

There are several heart rhythm representations. The simplest one is the interval tachogram, which is a signal composed of successive NN intervals. From this, the inverse interval tachogram can be obtained, which is the inverse of interval tachogram and gives information about the heart rate. However, heart beats occur non-uniformly in time, so it is more common to use functions which represents the same information plus the time instant when each heartbeat occurs. These functions are known as interval function and inverse interval function and both of them consist in a train of pulses occurring at the time when a beat takes place and scaled by the length of the preceding NN interval (interval function) or by the preceding rate (inverse interval function). An example of these four different representations is shown in Figure 1.8.

Another plausible model for HRV is the integral pulse frequency modulation (IPFM) model. This model assumes the existence of a modulating signal that carries information about the ANS activity, and the beat trigger impulse is generated when

(a)

(b)

(c)
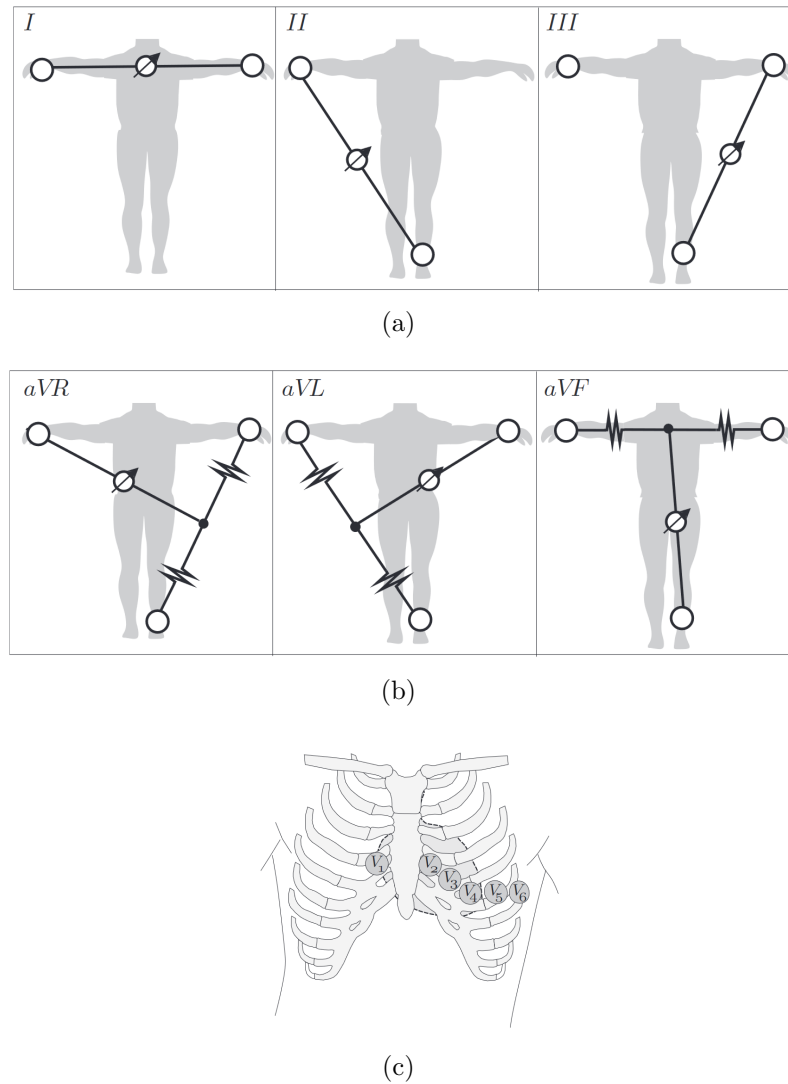
Figure 1.6: Electrode positions for recording (a) the standard bipolar limb leads (I, II and III); (b) the augmented unipolar limb leads (aVF,aVL and aVR); and (c) the six unipolar precordial leads (V1 to V6), from [26].

the integral of this function reaches a threshold [28, 29]. In situations where the mean heart period is not constant, such as in exercise stress testing, IPFM model with a constant threshold is not appropriate, so an evolution of this model was done taking into account the time varying mean heart rate, called the time-varying integral pulse frequency modulation (TVIPFM) model [30]. This last model will be used in this dissertation and will be more explained in Section 2.3.1.
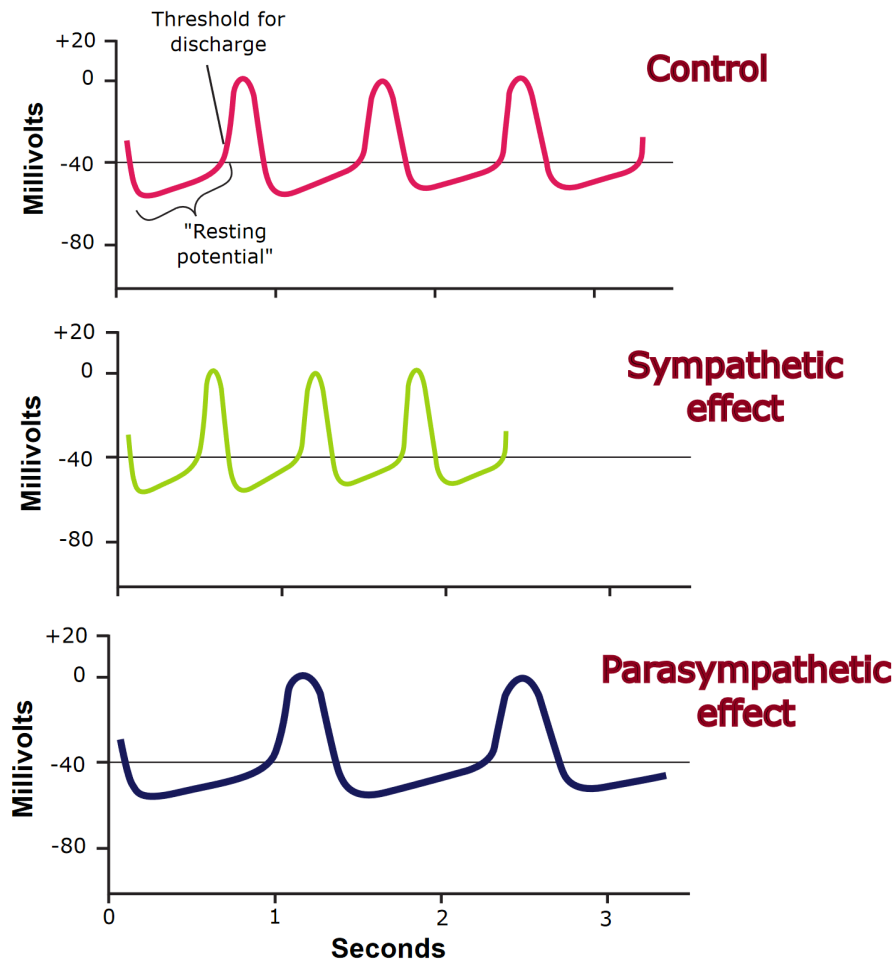
Figure 1.7: Effects of ANS activity on the sinus node cells, from [23].

The most extended approaches for HRV measurements are those based on time and frequency domains, as well as non-linear analysis. All of them have their own particularities, and result more appropriate for certain scenarios. A brief description of these parameters is provided below.

Time domain parameters are focused on statistical or geometric properties of the NN interval series. They are computationally simple, and the most employed parameters are: the mean and the standard deviation of the NN interval series (NN and $SDNN$), the standard deviation and the root mean square of the difference between adjacent NN intervals ($SDSD$ and $RMSSD$), and the percentage of successive differences of NN intervals differing by more than 50 ms ($pNN50$). About the

Figure 1.8: Representation of: a) an ECG with the beat occurrence times; b) interval tachogram; c) inverse interval tachogram; d) interval function; e) inverse interval function. Reproduced from [26].

physiological interpretation of each one, NN and $SDNN$ are related with the overall activity of HRV, and $SDSD$, $RMSSD$ and $pNN50$ are associated with short-term variations that are reflected in the parasympathetic branch of the ANS response [27].
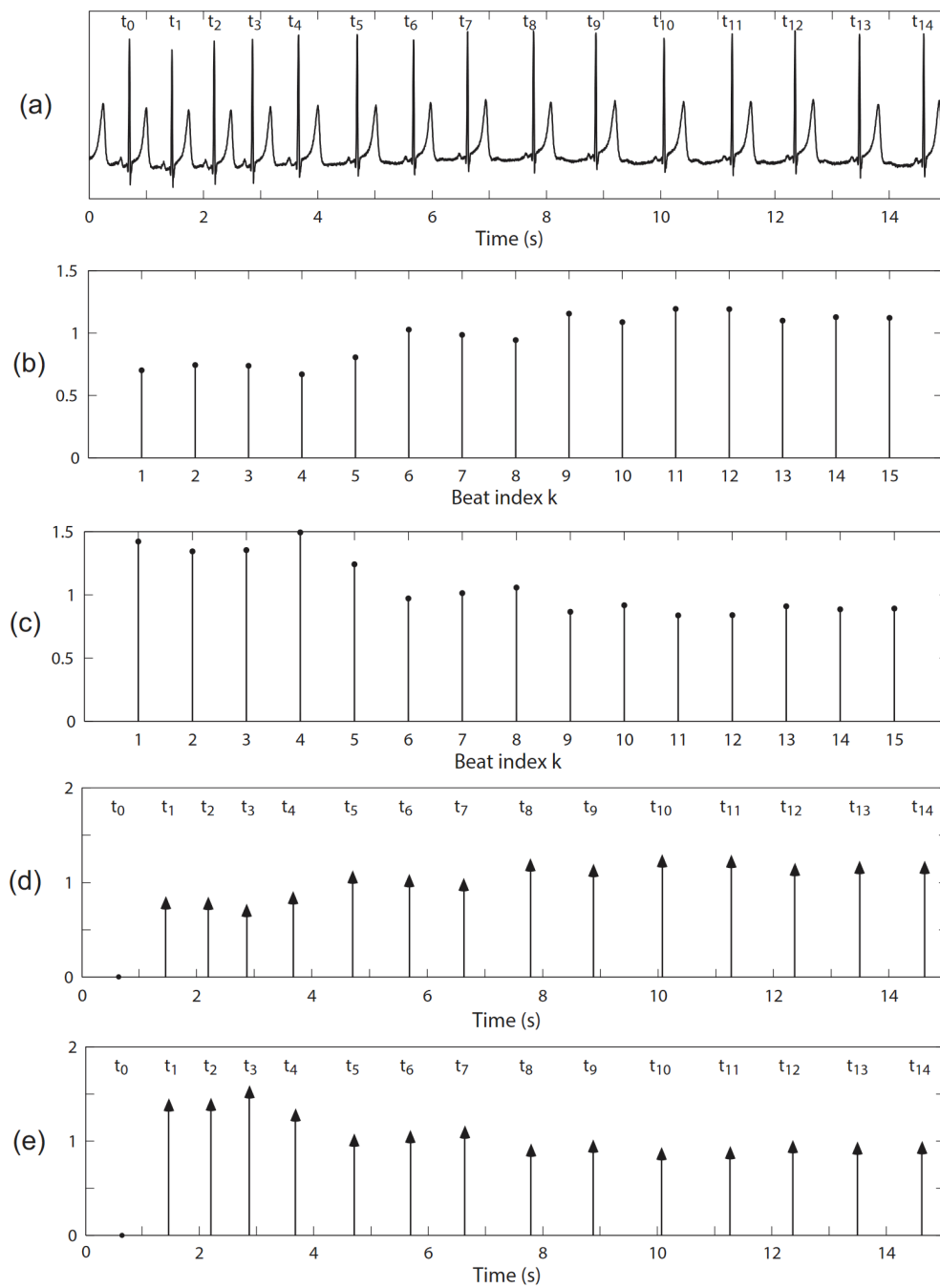
Frequency domain parameters consists in the analysis of the Power Spectral Distribution (PSD) in three main frequency bands of interest: the very low frequency (VLF) band, ranging from 0 to 0.04 Hz, the low frequency (LF) band, which extends from 0.04 up to 0.15 Hz, and the high frequency (HF) band, which goes from 0.15 to 0.4 Hz [27]. Figure 1.9 illustrates a classic spectral representation of HRV, with their bands separated.
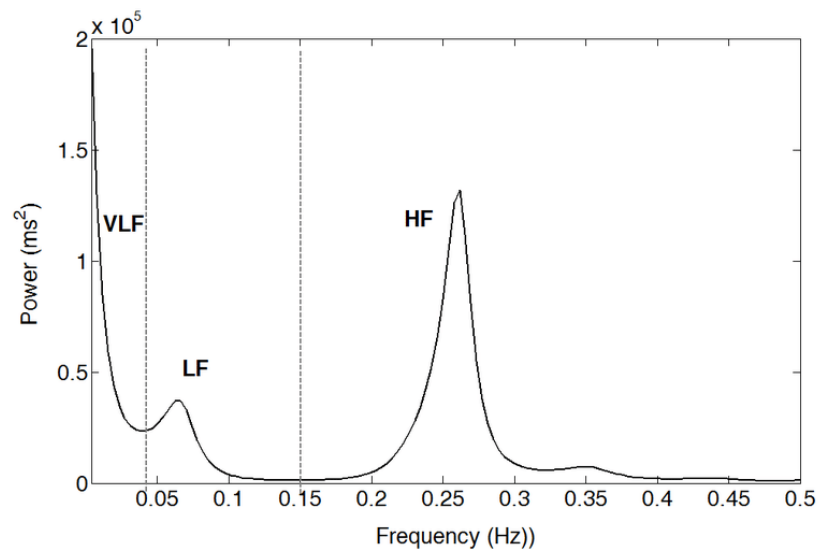
Figure 1.9: HRV power spectral distribution with its 3 classic frequency bands, extracted from [31].

The physiological interpretation of HRV frequency components has been studied by inferring sympathetic and/or parasympathetic blockades. The physiological interpretation of the power in the VLF band (P_{VLF}) has been related with thermoregulation and the rennin-angiotensin system [32]. The power in the LF band (P_{LF}) has been suggested to represent both sympathetic and parasympathetic modulation, where as the power in the HF band (P_{HF}) has been related only with parasympathetic activity. Apart from these parameters, also the normalized power in the low frequency band (P_{LFn}) and the ratio between powers in LF and HF band ($R_{LF/HF}$) are widely employed. P_{LFn} is interpreted as a marker of sympathetic activity, while $R_{LF/HF}$ is used as a measurement of the sympathovagal balance [33].

Finally, in the recent years a great amount of **non-linear parameters** have been developed, based on quantitative measurements of the complexity or regularity of HRV. Some examples are the correlation dimension, the approximate entropy, the sample entropy or the Poincarè plot. Another technique that account to linear and non-linear parameters is the PDM analysis, which is able to extract and separate sympathetic and parasympathetic dynamics [34]. This non-linear analysis will be used in this dissertation and will be more explained in Section 5.3.5.

1.4.2 Photoplethysmography

Pulse photoplethysmography, introduced by Hertzman [35], is a non-invasive method for measuring the relative blood volume changes in the microvascular bed of peripheral tissues and evaluating peripheral circulation [36]. This signal is obtained through non-invasive pulse oximetry systems and it is based on blood light absorption [37]. PPG consists of illuminating the tissue and simultaneously measuring the transmitted (transmission mode) or the reflected light (reflection mode) using a specific wavelength. About the wavelengths, green (530 nm), red (660 nm) and infrared (940 nm) are the most common, being deeper the light penetration when the wavelength increases. The PPG signal has two components: one component reflecting the arterial pulse produced by the heartbeats (AC component), and another component due to the non-pulsating blood volume and the surrounding tissue, producing a signal with slow changes (DC component). An example of the AC component of a PPG signal, labelled x_{PPG}, can be observed in Figure 1.10.
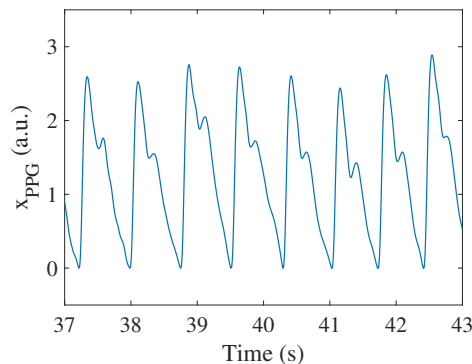
Figure 1.10: An example of the AC component of a PPG signal, measured in arbitrary units (a.u.).

The morphology of the PPG pulses can be divided into two phases. On one hand, the rise of the pulse which corresponds to the systole, and the descent of the pulse which corresponds to the diastole and the wave reflections. PPG pulses from subjects with no arterial compliance problems usually present a dichrotic notch, which is an inflection point on the pulse downward slope. Not all the PPG pulses have the same waveform, in fact, morphological changes have been observed due to the body location where PPG is registered [38], as Figure 1.11 shows.
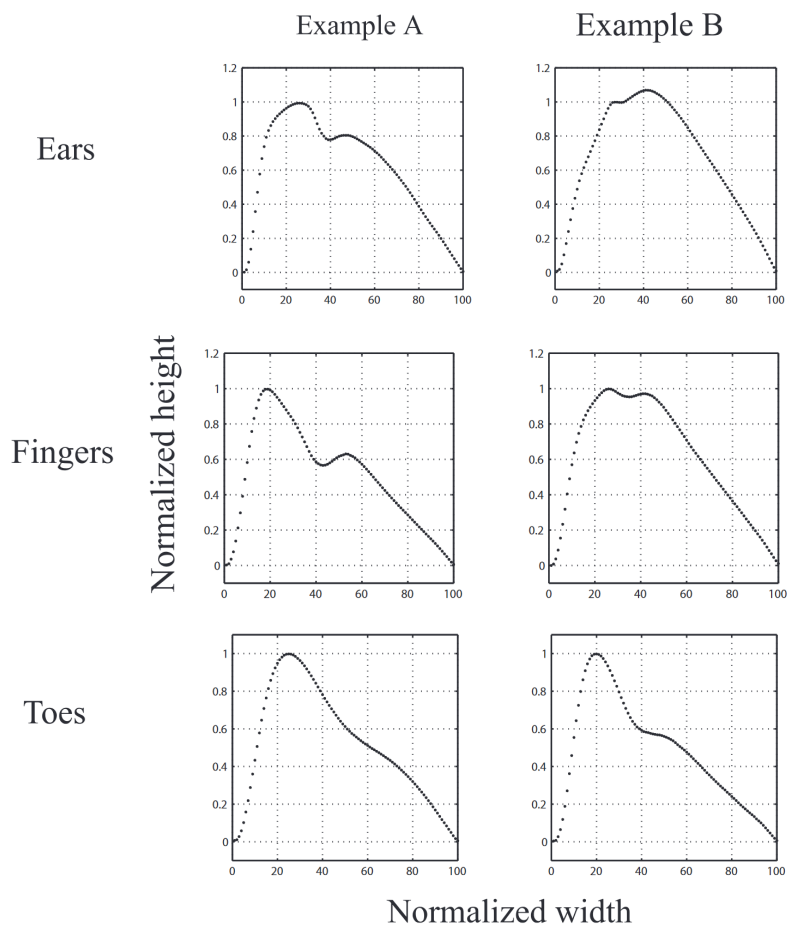
Figure 1.11: PPG pulses in different body locations, from [39].

The main advantage of PPG signal is that it could provide multiple information using only one sensor, making its use simpler, more comfortable and cheaper than multiple sensor devices. Among its applications, the most highlighted are [39]:

- Vascular assessment: measuring the arterial disease, compliance or ageing among others characteristics of the vascular tissue [40].

- Blood pressure (BP) measurement [41]: BP is the pressure exerted by the blood flux over the arteries walls. When the heart beats, a blood volume is pumped out to the arteries increasing BP and reaching its maximum, known as systolic pressure. When the heart relaxes, BP decreases and it falls to its minimum value, which is known as diastolic pressure. BP is usually quantified with a pair of numbers which correspond to the systolic and the diastolic pressures, e.g., 120/80 mmHg. BP can be estimated from the PPG using the pulse transit time (PTT), which is the time that the heart beat pulse takes to propagate from the heart to the body peripherals [42], or using time domain features of the PPG signal [43] or its derivatives [44], although usually a calibration is needed.

- Oxygen saturation (SpO_2) estimation [45]: is the fraction of oxygen-saturated hemoglobin relative to total hemoglobin (unsaturated + saturated) in the blood. As oxygenated hemoglobin and non-oxygenated hemoglobin have different light-absorption properties, SpO_2 can be measured by using two PPG signals (usually two different wavelengths, the red and infrared bands) acquired at the same location. The method is based on the ratio between AC and DC components of the two PPG signals.

Autonomic information in the PPG signal

In a similar way than in the ECG, ANS information in the PPG signal can be found in the PRV signal, which has been proved to be a surrogate measurement of the HRV [4, 5, 6, 7], although some controversy still exists [8]. While in the ECG the HRV signal is extracted from the NN intervals, in the PPG signals the fiducial points varies, using the apex points [46], the medium points [47], the maximum of PPG derivatives [48] or the tangent intersection points [49]. Irrespective of the fiducial points used, the same time and frequency domains parameters obtained from the ECG signal can be extracted from the pulse rate and its variability.

Furthermore, not only PRV contains information about the ANS response. Also, PPG morphology can provide a great amount of information about vascular as-

sessment or arterial compliance, since pulse pressure propagation in arteries causes alterations in blood volume and therefore changes in the PPG pulse shape [39, 50]. In fact, these distortions in the pulse waveform have been related to physiological changes in the subjects [9]. For example, a reduction in the pulse amplitude may be directly attributable to a loss of central arterial pressure, which could be related to an activation of the sympathetic system of the subject [51]. The ratio between the pulse-to-pulse interval and the systolic amplitude could provide an understanding of the properties of a person's cardiovascular system [52]. Talking about ratios, the relationship between the amplitude of the systolic peak and the diastolic peak of the PPG, called Reflection Index (RI), has been used as an estimator of the vascular resistance of the peripheral arteries [40, 53]. Also, the ratio between the age of the subject and the time delay between the systolic and diastolic peaks, called large artery stiffness (SI), formulated an index of the contour of the PPG that is related to large artery stiffness [54]. The ratio of two PPG subareas (divided at the dicrotic notch) can be used as an indicator of total peripheral resistance [55]. The PPG pulse width is also important, since some studies suggest that the PPG width correlates better with the systemic vascular resistance than the PPG amplitude [56]. Therefore, the PPG morphology is another tool for measuring the ANS information.

1.4.3 Respiratory signal

The respiratory signal reflects changes in the thoracic cavity or in the airflow of the respiratory system during breathing. Breathing is a rhythmic process (generally unconscious) which involves the exchange of air between the atmosphere and the lungs, providing oxygen to the tissues and removing carbon dioxide. The movement of air into the lungs is called inspiration and it involves the contraction of the diaphragm and of the external intercostal muscles, increasing the diameter of the thoracic cavity and allowing the entrance of O_2. The movement of air out of the lungs is called expiration and it supposes a relaxation of the diaphragm and external intercostal muscles, compressing the chest wall and expelling CO_2 of the lungs [57].

Among others, respiratory related chest movements can be measured using a respiratory belt made from a piezoelectric sensor, which changes the electrical charge concentration in response to the chest movement. Also, respiratory rate can be di-

rectly estimated with the changing impedance of the thoracic cavity, which varies with each inhalation (increasing) and exhalation (decreasing), that results in a corresponding voltage change that can be measured with electrodes.

Furthermore, respiratory signals can be derived indirectly from other biological signals, as the ECG and the PPG, that contain respiratory influences [58]. For example, respiration modulates the beat-to-beat/pulse-to-pulse intervals, which are smaller during inspiration than during expiration. This phenomenon is known as respiratory sinus arrhythmia (RSA) and could be noticed in the ECG and PPG signals as a Frequency modulation (FM) [59, 60]. It has been reported that the amplitude of these heart rate oscillations decreases as the respiratory rate increases [61]. Also, an Amplitude modulation (AM) phenomena is found since inspiration can lead to a reduction in tissue blood volume, lowering the ECG and PPG signal amplitude. This reduction in tissue blood volume is generated by two different mechanisms: a reduction of cardiac output, and a reduction of intra-thoracic pressure [59, 62]. Alterations in intra-thoracic pressure also causes the Baseline modulation (BM) [60, 63, 64, 65], which is a variation of perfusion baseline that arises from respiratory-induced variations in venous return to the heart. The effects of these modulations over ECG and PPG signal can be seen in Figure 1.12.
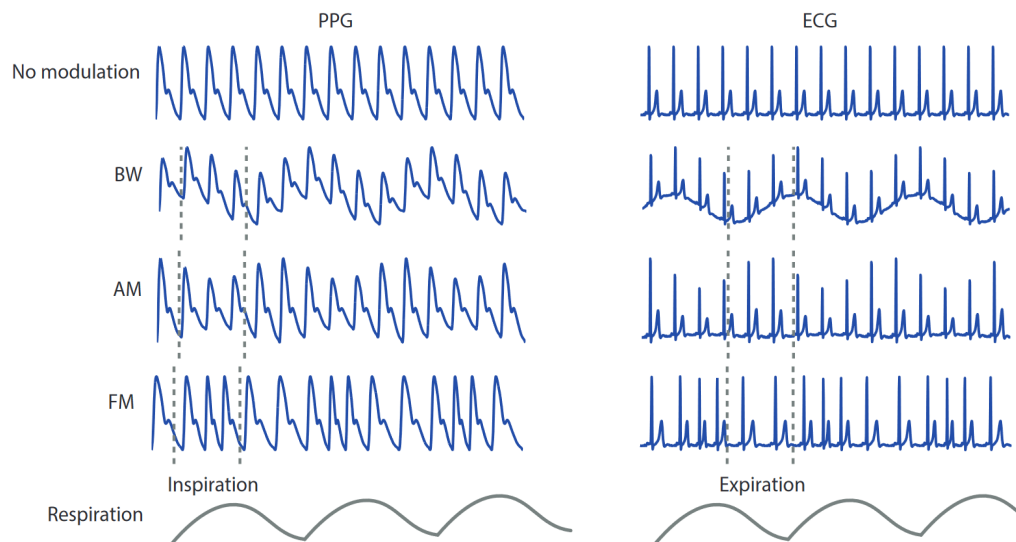

Figure 1.12: Respiratory modulations over PPG and ECG signals, reproduced and modified from [58].

Apart from these modulations, ECG morphology could also be affected by respiration through relative movements of the electrodes with respect to the heart, and changes of impedance distribution in thorax due to the filling and emptying of the lungs [66]. Taking this into account, ECG can be used to estimate the respiratory signal through the ECG derived respiratory (EDR) signals, that reflects the variations in ECG morphology due to the effect of respiration, including the QRS amplitude and the up-slope and down-slope of the QRS complexes [67]. This last method will be used in this dissertation to obtain a respiratory rate estimation from the ECG signal and will be more explained in Section 2.3.2.

Respiratory signal is also estimated from the PPG signal, based on the assumption that respiration modulates PPG signal through several effects [59]. A lot of works have developed algorithms to estimate respiratory rate from PPG signal directly, as in [68, 69, 70, 71, 72]. Other works prefer to develop their algorithms over PPG derived respiratory (PDR) signals, which contain information about the respiratory modulation. Some of these PDR signals are: respiratory-induced intensity variability (RIIV) signal, that reflects the BM [60, 63, 64, 65]; respiratory-induced frequency variation (RIFV) signal or PRV signal, that reflects the FM [59, 60, 73, 74]; respiratory-induced amplitude variation (RIAV) o Pulse Amplitude Variability (PAV) signal, which reflects the AM [60, 65, 73, 74]; and the Pulse Width Variability (PWV), which exploits the respiratory information present in the pulse wave velocity and dispersion, and it is modulated by blood vessels stiffness in addition to the pressure changes in the thorax during respiratory cycle [73]. The method explained in [73] will be used in this dissertation to obtain a respiratory rate estimation from the PPG signal and will be more explained in Sections 2.3.2 and 3.3.2. It must be noticed than PPG morphology is also dependent on the location of the sensor, so where should be placed the PPG device is another factor to be taken into account.

Autonomic information in the respiratory signal

Respiration plays a vital role in hyperbaric environments, since when hydrostatic pressure increases, air consumption increases, respiratory effort increases, and fatigue occurs. Some techniques based on breathing slowly and deeply with the diaphragm are proposed to control the rhythm and minimize the oxygen consumption.

Cardio-respiratory system is characterized by a complex interplay of several linear and non-linear subsystems, with iterations between them. In this regard, it has been shown that changes in the respiratory pattern alter the spectral content of HRV/PRV [75] and, consequently, the interpretation of sympathetic or vagal activations [76, 77, 78]. In fact, RSA could affect the interpretation of frequency domain parameters, since respiration, which is mediated by the parasympathetic system, is reflected in different frequencies. Normal range of human respiration in rest conditions is [0.08, 0.5] Hz, so it is not a surprising situation that respiration is in the LF band or exceeds the upper limit of the classic HF band. Because of this, the inclusion of respiratory rate information in HRV analysis can improve the ANS assessment: some works discard those subjects whose respiratory rate falls into the LF band [78]; in other studies, the HF band is centered at the respiratory rate using either a constant or a time-dependent bandwidth [76]. Other approximation to this situation is to separate respiratory influences from the heart rate for a better estimation of the sympathovagal balance, as the OSP method does [79]. During this thesis, both solutions will be applied, discarding those subjects with a respiratory rate lower than 0.15 Hz in Chapter 2 and applying the OSP method in Chapter 4.

1.5 Objective and structure of the thesis

The main objective of this thesis is the study of the ANS response in hyperbaric environments, through the variations of time, frequency and non-linear parameters extracted from biological signals in a non-invasive way. The content of this thesis is organized as follows:

- **Chapter 2:** A comparison between ECG and PPG time and frequency domain parameters is performed to see if the PRV signal can be used as a surrogate measurement of the HRV signal to study the ANS response in a hyperbaric environment. To that end, a new dataset was created with subjects into a hyperbaric chamber. The main differences from this dataset to others in the bibliography are: i) the increase in the number of physiological signals recorded (ECG and PPG vs. only ECG); ii) the increase in the number of subjects (28 vs. 8 to 12); iii) the increase in the number of stages with different atmospheric

pressure (5 stages with 1 atm; descent to 3 and 5 atm; ascent to 3 and 1 atm vs. 1 stage between 2,5 or 3 atm). A study of the ANS response based in the time and frequency parameters was also done, taking into account the respiratory information. The study of this new dataset generated the following publications:

- C. Sánchez, M.D. Peláez-Coca, M.T. Lozano, M. Aiger, **A. Hernando** and E. Gil. "Autonomic Nervous System Non-stationary Response to Controlled Changes in Barometric Pressure", *Proceedings of the XLIV International Conference on Computing in Cardiology (CinC), Rennes, France*, 2017.

- C. Pérez, M.D. Peláez-Coca, **A. Hernando**, E. Gil and C. Sánchez. "Multivariable Relationships between Autonomic Nervous System Related Indices in Hyperbaric Environments", *41st International Conference of the IEEE Engineering in Medicine & Biology Society (EMBC), Berlin, Germany*, 2019.

- **A. Hernando**, M.D. Peláez-Coca, M.T. Lozano, M. Aiger, D. Izquierdo, A. Sánchez, M.I. López-Jurado, I. Moura, J. Fidalgo, J. Lázaro and E. Gil. "Autonomic nervous system measurement in hyperbaric environments using ECG and PPG signals", *IEEE Journal of Biomedical and Health Informatics*, 23(1), 132-142, 2019.

- C. Sánchez, **A. Hernando**, J. Bolea, D. Izquierdo, M.T. Lozano, M.D. Peláez-Coca. "Safety Ranges for Heart Rate Variability Parameters in Hyperbaric Environments", *Proceedings of the XLVII International Conference on Computing in Cardiology, Rimini, Italy*, 2020.

• **Chapter 3:** An evaluation of the PPG sensor location for respiratory rate estimation is performed in this Chapter, due to respiratory rate is necessary to complete the study of the ANS response. In this Chapter, respiratory rate is estimated only from PPG signal because results in Chapter 2 show that PRV provides a surrogate measurement of HRV, indicating than only PPG could be used to characterize the ANS response. A dataset with 35 subjects breathing spontaneously and with a controlled respiration at a constant rate

from 0.1 Hz to 0.6 Hz, in 0.1 Hz steps, was created for that end. Respiratory signal and finger and forehead PPG were recorded simultaneously and four PDR signals were extracted from each one of the recorded PPG signals. The research described in this Chapter generated the following publications:

– **A. Hernando**, M.D. Peláez-Coca, M.T. Lozano, M. Aiger, E. Gil and J. Lázaro. "Finger and Forehead PPG Signal Comparison for Respiratory Rate Estimation Based on Pulse Amplitude Variability", *25th European Signal Processing Conference (EUSIPCO), Kos, Greece*, 2130-2134, 2017.

– **A. Hernando**, M.D. Peláez-Coca, M.T. Lozano, J. Lázaro and E. Gil. "Finger and forehead PPG signal comparison for respiratory rate estimation", *Physiological Measurement*, 40, 095007 (12pp), 2019.

- **Chapter 4:** A new algorithm to decompose the PPG pulse into two waves related with the systolic and the diastolic peaks is presented in this Chapter. The first wave is extracted directly from the PPG pulse waveform and the second wave is modelled by a lognormal curve. From these two waves, some parameters such as the amplitude, the width, the time instant, the area under the curve and some ratios are computed. This algorithm is applied into the hyperbaric chamber dataset to identify alterations in the morphology of the PPG pulse due to the exposure of the subjects to the hyperbaric environment. The following publications associated with the PPG morphology were generated:

  – M.D. Peláez-Coca, **A. Hernando**, C. Sánchez, M.T. Lozano, D. Izquierdo and E. Gil. "Photoplethysmographic Waveform in Hyperbaric Environment", *41st Annual International Conference of the IEEE Engineering in Medicine & Biology Society (EMBC), Berlin, Germany*, 2019.

  – M.D. Peláez-Coca, M.T. Lozano, **A. Hernando**, M. Aiger and E. Gil. "Photoplethysmographic Waveform Versus Heart Rate Variability to Identify Low Stress States. Attention Test", *IEEE Journal of Biomedical and Health Informatics*, 23(5), 1940-1951, 2019.

  – M.D. Peláez-Coca, **A. Hernando**, M.T. Lozano, C. Sánchez, D. Izquierdo and E. Gil. "Photoplethysmographic Waveform and Pulse Rate Variabil-

ity Analysis in Hyperbaric Environments", *IEEE Journal of Biomedical and Health Informatics*, 2020.

– **A. Hernando**, M.D. Peláez-Coca and E. Gil. "Photoplethysmogram waveform decomposition into systolic and diastolic waves for Autonomic Nervous System characterization in hyperbaric environments", *IEEE Transactions on Biomedical Engineering, Under Review*

- **Chapter 5:** The objective of this Chapter is the characterization of the ANS response in three different hyperbaric environments: a) in the hyperbaric chamber dataset, presented in the Chapter 2; b) in a controlled water immersion where divers remained static in order to minimize the effects of different variables; c) in an uncontrolled water immersion where divers performed physical activities during the immersion, which is expected to alter ANS dynamics. The effects of different factors over the ANS response, such as the pressure, the cold water or the physical activity during the dive, are analyzed in this Chapter. To do that, OSP and PDM methods are used to overcome the limitations of classic PSD frequency domain parameters when the respiratory rate falls in the LF band and in the account of linear and non-linear properties. The research described in this Chapter generated the following publications:

  – C. Varon, J. Lázaro, J. Bolea, **A. Hernando**, J. Aguiló, E. Gil, S. Van Huffel and R. Bailón. "Unconstrained Estimation of HRV Indices after Removing Respiratory Influences from Heart Rate", *IEEE Journal of Biomedical and Health Informatics, 23(6), 2386-2397*, 2019.

  – **A. Hernando**, M.D. Peláez-Coca, C. Sánchez, J. Bolea, D. Izquierdo, M.T. Lozano and E. Gil. "Autonomic Nervous System Response During Scuba Diving Activity", *Proceedings of the XLVII International Conference on Computing in Cardiology. Rimini, Italy*, 2020.

  – **A. Hernando**, H. Posada-Quintero, M.D. Peláez-Coca, E. Gil, K.H. Chon. "Respiratory component and non-linear analysis of Heart Rate Variability for Autonomic Nervous System characterization in hyperbaric environments", *Computer Methods and Programs in Biomedicine, Under review.*

- **Chapter 6:** The final chapter contains the conclusions and the possible future lines of this thesis.

Chapter 2

PRV as a surrogate measurement of HRV in hyperbaric environments

2.1 Introduction

As it is said in Section 1.2, the fact of being under the water, since this element is almost 800 times denser than air, supposes that a descent of 10 meters implies a pressure increase of one atmosphere. To regulate this pressure change, the diver's body needs to adapt itself to the new environments in the best possible manner, trying to maintain the homeostasis.

The fast response to changes that occur during a dive is reflected by the two branches of the ANS, the sympathetic and parasympathetic nervous systems. The most popular way to measure the ANS activity in a non-invasive way is the HRV signal, extracted from the ECG. However, the fact of using electrodes on the subject's chest maybe is not the best option in hyperbaric environments, especially during a real immersion. That is the reason to propose the PRV signal extracted from the PPG as an alternative non-invasive measure of the ANS response. PRV has been proved to be a surrogate measurement of the HRV [4, 5, 6, 7], although some controversy still exists [8]. The advantages of using PPG are: it requires only one low-cost device; this device can be located in several parts of the body; PPG allows

to obtain extra information that ECG does not, as the oxygen saturation. For these reasons, PPG signal could be better suited to measure the ANS response in hyperbaric environments.

The ANS response has been analysed in several studies simulating atmospheric pressure conditions inside a hyperbaric chamber, without needing to go under water [1, 15, 16, 17, 18]. The results of these studies suggest an increase in parasympathetic activity, that could lead to a reduction in the heart rate. All the cited studies inside a hyperbaric chamber are characterised by: a low number of subjects (between 8 and 12); the use of only the HRV to characterise the ANS behaviour; and the measurement of only one hyperbaric stage between 2.5 and 3 atm.

In light of the above, the main goal of this Chapter is to determine if PRV is a surrogate measurement of HRV in hyperbaric environments. To that end, an analysis of HRV, PRV and respiratory rate was performed in 26 healthy subjects inside a hyperbaric chamber during five stages, with pressure increasing from 1 atm to 3 and 5 atm and later decreasing it to 3 and 1 atm again. ECG and PPG signals were recorded and respiratory rate was estimated from these signals, and was included in the HRV and PRV analysis to obtain a more reliable interpretation of the results [76, 77, 78]. An statistical analysis and a correlation of the time and frequency domain parameters was made to compare ECG and PPG signals. Also, the ANS response to atmospheric pressure changes and the time spent in a hyperbaric environment was studied, with a higher number of subjects and more stages with varying atmospheric pressures in comparison to previous studies.

2.2   Materials

A total of 26 subjects (22 males and 4 females), with a mean age of 28.73 ± 6.39 years and a strong component of military personnel (21 out of 26, 80.78% of the total study population) were recorded inside the hyperbaric chamber of the Hospital General de la Defensa de Zaragoza (it can be seen in Figure 2.1). The study protocol was approved by "Comité de ética de la investigación con medicamentos de la inspección general de sanidad de la Defensa", the hospital Review Board, and all subjects signed the written informed consent.

Figure 2.1: The hyperbaric chamber used in this study.

The protocol consisted of five different pressure stages at 1 atm (sea level), 3 atm (simulating 20 metres depth) and 5 atm (simulating 40 meters depth), and sub-sequently returning to 3 atm and 1 atm. Subjects remained relaxed and sitting comfortably, and the chamber was correctly ventilated throughout the protocol in an attempt to avoid major changes in temperature and humidity. During the five different stages, there were 5 min stops where the subjects remained in silence and without any movements for a good ECG and PPG recording. Therefore, a total of five stages, referred to as S1D, S3D, S5, S3A and S1A (the letter S from stage; the number 1, 3, or 5 reflects the pressure in atm; the letter D or A refers to descent or ascent) were studied. A schematic representation of the entire protocol is shown in Table 2.1. The complete duration of the protocol was about two hours and most of the time was spent in the decompression stops between 3 atm and 1 atm, as recom-mended in standard decompression tables. In 21 subjects, this decompression time was 44 min, distributed as follows: 2 min at 1.9 atm, 16 min at 1.6 atm and 26 min at 1.3 atm. In the rest of the cases, the decompression time was slightly fewer, but always upper than 30 min.

Recordings were performed using a Nautilus device [80], which recorded the ECG signal with three frontal bipolar leads at a sampling frequency (f_s) of 2000 Hz, along with the PPG signal ($f_s = 1000$ Hz) on the finger with two possible wavelengths (red and infrared) and the atmospheric pressure ($f_s = 250$ Hz) inside the chamber.

Table 2.1: Explanation of the protocol, showing the atmospheric pressure, the different parts and their respective durations.

Pressure	1 atm (sea level)	1-3 atm	3 atm	3-5 atm	5 atm	5-3 atm	3 atm	3-1 atm	1 atm (sea level)
Explanation	S1D	Descending	S3D	Descending	S5	Ascending	S3A	Ascending	S1A
Duration	5 min	6-8 min	5 min	6-8 min	5 min	6-8 min	5 min	50-55 min	5 min

2.3   Methods

2.3.1   ECG and PPG analysis

ECG and PPG signals needed some preprocessing before analysis. ECG was first down-sampled to 1000 Hz to obtain the same sampling frequency as the PPG signal. A low-pass finite impulse response (FIR) filter was then applied to the two signals to estimate the baseline interference and to remove this noise from the signal (cut-off frequency of 0.03 Hz and 0.07 Hz for ECG and PPG signals respectively) [26]. Another low-pass FIR filter was applied over the PPG signal (cut-off frequency of 35 Hz) to remove the high frequency noise [73]. The filtered ECG and PPG signals were labelled as x_{ECG} and x_{PPG} respectively.

Heart beats were detected in the ECG using a wavelet-based algorithm over the second lead of the recorded ECG signal [81]. In addition, ectopic beats and missed and false detections were identified and corrected [82]. As a result, the QRS complex could be located in each beat (i) of the ECG, and the difference between consecutive R waves was used to generate the beat-to-beat RR time series.

Artefacts in the PPG signal pulses were suppressed using the detector described in [83]. From each pulse (i), the medium points (n_{M_i}) of the PPG pulses were then detected automatically using an algorithm based on a low-pass differentiator filter [46], since they were considered the fiducial points because of their robustness [47, 84], so the difference between them was used to compute the pulse-to-pulse PP time series. Figure 2.2 shows an example of how time series from the ECG and PPG signals were estimated using the fiducial points of both signals.
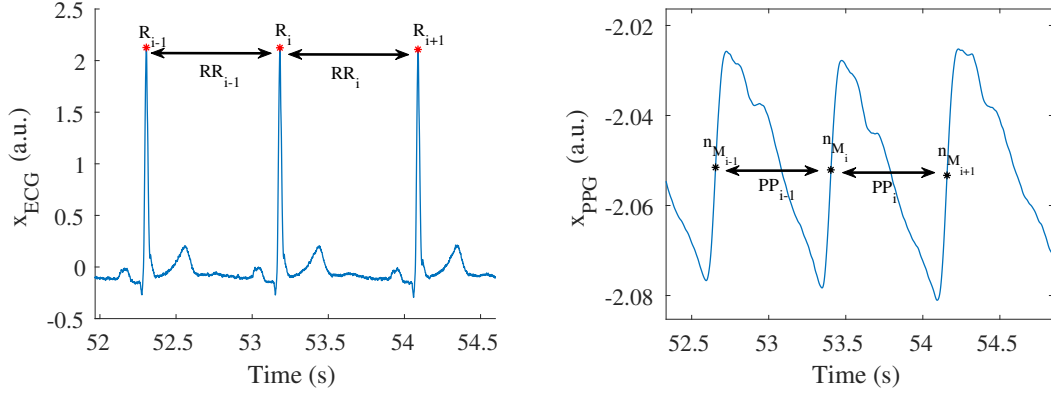
Figure 2.2: Left, ECG signal with the R peaks of the QRS complexes highlighted and the RR time series delimited with an arrow; right, PPG signal with the medium points of the pulse wave highlighted and the PP time series delimited with an arrow.

Four time domain parameters were computed for both signals using the beat-to-beat/pulse-to-pulse time series for each stage:

- $NN(s)$: median of the Normal-to-Normal intervals between the fiducial points of both signals.

- $IQR(s)$: Interquartile range as a measure of statistical dispersion, which reflects the difference between the upper and lower quartiles.

- $RMSSD(s)$: root mean square of successive differences between adjacent NN intervals.

- $pNN50(\%)$: number of pairs of successive NNs that differ by more than 50 ms, divided by the total number of NN intervals.

The frequency domain parameters were extracted from the TVIPFM model. This model assumes that the beat/pulse occurrence times (R_i or n_{M_i}) were supposed to be generated by a modulating signal, $m_X(n)$, with X $\in$ [H,P], extracted from ECG and PPG respectively, which has zero-mean and carries the information of ANS modulation. The input signal, consisting in $m_X(n)$ superimposed to a DC level, was integrated until the threshold $T_X(n)$, which represents the time-varying mean heart period, was reached. Then, a beat occurred and the integration process was reset. A schematic of the TVIPFM model is displayed in Figure 2.3.
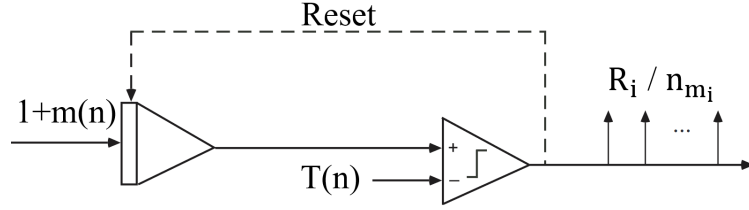
Figure 2.3: Schematic representation of the time-varying integral pulse frequency modulation (TVIPFM) model. Adapted and reproduced from [76].

From this model, the instantaneous heart/pulse rate signal $(d_{XR}(n))$, sampled at 4 Hz, was represented by:

$$d_{XR}(n) = \frac{1 + m_X(n)}{T_X(n)}. \tag{2.1}$$

Assuming that the variations in the term $1/T_X(n)$ are slower than those in the term $m_X(n)/T_X(n)$, the time-varying mean HR or PR $(d_{XRM}(n))$ could be obtained by low-pass filtering $d_{XR}(n)$, with a cut-off frequency of 0.03 Hz, as follows:

$$d_{XRM}(n) = \frac{1}{T_X(n)}. \tag{2.2}$$

HRV and PRV signals $(d_{XRV}(n))$ were subsequently obtained as:

$$d_{XRV}(n) = d_{XR}(n) - d_{XRM}(n) = \frac{m_X(n)}{T_X(n)}. \tag{2.3}$$

Finally, $m_X(n)$ was estimated by correcting $d_{XRV}(n)$ by $d_{XRM}(n)$:

$$m_X(n) = \frac{d_{XRV}(n)}{d_{XRM}(n)}. \tag{2.4}$$

Figure 2.4 shows an example of $d_{XR}(n)$, $d_{XRM}(n)$, and $m_X(n)$ signals extracted from the ECG and from the PPG.

As the five stages were considered stationary, four frequency domain parameters were calculated based on the PSD analysis of the modulating signal $m_X(n)$, using Welch's power spectral density estimation, with nine 1-min Hamming windows and an overlap of 50%. The parameters computed were:
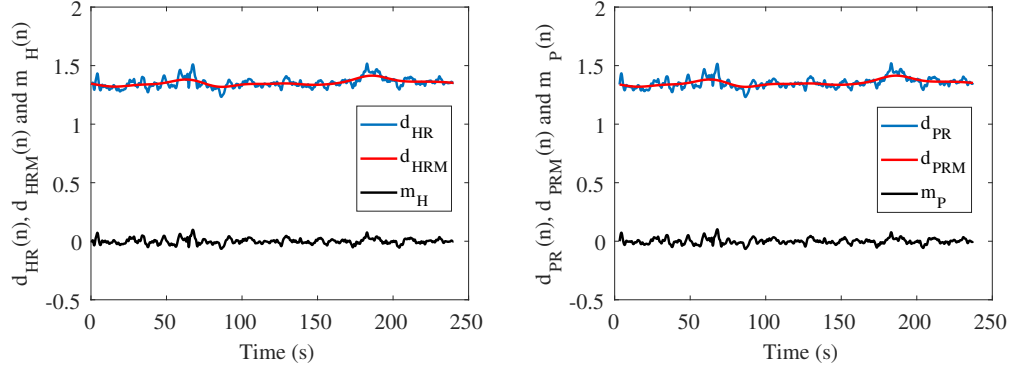
Figure 2.4: $d_{XR}(n)$ (in blue), $d_{XRM}(n)$ (in red), and $m_X(n)$ (in black) signals extracted from the ECG (left) and from the PPG (right).

- $P_{LF}(a.u.)$: power inside the LF band (0.04-0.15 Hz). Measurement units: $a.u.$, arbitrary units.

- $P_{HF}(a.u.)$: power inside the HF band (0.15-0.4 Hz).

- $P_{LFn}(n.u.)$: power in LF band normalised with respect to those of the LF and HF bands. Measurement units: $n.u.$, normalized units.

- $R_{LF/HF}(n.u.)$: ratio between LF and HF powers.

These eight time and frequency domain parameters allowed a comparison among ECG and PPG estimations in order to determine whether both signals provide the same information in hyperbaric environments. Furthermore these parameters also permitted to characterise the ANS response to atmospheric pressure changes and time spent in the hyperbaric chamber.

2.3.2 Respiratory rate extracted from ECG and PPG signals

As it was explained in Sections 1.4.1 and 1.4.2, respiratory information affects the interpretation of frequency parameters, since respiration, which is parasympathetic related, has a normal range of [0.08, 0.5] Hz in rest conditions, so it is not a surprising situation that respiration is in the LF band or exceeds the upper limit of the classic HF band. Therefore, an estimation of the respiratory rate of the five stages is necessary to avoid misinterpretations of the frequency parameters. Since there is

not a respiratory device or a chest band that estimates respiratory rate directly, in this Chapter respiratory rate should be extracted from the ECG and PPG signals. The first step was obtaining all the EDR and PDR signals. Secondly, and after combining the EDR and PDR signals, the same algorithm was applied to them to obtain the respiratory rate. Finally, a combined respiratory rate was averaged if both estimations provided a similar value during at least one minute of the analysis window. If not, no respiratory rate estimation was performed for that subject at that stage. Those subjects with an averaged respiratory rate lower than 0.15 Hz (upper limit of the LF band) were discarded to avoid possible misinterpretations when studying the ANS results, as in [78].

EDR signals extraction from the ECG

The method for estimating respiratory rate from ECG presented in [67] was used to obtain the EDR signals. This method exploits respiration-induced morphology variations in the QRS slope and R-wave angle of the ECG signal [85].

For each QRS complex, two slopes were measured: upward slope of the R wave and downward slope of the R wave. To do that, first time instants associated with the maximum variation points of the ECG signal between Q and R points ($n_{Q_{l,i}}$ and $n_{R_{l,i}}$), and between R and S points ($n_{R_{l,i}}$ and $n_{S_{l,i}}$), were computed as:

$$n_{U_{l,i}} = \max_{n \in [n_{Q_{l,i}}, n_{R_{l,i}}]} \{|l'_l(n)|\} \, ; \tag{2.5}$$

$$n_{D_{l,i}} = \max_{n \in [n_{R_{l,i}}, n_{S_{l,i}}]} \{|l'_l(n)|\} \, , \tag{2.6}$$

where l' is the first derivative of lead l and i indicate the beat index.

Then, a straight line was fitted to the ECG signal by least squares in two 8 ms-length intervals, one of them centred at $n_{U_{l,i}}$ and the other one at $n_{D_{l,i}}$. The slopes of these lines are denoted $\mathcal{I}_{US_{l,i}}$ and $\mathcal{I}_{DS_{l,i}}$, respectively.

A R-wave angle was also used to derive respiratory rate. This angle corresponds to the smallest one formed by the straight lines that define $\mathcal{I}_{US_{l,i}}$ and $\mathcal{I}_{DS_{l,i}}$ [86]. The equation that defines this angle is:

$$\phi_{R_{l,i}} = \arctan \left| \frac{\mathcal{I}_{US_{l,i}} - \mathcal{I}_{DS_{l,i}}}{0.4(6.25 + \mathcal{I}_{US_{l,i}} \cdot \mathcal{I}_{DS_{l,i}})} \right| . \tag{2.7}$$

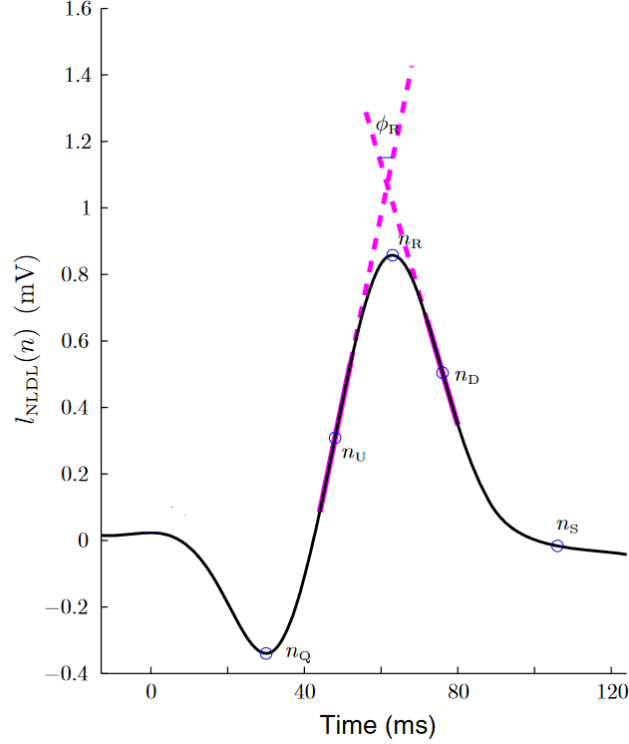Figure 2.5 shows an example of this algorithm over one QRS complex.

Figure 2.5: Estimation of the up-slope, down-slope and R-wave angle, extracted from [67]. Thick magenta lines represent the two straight lines from which the slope series are obtained. R-wave angle series are obtained from the smallest angle formed by these two lines.

An EDR signal was generated for each one of the QRS slopes series by assigning to each beat occurrence ($R_{l,i}$), the value of its associated QRS slope:

$$d^u_{US,DS_l}(n) = \sum_i \mathcal{I}_{US,DS_{l,i}} \cdot \delta(n - R_{l,i}), \qquad (2.8)$$

$$d^u_{R_l}(n) = \sum_i \phi_{R_{l,i}} \cdot \delta(n - R_{l,i}). \qquad (2.9)$$

As these signals were unevenly sampled, a resampling at 4 Hz was necessary to standardise them. Finally, a mad-based-outlier rejection and a band-pass filter were applied (0.07 - 1 Hz cut-off frequencies) to study only the frequency range where the respiratory rate was expected to be found [87]. Therefore, the three filtered EDR signals were called Ra, Us, and Ds and an example of these three signals can be

seen in Figure 2.6. Three leads were registered in this study, with three EDR signals estimated for each lead, thus meaning that nine final EDR signals were used in the ensemble to extract respiratory information.
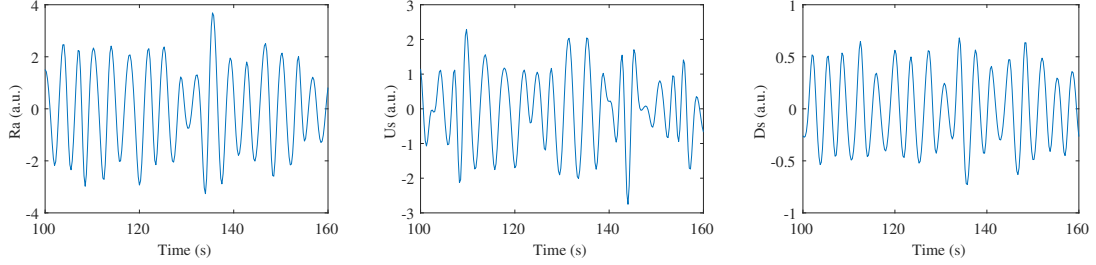

Figure 2.6: An example of the three EDR signals extracted from one ECG lead.

PDR signals extraction from the PPG

The algorithm explained in [73] was applied to obtain three morphology-based PDR signals from the PPG. The first one is related with the PRV signal:

$$d^u_{PRV}(n) = \sum_i f_s \cdot \frac{1}{n_{M_i} - n_{M_{i-1}}} \cdot \delta(n - n_{M_i}). \tag{2.10}$$

Then, the PAV signal, which reflects the amplitude variation between the apex (n_{A_i}) and the basal (n_{B_i}) points, detected as in [46], was also obtained:

$$d^u_{PAV}(n) = \sum_i \left[\mathrm{x_{PPG}}(n_{A_i}) - \mathrm{x_{PPG}}(n_{B_i}) \right] \cdot \delta(n - n_{A_i}). \tag{2.11}$$

Finally, the PWV signal, which reflects the width variation of the PPG pulse, was also estimated. In order to measure the pulses width in PPG signal, it is necessary to locate the onset (n_{O_i}) and the end points (n_{E_i}) of each pulse wave. To do that, the maximum up-slope point $(n^{PPG}_{U_i})$ was found inside a determined region around the apex point in the low-pass derivative PPG signal $(\mathrm{x'_{PPG}}(n))$:

$$n^{PPG}_{U_i} = \arg\max_n \left\{ \mathrm{x'_{PPG}}(n) \right\}, n \in [n_{A_i} - 0.3 f_s, n_{A_i}]. \tag{2.12}$$

The pulse wave onset, n_{O_i}, search is limited to Ω_{O_i} interval and is determined as:

$$\Omega_{O_i} = \left[n_{A_i} - 0.3 f_s, n_{U_i}^{PPG} \right] \tag{2.13}$$

$$
n_{O_i} = \begin{cases}
\arg \min\limits_{n \in \Omega_{O_i}} \left\{ \left| \mathrm{x}_{\mathrm{PPG}}'(n) - \eta \cdot \mathrm{x}_{\mathrm{PPG}}'(n_{U_i}^{PPG}) \right| \right\} & \text{if } C_1 \\
\text{last relative minimum of } \mathrm{x}_{\mathrm{PPG}}'(n) \text{ if } C_2 \\
\arg \min_{n \in \Omega_{O_i}} \left\{ \mathrm{x}_{\mathrm{PPG}}'(n) \right\} & \text{otherwise}
\end{cases} \tag{2.14}
$$

where $\eta \cdot \mathrm{x}_{\mathrm{PPG}}'(n_{U_i}^{PPG})$ represents a beat varying threshold dependent on maximum up-slope value of each pulse wave, and conditions C1 and C2 are defined by:

- C_1: $\exists \, m \in \Omega_{O_i} \ni \mathrm{x}_{\mathrm{PPG}}'(m) \leq \eta \cdot \mathrm{x}_{\mathrm{PPG}}'(n_{U_i}^{PPG})$

- C_2: $\overline{C_1} \wedge$ exists a relative minimum of $\mathrm{x}_{\mathrm{PPG}}'$ in Ω_{O_i}

Pulse wave ends, n_{E_i}, were detected in a similar way as n_{O_i}, but using maximum down-slope $(n_{D_i}^{PPG})$ instead of $n_{U_i}^{PPG}$, in the interval $[n_{A_i}, \, n_{A_i} + 0.3 \cdot f_s]$ and $\Omega_{O_i} = \left[n_{D_i}^{PPG}, n_{A_i} + 0.3 \cdot f_s \right]$.

Once n_{O_i} and n_{E_i} were detected, the PDR signal based on pulse width variability was computed as:

$$d_{PWV}^u(n) = \sum_i \frac{1}{f_s} \cdot (n_{E_i} - n_{O_i}) \cdot \delta(n - n_{M_i}) \tag{2.15}$$

Figure 2.7 shows an example of the n_{O_i} and n_{E_i} points detection and the estimation of $d_{PWV}^u(n)$.

As the three PDR signals were unevenly sampled, a resampling at 4 Hz was applied to standardise them, along with a mad-based-outlier rejection and a band-pass filter (0.07 - 1 Hz cut-off frequencies). PRV, PAV and PWV conformed the ensemble used to extract respiratory information from the PPG. Figure 2.8 shows an example of these three PDR signals obtained from the PPG.

Respiratory rate estimation

The same fusion algorithm based on [67] was applied to the nine EDR signals (j = 1...9) and the three PDR signals (j = 1...3) to estimate respiratory rate (F_R^X), with X $\in$ [H,P], from peaked-conditioned averaged spectra. A power spectrum density
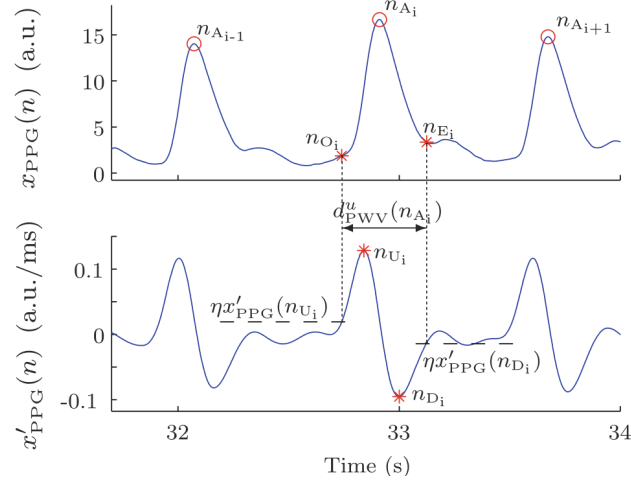
Figure 2.7: Estimation of the n_{O_i} and n_{E_i} points, together with the estimation of the PDR signal based on pulse width variability. Extracted and modified from [73].
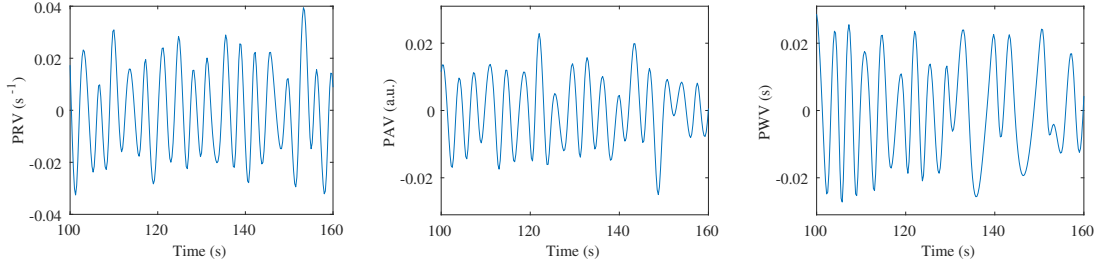

Figure 2.8: An example of the three PDR signals extracted from the PPG.

$S_{j,k}^X(f)$ was estimated every 5 seconds from the kth 40 s length running window using the Welch's periodogram with sub-windows of 12 s and a 50% overlap, for each EDR and PDR signal (j). The location of the largest peak $f_I^X(j,k)$ was determined for each $S_{j,k}^X(f)$. A reference interval $\Omega_R^X(j,k)$ was subsequently established as:

$$\Omega_R^X(j,k) = \left[F_R^X(j,k-1) - \delta, F_R^X(j,k-1) + 2\delta \right], \qquad (2.16)$$

where $F_R^X(k-1)$ is the respiratory rate estimated from the previous $(k-1)$ window, and $\delta = 0.1$.

All peaks larger than 85% of $f_I^X(j,k)$ inside $\Omega_R^X(j,k)$ were detected, and $f_{II}^X(j,k)$ was chosen as the nearest peak to $F_R^X(j,k-1)$, since respiratory variation in 5 s is supposed to be slow. Note that $f_{II}^X(j,k)$ could be the same $f_I^X(j,k)$ if the largest

peak was also the nearest peak to $F_R^X(j, k-1)$. An example of selection of $f_I^X(j,k)$ and $f_{II}^X(j,k)$ is shown in Figure 2.9.
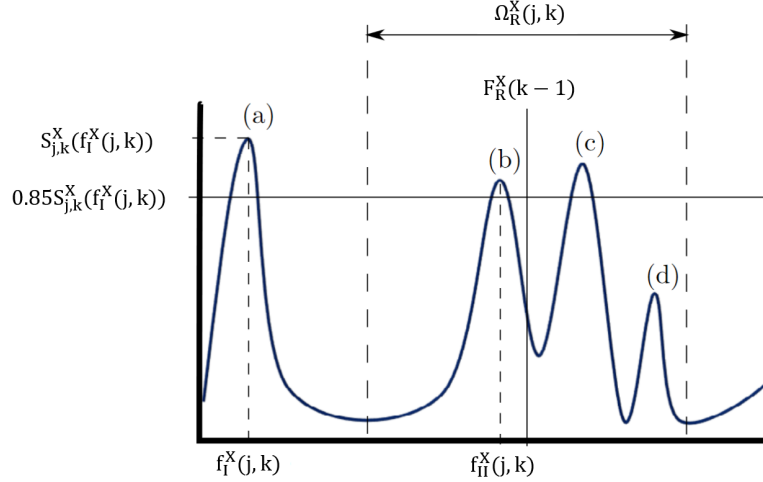

Figure 2.9: Example of selection of $f_I^X(j,k)$ and $f_{II}^X(j,k)$ for an hypothetical $S_{j,k}^X(f)$ and for a given $F_R^X(k-1)$, extracted and modified from [67]. Peak (a) was selected as $f_I^X(j,k)$ because is the highest peak. Then, peaks higher than 85% of $f_I^X(j,k)$ within $\Omega_R^X(j,k)$ were detected. Peak (b) was selected as $f_{II}^X(j,k)$ because is the nearest to $F_R^X(k-1)$. Extracted and modified from [67].

A measure of peakness was subsequently obtained from $S_{j,k}^X(f)$ as the percentage of power around the $f_{II}^X(j,k)$ with respect to the reference interval $\Omega_R^X(j,k)$. This is the only difference between the respiratory rate estimation from ECG and PPG signals, while the peakness for EDR signals was determined as:

$$P_{j,k}^H = \frac{\int_{f_{II}^H(j,k)-0.6\delta}^{f_{II}^H(j,k)+0.6\delta} S_{j,k}^H(f)df}{\int_{F_R^H(k-1)-\delta}^{F_R^H(k-1)+2\delta} S_{j,k}^H(f)df} \cdot 100. \tag{2.17}$$

A different peakness formulation, which follows the criterion described in [88], changing the peakness conditions and limits to enhance the high frequencies, was used for PDR signals:

$$P_{j,k}^P = \frac{\displaystyle\int_{(1-g)f_{II}^P(j,k)}^{(1+g)f_{II}^P(j,k)} S_{j,k}^P(f)df}{\displaystyle\int_{F_R^P(k-1)-\delta_P}^{F_R^P(k-1)+\delta_P} S_{j,k}^P(f)df} \cdot 100, \tag{2.18}$$

where $g = 0.5$ and $\delta_P = 0.2$.

Then, a peaked-conditioned average spectra, $\overline{S_k^X(f)}$, was obtained by averaging those $S_{j,k}^X(f)$ which were sufficiently peaked:

$$\overline{S_k^X(f)} = \sum_{l=-L_s}^{L_s} \sum_{j=1}^{N_s} \chi_{j,k-l}^A \cdot \chi_{j,k-l}^B \cdot S_{j,k-l}^X(f), \tag{2.19}$$

where L_s was set to 2 in order to average a maximum of 5 spectra for each EDR and PDR signal as in [67], N_s is the number of signals (9 for ECG and 3 for PPG), and $\chi_{j,k-l}^A$ and $\chi_{j,k-l}^B$ are two criteria used to determine whether the power spectrum $S_{j,k-l}^X(f)$ was sufficiently peaked:

$$\chi_{j,k}^A = \begin{cases} 1, & P_{j,k}^X \geq 85 \\ 0, & otherwise \end{cases}, \tag{2.20}$$

$$\chi_{j,k}^B = \begin{cases} 1, & P_{j,k}^X \geq \max_j \left(P_{j,k}^X\right) - \lambda \\ 0, & otherwise \end{cases}. \tag{2.21}$$

Therefore, only those $S_{j,k}^X(f)$ whose peakness $P_{j,k}^X$ was above 85% and had a total power close to the maximum ($\lambda = 0.05$) were averaged. Figure 2.10 shows an example of two spectra, one with $P_{j,k}^P > 85\%$ (sufficiently peaked to be used for the average), and another one with $P_{j,k}^P < 85\%$ (insufficiently peaked to be used for the average).

Consequently, the respiratory rate was estimated for both signals as the maximum of $\overline{S_k^X(f)}$:

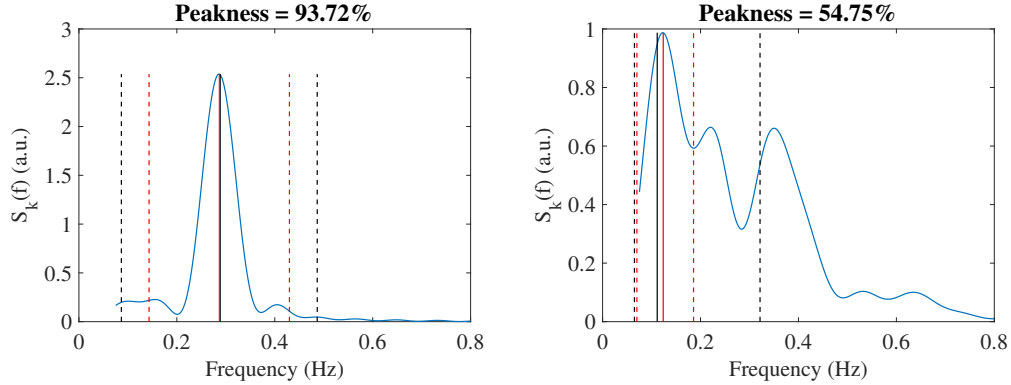$$F_R^X(k) = \arg \max_f \overline{S_k^X(f)}. \tag{2.22}$$

Figure 2.10: Differences between one spectrum (extracted from the PPG) that satisfy the peakness condition and one spectrum that do not. Red dashed lines illustrate the limits of the integrating interval of the numerator in $P_{j,k}^P$ with the solid line marking the $f_{II}^P(k)$ value. Black dashed lines illustrate the limits of the integrating interval of the numerator in $P_{j,k}^P$, with the solid line marking the $F_R^P(k-1)$ value.

Finally, a combined respiratory rate $(F_R^C(k))$ was calculated as the mean of both estimations if they were similar. The difference between PPG and ECG respiratory rate estimations must be less than 0.05 Hz for at least 25% of the analysis window. This restriction was defined based on the estimation errors found in [67, 73], and imposes that, to obtain the mean respiratory rate value representing the entire stage $(\overline{F_R^C})$, both estimations have to be similar during 1 min at least. If this criterion was not fulfilled, the combined respiratory rate was not estimated for the subject in that stage. If this criterion was fulfilled, but $\overline{F_R^C}$ is lower than 0.15 Hz, the subject was discarded in this stage to avoid misinterpretations in the ANS response.

The percentage of time (P_T) during which both estimations matched was also calculated:

$$P_T(\%) = \frac{100}{N_t} \cdot \sum_{k=0}^{T_n} C_f(k), \tag{2.23}$$

where $C_f(k) = 1$ if both estimations match and $C_f(k) = 0$ if not, and N_t is the total number of time instants during the entire stage.

2.3.3 Oxygen saturation

Oxygen saturation can be computed using both wavelengths (red and infrared) of the PPG signal, applying the decomposition in AC and DC components [36]. Both

signals were initially band-pass-filtered with cut-off frequencies of 0.4 and 10 Hz. They were then divided into series of 0.8 s and the maximum and minimum for each series were determined. The AC component in the red and infrared wavelengths was described as the difference between the maximum and minimum values, whereas the DC component was just the maximum value. This defined two ratios, namely the red ratio, which is obtained by dividing the AC component by the DC component, and the infrared ratio, which is the same operation but for the infrared wavelength. The division of these two ratios gave the so-called ratio of ratios ($R(n)$), computed for each serie (n). Finally, the oxygen saturation, SpO_2, was calculated (and expressed as a percentage) according to the device manufacturer's instructions. The oxygen saturation equation was extracted from an experimental calibration curve obtained by comparing this device's recordings with a reference device to obtain the same oxygen saturation measures:

$$SpO_2(\%) = \left[-4.73R(n)^2 + 1.12R(n) + 99.7 \right] \cdot 100. \tag{2.24}$$

2.3.4   Statistical analysis

Two different statistical tests were used to analyse if PRV is a surrogate measurement of HRV. The first was a comparison between ECG and PPG likeness by means of the correlation of the modulating signal $m_X(n)$ extracted from the ECG and from the PPG. The second one involved an analysis of the difference for each parameter extracted from HRV and PRV, with a Shapiro-Wilk test being applied to verify the normal distribution of the eight parameters and then a paired sample Student's t-test being applied to the same parameter extracted with both signals. The correlation between the parameters extracted was also studied as a marker of the similarity between the two signals.

One statistical analysis was applied to each parameter to determine the presence of significant differences between the five stages of the protocol looking for differences in the ANS response. Thus, a Shapiro-Wilk test was applied to check the normal distribution of the parameter, with Student's t-test being applied to every pair of stages if the distribution was normal and the Wilcoxon paired test if not. In all the methods, a p-value < 0.05 indicated statistical significance.

2.4   Results

In this Section, data for the two final stages were not recorded in one subject, thus meaning that there were 26 subjects for S1D, S3D and S5 and only 25 subjects for S3A and S1A. As the results obtained for the red and infrared wavelengths in the PPG signal were very similar, only those for the red configuration were shown to help the reader's understanding.

2.4.1   Respiratory parameters

As mentioned above in Section 2.3.2, respiratory rate was estimated from the ECG and the PPG signals. When both estimations were very close for at least one minute during the stage, a mean combined respiratory rate was computed. As this requirement was not always fulfilled, the number of final subjects in each stage varies: 22 in S1D and S3A; 21 in S1A; 20 in S3D; and 19 in S5. The mean and standard deviation (SD) for the combined respiratory rate and the percentage of time that both estimations have a similar value for each stage are presented in Table 2.2. As the normal distribution was verified, a paired Student's t-test was performed to detect any differences in respiratory rate among stages. The number of subjects in each paired comparison were: 15 for S3A versus (vs.) S3D; 16 for S3A vs. S1D, S5 vs. S3D, S1A vs. S3D, S3A vs. S5 and S1A vs. S5; 17 for S5 vs. S1D and S1A vs. S1D; 18 for S3D vs. S1D; and 20 for S1A vs. S3A.

Table 2.2: Mean and sd for the combined respiratory rate estimation $\left(\overline{F_R^C}\right)$ and the percentage of time when both estimations match $\left(\overline{P_T}\right)$. Statistical differences (p<0.05) are represented by a $\star$ when compared with S1D.

Stages	S1D	S3D	S5	S3A	S1A
$\overline{F_R^C}(Hz)$	0.21 ± 0.07	0.23 ± 0.06	0.25 ± 0.05 $\star$	0.26 ± 0.06 $\star$	0.24 ± 0.07
$\overline{P_T}(\%)$	81.29 ± 18.75	78.08 ± 18.67	75.68 ± 20.53	83.06 ± 16.29	81.17 ± 15.84

The overall results show that the respiratory rate was higher in the latter stages than in the initial ones, with a significant difference being found when comparing S5

and S3A with S1D. The percentage of time with a match between both estimations decreased as the atmospheric pressure increased, although the difference was not significant. It must be noted that three subjects in S1D, and one subject in S3D, S5, S3A and S1A, had a respiratory rate value lower than 0.15 Hz, thus meaning that in this study they were discarded in the ANS interpretation.

2.4.2 HRV and PRV parameters

With the elimination of those subjects whose combined respiratory rate was not computed due to EDR and PDR estimations did not match during one minute and those subjects whose combined respiratory rate was lower than 0.15 Hz, there was a total of 21 subjects in S3A stage, 20 in S1A, 19 in S1D and S3D, and 18 in S5. Figure 2.11 shows one example when the combined respiratory rate is lower than 0.15 Hz and other when is higher than 0.15 Hz.
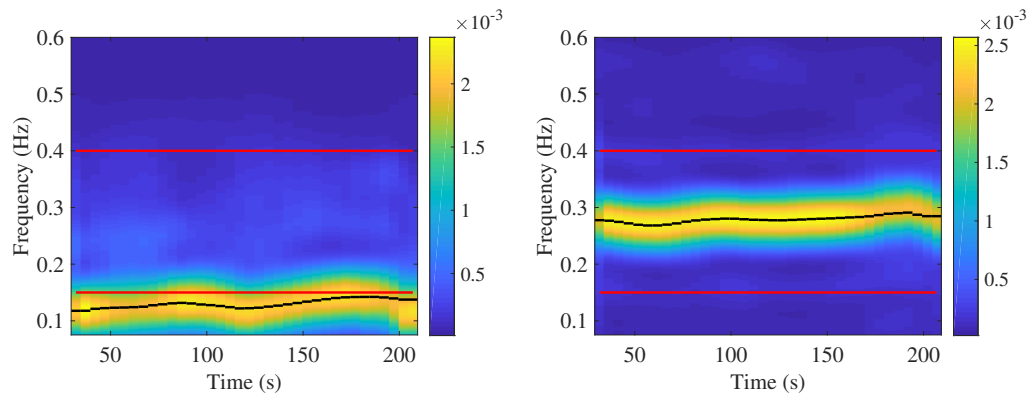

Figure 2.11: Time-frequency map of the combined respiratory rate estimation for two subjects in the same stage: a) the combined respiratory rate (highlighted in black) is lower than 0.15 Hz, so respiration is inside the LF band and therefore this subject will be discarded of the analysis; b) the combined respiratory rate (highlighted in black) is higher than 0.15 Hz, so respiration is within the HF band (whose limits are marked in red) and therefore this subject will be analyzed.

Table 2.3 presents the mean and SD for the eight parameters extracted from the ECG and PPG signals in every stage, together with the p-value (T-TEST) and the correlation (CORR) of each parameter extracted from the ECG and PPG signals. Figure 2.12 shows one boxplot for each parameter to highlight the similarity between the ECG and PPG parameters and to follow the trend of each one during the various stages. In these boxplots, a paired statistical test was carried out comparing the

different stages in pairs, with different numbers of subjects involved in the comparison depending on the stages analysed: 15 subjects for S5 vs. S3D, S1A vs. S3D and S1A vs. S5; 18 for S1A vs. S3A; and 14 for the remaining comparisons.

Table 2.3: Mean $\pm$ sd for time and frequency domain parameters in each stage extracted from ECG and PPG signals, along with p-value and correlation for each parameter extracted from the ECG and PPG signals.

Stage	Parameters	$\overline{NN}(s)$	$\overline{IQR}(s)$	$\overline{RMSSD}(s)$	$\overline{pNN}50(\%)$	$\overline{P_{LF}}(a.u.)$	$\overline{P_{HF}}(a.u.)$	$\overline{P_{LFn}}(n.u.)$	$\overline{R_{LF/HF}}(n.u.)$
	ECG	0.92 ± 0.14	0.08 ± 0.03	0.92 ± 0.14	11.96 ± 10.02	2.90 ± 1.56	1.44 ± 0.98	0.67 ± 0.12	2.67 ± 1.78
S1D	PPG	0.92 ± 0.15	0.09 ± 0.03	0.93 ± 0.13	13.58 ± 10.21	2.88 ± 1.46	1.58 ± 1.03	0.66 ± 0.13	2.49 ± 1.75
	T-TEST	0.99	0.77	0.86	0.64	0.98	0.69	0.54	0.78
	CORR	0.99	0.99	0.94	0.99	0.96	0.98	0.89	0.90
	ECG	0.99 ± 0.18	0.11 ± 0.05	1.01 ± 0.18	16.58 ± 11.99	3.53 ± 2.42	1.37 ± 0.81	0.66 ± 0.18	3.31 ± 2.58
S3D	PPG	0.99 ± 0.18	0.12 ± 0.05	0.99 ± 0.17	19.21 ± 11.74	3.79 ± 2.63	1.60 ± 0.87	0.65 ± 0.17	2.76 ± 1.71
	T-TEST	0.97	0.60	0.78	0.52	0.79	0.48	0.90	0.49
	CORR	0.99	0.99	0.99	0.96	0.99	0.87	0.96	0.88
	ECG	1.00 ± 0.17	0.13 ± 0.08	1.01 ± 0.16	21.99 ± 13.75	3.77 ± 3.09	2.44 ± 2.30	0.60 ± 0.18	2.26 ± 2.04
S5	PPG	0.99 ± 0.17	0.15 ± 0.08	0.99 ± 0.17	24.43 ± 13.03	3.84 ± 3.30	2.71 ± 2.45	0.58 ± 0.18	2.05 ± 1.69
	T-TEST	0.99	0.55	0.74	0.65	0.95	0.75	0.77	0.76
	CORR	0.99	0.88	0.98	0.98	0.99	0.99	0.99	0.98
	ECG	1.06 ± 0.19	0.11 ± 0.06	1.06 ± 0.19	18.74 ± 11.84	2.38 ± 2.01	1.37 ± 0.96	0.59 ± 0.15	1.98 ± 1.52
S3A	PPG	1.05 ± 0.19	0.12 ± 0.05	1.05 ± 0.18	21.43 ± 11.58	2.34 ± 1.98	1.57 ± 1.04	0.57 ± 0.14	1.60 ± 0.84
	T-TEST	0.97	0.75	0.90	0.47	0.90	0.60	0.55	0.40
	CORR	0.99	0.99	0.99	0.98	0.97	0.98	0.92	0.87
	ECG	1.07 ± 0.19	0.13 ± 0.07	1.08 ± 0.20	19.38 ± 11.07	2.42 ± 2.08	1.64 ± 1.34	0.58 ± 0.18	2.04 ± 1.55
S1A	PPG	1.07 ± 0.19	0.14 ± 0.09	1.07 ± 0.18	20.92 ± 10.51	2.64 ± 2.31	1.68 ± 1.27	0.58 ± 0.18	2.03 ± 1.48
	T-TEST	0.96	0.58	0.87	0.65	0.75	0.98	0.99	0.99
	CORR	0.99	0.88	0.95	0.97	0.96	0.98	0.94	0.94

The similarity between HRV and PRV is demonstrated by the correlation between the signals and the parameters extracted from them. The median value for the correlation between the modulating signals from the ECG and PPG is higher than 95% for all stages. Moreover, the time and frequency domain parameters extracted from them are also essentially identical: both distributions are similar (p>0.05) for all the parameters during all stages and the correlation is higher than 90% in almost all cases (see Table 2.3).

About the evolution between stages of time domain parameters, NN and $RMSSD$ increased their value during the entire test, whereas IQR and $pNN50$ had their maximum at stage S5, when the highest pressure was reached. It must be highlighted that the evolution of these parameters was the same, no matter if ECG or PPG signal was used. For the four time domain parameters, all stages were significantly different when compared to the first one. The last two stages (S3A and S1A) also presented statistically significant differences with the previous two stages (S3D and S5) for
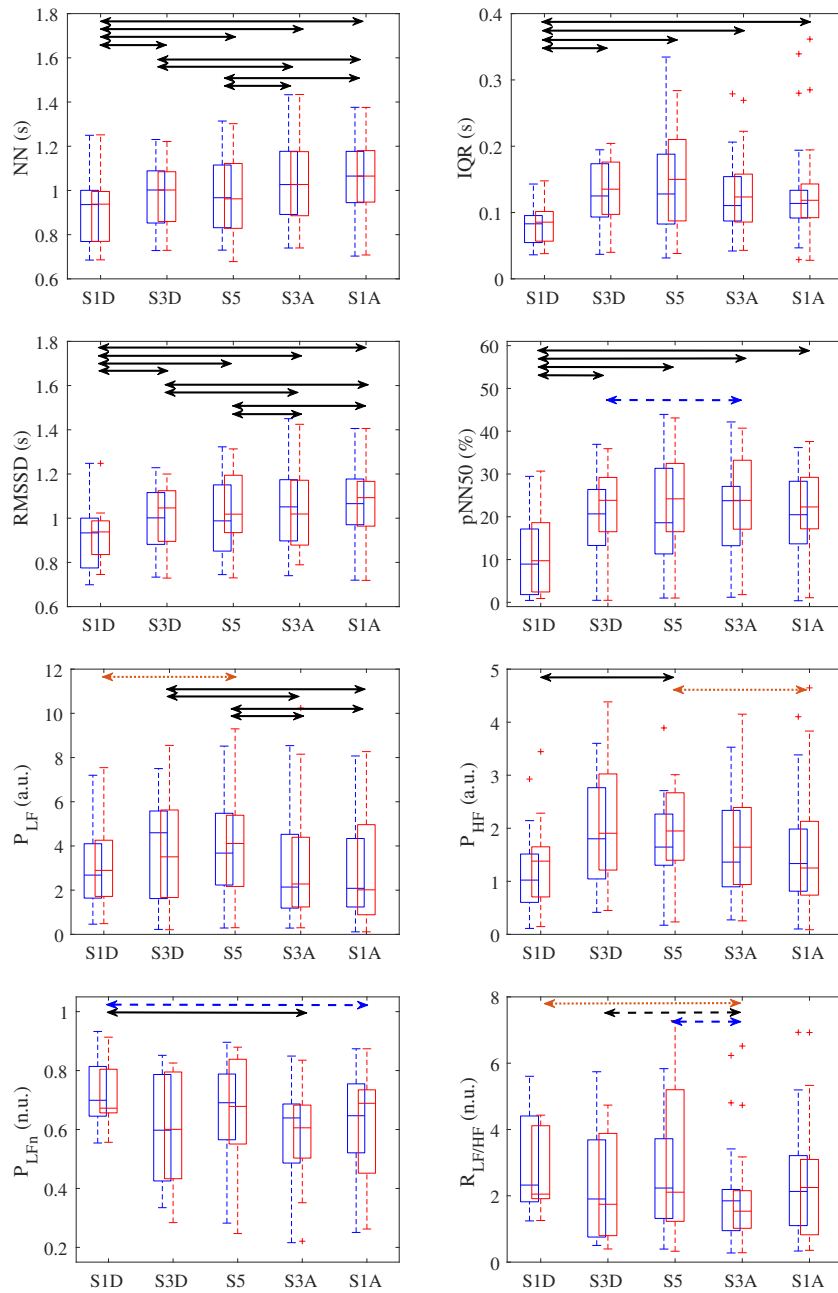
Figure 2.12: Boxplots of the ECG (in blue) and PPG (in red) parameters. Significant differences between stages are represented by an arrow joining the two stages analysed: black arrow if differences are found in both ECG and PPG; blue dashed arrow when differences are only in ECG; red dotted arrow when only in PPG.

NN and $RMSSD$. However, $pNN50$ had a different distribution, with significant differences being found for S5 vs. S3D and S3A vs. S3D.

With regard to the frequency domain parameters, P_{HF} exhibited the main difference, being slightly higher in the PPG signal than in the ECG signal, thus affecting the normalised power and the ratio. About the trend of each frequency domain parameter, P_{LF} and P_{HF} increased during the descent, reaching their maximum at the deepest stage S5 and then decreasing in value during the ascent. Significant differences were found in P_{LF} when comparing S3A and S1A with S3D and S5, and S5 was significantly different from S1D, but only when P_{LF} was extracted from the PPG signal. P_{HF} was significantly higher in S5 than S1D, and S1A exhibited a significant difference with respect to S5, but only with the PPG signal. In general terms, P_{LFn} and $R_{LF/HF}$ were higher during the initial stages and their values decreased continuously in the latter stages. Significant differences were found for S5 vs. S1D, S3A vs. S1D and S3A vs. S3D in both markers of sympathetic dominance.

2.4.3   Oxygen saturation

The mean of the SpO_2 was computed for each subject in each stage. Table 2.4 shows the inter-subject mean of SpO_2 for each stage. As can be seen, oxygen saturation remained stable during all the stages.

Table 2.4: Mean $\pm$ sd for the percentage of oxygen saturation during each stage.

Stages	S1D	S3D	S5	S3A	S1A
$\overline{SpO_2}(\%)$	96.16 $\pm$ 0.10	96.12 $\pm$ 0.08	96.15 $\pm$ 0.08	96.13 $\pm$ 0.06	96.18 $\pm$ 0.09

2.5   Discussion

ECG and PPG signals have been recorded for subjects inside a hyperbaric chamber when the atmospheric pressure varies, subsequently analysing the five stages proposed. The main goal of this Chapter is to corroborate if PPG signal provides the

same information in terms of ANS response than ECG signal, because PPG could be a more suitable signal in these environments, since PPG device is easier to locate and PPG could estimate some parameters, as the oxygen saturation, than ECG could not. To that end, an analysis of HRV and PRV time and frequency domain parameters is performed and the correlation among them is studied. Also a characterization of how the ANS reacts to pressure changes and the time spent in the hyperbaric environment is done with these parameters, taking into account the respiratory information extracted from the ECG and PPG signals in order to complete the study of the ANS response.

The main limitation of this work is the lack of a respiratory rate reference. To minimize this problem, two validated algorithms were implemented to extract respiratory information from the ECG and PPG signals in order to guide the HRV and PRV analysis. If these techniques provided similar results, respiration was assumed to have been correctly measured. This similarity criterion among the two estimations was impose in order to maximize the robustness of the estimation by merging the respiratory information from both signals and attempt to minimise the limitation resulting from this lack of respiratory reference. It must be noted that the two algorithms used [67, 73] were tested with respect to a reference device and the good results obtained validate their use for estimating respiratory rates. In addition, the possibility of both algorithms providing the same wrong result at the same time is considered highly unlikely in this work as they are based on different physiological principles. The threshold of the similarity criterion is based on the margin of error reported for the EDR [67] and PDR [73] methods. In the worst case, the error has an SD of approximately 0.025 Hz, therefore this value was doubled (0.05 Hz) to provide the threshold of likeness. In addition, the similarity must be maintained for at least 1 min of each 4 min stage (25%) in order to correctly characterize the respiratory rate of the entire stage. The peakness criteria and thresholds were strictly imposed because in this Chapter, more importance was given to having a clear respiratory component than to having more time during which the respiratory rate can be estimated. However, the parameters and algorithms could be modified depending on the final application, so for future applications in which only one signal is available this respiratory rate estimation could change, modifying the peakness criteria and

thresholds in order to be less restrictive and be able to estimate the respiratory rate over a longer period of time even though the respiratory information may be less clear.

Talking about the results of the respiratory rate inside the hyperbaric chamber, the general trend is an increase in the respiratory rate as the pressure increases, with a lower value at 1 atm than at 3 atm and a maximum for 5 atm. The fact that almost the same result was obtained for S5 and S3A can be explained by considering that these two stages are very close in time and therefore there may not have been enough time to recover for the high pressure effects. These similar measurements explain the fact that differences in the complete dataset are significant when comparing S5 and S3A with respect to S1D. No statistically significant differences between stages were found when considering the percentage of time than EDR and PDR estimations match (P_T). However, an increase in the mismatch between the two respiratory rates when the pressure increased could be distinguished. One possible explanation for this pattern may be a change in the PPG waveform morphology as a result of the pressure variations. This change may lead to differences in the PDR signals, which could affect the respiratory rate estimation. Another possible explanation for the mismatch between respiratory rates, especially when high pressures were reached, could be that respiratory modulation in the ECG and PPG does not behave the same in all cases. As it was shown in [87], respiratory modulation can be affected by different factors and varies between subjects, so it is possible that pressure changes modify the respiratory modulation, at least in some subjects. While respiratory rate estimation based on the ECG exploits the morphological changes in QRS complexes provoked by the movement of the electrodes with respect to the heart, and by the impedance changes in the thorax, respiratory rate estimation based on the PPG exploits ANS control over the cardiovascular system and intrathoracic pressure changes, so if one of these factors is altered by the pressure, respiratory modulation could be affected. This, together with the high variability between subjects, means that respiratory information is sometimes very clear in the modulating signals whereas sometimes it is not, thus increasing the results variability. Furthermore, as the peakness criteria in this work are very strict, if the respiratory component is not very clear, the algorithm uses the previous estimated respiratory rate and does not update it. If this behaviour

is repeated for a long period of time with ECG or PPG signals, and new estimations are calculated in the other one, it is possible that the final results do not match, thereby increasing the time during which the two estimations do not match and its variability.

The respiratory rate was used to complement the ANS information extracted from the HRV and PRV analysis, discarding those subjects with a respiratory rate lower than 0.15 Hz to avoid misinterpretations of the ANS response [75, 77, 78]. The first interesting point arising from our observations is that the ECG and PPG signals provide the same information. A similar behaviour has been reported previously [4, 5, 6, 7], although there are no studies of the ECG and PPG at different atmospheric pressures. The results provided by ECG and PPG are very similar, as can be seen from Table 2.3 and Figure 2.12, being all the p-values comparing ECG and PPG parameters higher than 0.05 and the correlation between parameters extracted from the ECG and PPG higher than 90% in almost all stages. There is only one difference between ECG and PPG parameters, that is a slightly increase in the P_{HF} when it is measured from the PPG signal. This behaviour has been reported previously in the literature [8] and could appear since respiration is differently represented in PRV than in HRV due to the PTT, that is the time the pulse wave takes to travel from the heart to the finger. Despite this minor difference, results from statistical test and correlation among ECG and PPG signals show that they provide the same information irrespective of atmospheric pressure.

Another interesting point from this Chapter is the study of the ANS response inside the hyperbaric chamber. It must be noticed than the variation of each parameter during the stages has the same behaviour when they are extracted from the ECG and from the PPG. The time domain parameters (NN, IQR, $RMSSD$ and $pNN50$) increase significantly their value with respect to the first stage, as shown in Figure 2.12. Despite this common behaviour, two different trends are observed: the increase in NN and $RMSSD$ values occurs during the entire test when comparing each stage with the previous one, whereas the increase in IQR and $pNN50$ ends at the deepest stage (S5). An increase in NN (and therefore a decrease in heart rate) related to the time spent in a hyperbaric environment has been reported previously [15, 17, 18]. This bradycardia could arise due to the fact that the increased

ambient pressure balances the systemic circulation, and shifts the blood from the lower part of body to the central circulation, contributing to a reduction of the heart rate [19] and by the presence of gases inside the body, since their partial pressure increases with the ambient pressure and this increased density of gases brings to reduced heart rate [2]. The behaviour observed for IQR and $pNN50$ could suggest that the vital signs of the subjects are more unstable at greater depths as these two parameters mostly reflect the stability of the signal. However, the IQR and $pNN50$ values in S3A and S1A are higher than in S3D and S1D, respectively, thus suggesting some degree of modification due to the time spent in the hyperbaric environment, as the significant differences between S5 and S3A vs. S3D suggest. Note that, although not statistically significant differences exist, some parameters change in opposite direction along hyperbaric variation trend. For instance, IQR decreases from S5 to S3A but increases from S3A to S1A. This behaviour could be due to the long period of time spent in the decompression stops (44 min in almost all the subjects), but future studies are needed to corroborate this.

Each frequency domain parameter is evaluated individually. P_{LF} increased to a maximum for the deepest stage (S5), and then decreased quickly, reaching a minimum value for stages S3A and S1A. Significant differences were found for S3A and S1A with respect to S3D and S5 because of this rapid decrease. A similar increase in LF power at higher atmospheric pressures has been reported in [1], but with no significant differences. The physiological interpretation of this parameter by itself is complicated as P_{LF} registers both sympathetic and parasympathetic responses, therefore no clear interpretation of this parameter is possible. As mentioned above, a difference was observed between the ECG and PPG signals in P_{HF}, although this had no effect on the statistical analysis. P_{HF} increases until the highest pressure is reached, as seen in previous studies [1, 15, 16, 17]. Significant differences were only found in the deepest stage with respect to the initial stage (S5 vs. S1D) and in the final stage with respect to the deepest one (S1A vs. S5) for the PRV signal, thus reinforcing this pattern. A possible reason for this increase in P_{HF} could be the rise in peripheral vascular resistance that may occur in hyperbaric environments, which would cause a higher blood pressure leading to a baroreflex system reaction and so, an observation of an increase of the parasympathetic tone [2, 19]. A detailed study

of the baroreflex system inside hyperbaric environments should be needed to confirm this hypothesis. The sympathetic indices (P_{LFn} and $R_{LF/HF}$) reach their maximum values in the first two stages (S1D and S3D) and then decrease, reaching a minimum in the final two stages (S3A and S1A). The decrease of these parameters in the final stages when a considerable time is spent inside the chamber has been corroborated in other studies [15, 16, 17]. The statistical differences in P_{LFn} found for S5 and S3A vs. S1D, and for S3A vs. S3D, supports this theory. To sum up the contribution of the frequency parameters, it should be noted that while the behaviour of the sympathetic components (P_{LFn} and $R_{LF/HF}$) varies with the time spent inside the hyperbaric chamber, the parasympathetic component (P_{HF}) varies with changes in atmospheric pressure, which is one of the novel findings of this study. However, since P_{LF} registers the influence of both sympathetic and parasympathetic components, P_{LF} behaviour does not show any clear pressure or time dependency.

Finally, oxygen saturation remains stable during all stages due to the ventilation system of the hyperbaric chamber, which maintains a steady gas concentration. The possibility of being able to measure SpO_2 is very interesting, especially when subjects are exposed to compressed air, as in real diving. The percentage of oxygen in the body will allow hyperoxia to be identified and controlled, thus meaning that decompression stops can be performed based on this concentration instead of the time established in the tables. Therefore, use of the PPG signal in real diving would appear to be very useful, although further studies are required to analyse all the possibilities that this signal can provide in terms of subject analysis.

2.6   Conclusion

It has been shown that the PRV signal provides a surrogate measurement of HRV in hyperbaric environments since correlation and statistical analysis from ECG and PPG signals show the similarity among both measures. Respiratory rate extracted from both signals provides a similar estimation in most of the subjects, allowing to include respiratory information in the ANS response. These two points, together with the fact that PPG signal provides very useful additional information such as the oxygen saturation, that ECG does not, makes PPG signal a suitable tool for measure

ANS response in hyperbaric environments. About the parameters variation inside the chamber, it has been shown that respiratory rate and P_{HF}, which is related with the parasympathetic activity, increase in those stages when the atmospheric pressure is high, and the heart rate and the sympathetic markers (P_{LFn} and $R_{LF/HF}$) decreases as more time is spent inside the chamber.

Chapter 3

Deriving Respiratory Rate from PPG signal

3.1   Introduction

As it was pointed out in Section 1.4.3, respiration plays an important role in hyperbaric environments, since it is necessary to breath slowly and deeply to maintain a low air consumption and avoid an increase in the respiratory effort that could cause fatigue. Besides, it is important to include respiratory information in the HRV/PRV analysis, since it has been shown that changes in the respiratory pattern alter the spectral content [75] and, consequently, the interpretation of sympathetic or vagal activations [76, 77, 78].

In Chapter 2, respiratory rate was obtained combining ECG and PPG because of the lack of a respiratory rate device. Now, if only PPG wants to be used, since in the previous Chapter it was concluded than PRV can be considered as a surrogate measurement of HRV in hyperbaric environments, a comparison among the PPG respiratory rate estimation and a respiratory rate reference is needed in order to study how reliable is this PPG estimation by itself. Therefore, this Chapter is focused in respiratory rate estimation from PPG signal. Some works have developed algorithms to estimate respiratory rate from PPG signal directly, as in [68, 69, 70, 71, 72]. Other works prefer to develop their algorithms over PDR signals, which contain information about the respiratory modulation, as in [59, 60, 63, 64, 65,

73, 74, 89]. Respiratory rate can be estimated over one of this PDR signals [63, 64, 89] or over an ensemble of them [60, 65, 73, 74], through the application of several algorithms as autoregressive decomposition [69, 90], fusion of fast Fourier transforms [60, 71], wavelet transform methods [65, 70], time-frequency maps [68] or peak-averaged combination of power spectra estimation [73]. This last method is the one chosen to estimate the respiratory rate in this Chapter.

The location of the PPG sensor has their importance in respiratory rate estimation, since morphological changes in PPG have been observed due to the body location where PPG is registered [38, 39]. Most of the cited works have the PPG recorded in the finger, but in some of them this signal was registered in the forearm [63, 64], in the earlobe [89] or in the forehead [74]. Few works in the bibliography have compared respiratory rate estimation extracted from different PPG locations and there is not an agreement between them: while some studies suggest than finger and forehead are good places to locate the PPG sensor [38, 91], other work indicates than only the finger is a good location [92] and another one even proposes the forearm as the best place [93].

Therefore, in this Chapter, PPG signal is recorded from finger and forehead and 4 PDR signals are extracted from each location: PRV, PAV, PWV and RIIV. Respiratory rate for these PDR signals (and all the possible combinations of them) is estimated and the success rate, the relative error and a confusion matrix are computed to evaluate how the location of the PPG sensor affects to the respiratory rate estimation. The power distribution of respiratory information and some morphological parameters of both PPG signals are studied too to complete the analysis.

3.2 Materials

Thirty-five subjects (18 males and 17 females) with a mean age of 35.1 ± 6.5 years conformed the whole dataset. During the whole test subjects remained comfortably seated during approximately half an hour. The protocol consisted of 7 different stages with a duration of 3 minutes each one: first, subjects were registered during spontaneous breathing; then a different respiratory rate was imposed in each of the remaining six stages, starting at 0.6 Hz and ending at 0.1 Hz in steps of 0.1 Hz.

A schematic representation of this protocol is shown in Table 3.1. This controlled breathing was given by a sinusoidal wave that the subjects had to follow, marking the moment of inhale and exhale.

Table 3.1: Explanation of the protocol, with the fixed respiratory rate of each stage and its duration.

Respiratory rate	Spontaneous (Spt)	0.6 Hz	0.5 Hz	0.4 Hz	0.3 Hz	0.2 Hz	0.1 Hz
Duration	3 min	3 min	3 min	3 min	3 min	3 min	3 min

Finger and forehead PPG signals were recorded simultaneously as well as a chest-band respiratory signal. These signals were registered with the Medicom System, ABP-10 module (Medicom MTD, Ltd, Russia), a device specifically created to acquire raw biomedical signals without any preprocessing. The sample frequency was $f_s = 250$ Hz. Only the last 2 minutes of each stage were used to extract the features of the wave morphology and the respiratory information from the PPG signals. Results of respiratory chest-band signal obtained the same respiratory rate imposed by the guided sinusoidal wave, so it was used as the reference to compare the respiratory rate estimated from finger and forehead PPG signals.

3.3 Methods

3.3.1 PDR signals

Preprocessing of finger and forehead PPG signals was very similar than the one described in Section 2.3.1. First of all, a band-pass filter (cut-off frequencies of 0.3 - 35 Hz) was applied to both PPG signals (x_{PPG}) in order to avoid baseline noise and possible interference [94]. Then, artefacts in the PPG signal pulses were suppressed using the detector described in [83]. Finally, the apex, n_{Ai}, the basal, n_{Bi}, and the medium, n_{Mi}, points of PPG pulses were automatically detected using an algorithm based on a low-pass differentiator filter [46]. The medium points were considered the fiducial points because of their robustness [47, 84], so the difference between them was used to compute the pulse-to-pulse time series (PP_i). Onset, n_{Oi}, and end, n_{Ei},

points of the pulses were detected as described in [73] and detailed in Section 2.3.2. Figure 3.1 shows an example of finger and forehead PPG signals with their most representative points highlighted.
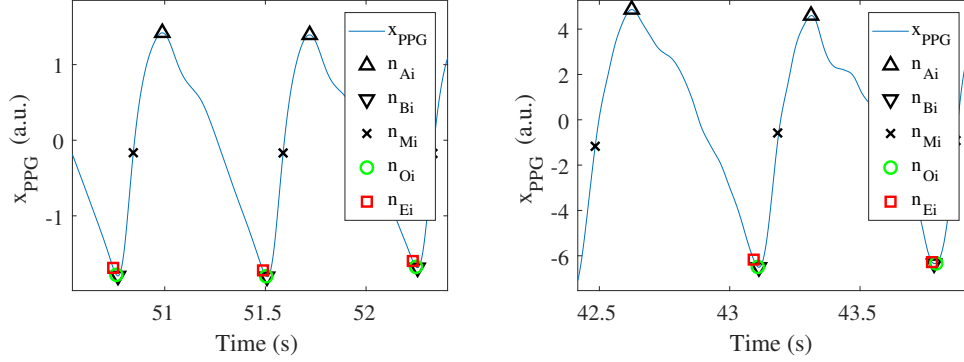
Figure 3.1: Two pulse waves of PPG signal recorded in the finger (left) and in the forehead (right), with their most representative points highlighted.

Finally, 4 unevenly sampled (superscript u) PDR signals were obtained, assuming that their variations were due to a modulation based on respiratory information.

- Pulse Rate Variability: it represents the time difference between two adjacent medium points [30, 59, 60, 73, 74]:

$$d_{PRV}^u(n) = \sum_i f_s \cdot \left[\frac{1}{(n_{Mi} - n_{Mi-1})} \right] \cdot \delta(n - n_{Mi}). \qquad (3.1)$$

- Pulse Amplitude Variability: it reflects the amplitude variation between the apex and the basal points [60, 65, 73, 74]:

$$d_{PAV}^u(n) = \sum_i \left[x_{PPG}(n_{Ai}) - x_{PPG}(n_{Bi}) \right] \cdot \delta(n - n_{Mi}). \qquad (3.2)$$

- Pulse Width Variability: it reflects the width variation of the pulses [73]:

$$d_{PWV}^u(n) = \sum_i \frac{1}{f_s} \cdot (n_{Ei} - n_{Oi}) \cdot \delta(n - n_{Mi}). \qquad (3.3)$$

- Respiratory-Induced Intensity Variability: it represents the intensity variations produced by the respiration [60, 63, 64, 65]. This signal was estimated from n_{Bi} points before the initial band-pass filter was applied.

$$d_{RIIV}^u(n) = \sum_i \mathrm{x}_{\mathrm{PPG}}(n_{Bi}) \cdot \delta(n - n_{Mi}). \tag{3.4}$$

Due to the presence of some outliers in these signals, a median-absolute-deviation-based outlier rejection rule was applied together with a resampling by cubic splines interpolation at 4 Hz to standardize the four PDR signals: PRV, PWV, PAV and RIIV. Then, a band-pass filter (cut-off frequencies of 0.07 - 1 Hz) was applied over the PDR signals in order to limit the analysis within the frequency range where respiratory information was [73]. An example of the four PDR signals is shown in Figure 3.2.
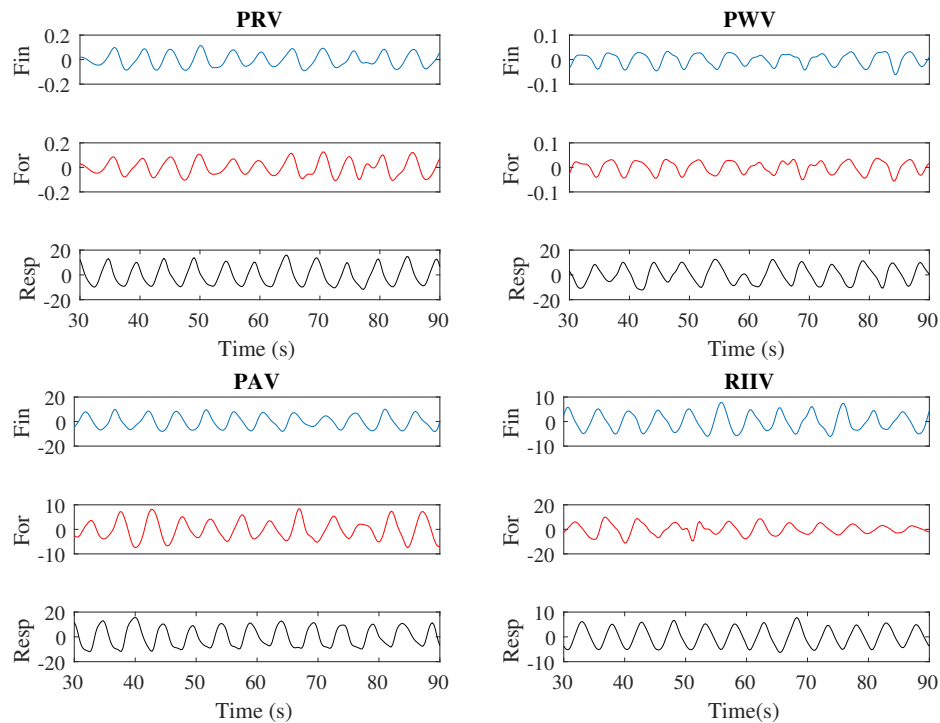
Figure 3.2: One minute representation of each PDR signal: PRV (top left), PWV (top right), PAV (bottom left) and RIIV (bottom right). PDR signals extracted in the finger (Fin) are represented in blue and in the forehead (For) are represented in red. The chest-band respiratory signal (Resp) is also represented in black.

3.3.2 Respiratory rate estimation

The same algorithm explained in Section 2.3.2 was applied to estimate the respiratory rate from both PPG signals. As a reminder, this algorithm is a fusion technique based on frequency analysis of PDR signals [73] to estimate the respiratory rate every 5 seconds from peaked-conditioned averaged spectra. Every 5 seconds, a Welch's periodogram from a 40 s length running window of each PDR signal was calculated and the biggest peak near the previous respiratory rate estimation was selected and the percentage of power around this peak with respect a reference interval was computed. If this percentage was higher than a established threshold (if the signal was peaked enough), the spectrum was promediated together to the other PDR spectra peaked enough and a peaked-conditioned average spectrum was obtained. The location of the largest peak in this average spectrum was selected as the new respiratory rate estimation (F_R). This algorithm was applied over a single PDR signal and over all the possible combinations of PDR signals.

The same method was applied over the respiratory chest-band signal in order to obtain chest-band respiratory rate estimation (F_C). This estimation was checked with the respiratory rate marked by the sinusoidal wave and all their estimations matched, thus this signal could be considered a reference of the real respiratory rate.

3.3.3 Performance measurements

A comparison among the respiratory rate estimated with the PDR signals and the reference was done every 5 seconds with an experimental margin of error of $\pm$ 0.05 Hz ($\pm$ 0.3 bpm). If the estimation matched with the reference, it was considered as a Correct Estimation (CE), while a Wrong Estimation (WE) was considered otherwise. The success rate (SR) was used as a performance measure:

$$SR = \frac{CE}{CE + WE} \cdot 100. \qquad (3.5)$$

The inter-subject mean of this percentage was calculated for every stage and for each PDR signal and all possible combination of them. Also, a confusion matrix was computed to analyse what happen when the respiratory rate was not successfully estimated. In addition, the relative error (e_r) of the respiratory rate estimation was

also calculated:

$$e_r = \frac{F_R - F_C}{F_C} \cdot 100. \tag{3.6}$$

Another interesting point of study was the power distribution for each PDR signal, specially the power associated with the respiratory information. Thus, for each stage, the power within a bandwidth of 0.1 Hz around the expected respiratory frequency (given by the respiratory chest-band) was compared with the total power in the averaged spectrum (from 0.07 to 0.65 Hz).

$$P_R(k) = \frac{\int_{f=F_C-0.05}^{f=F_C+0.05} \overline{S_k(f)} df}{\int_{f=0.07}^{f=0.65} \overline{S_k(f)} df}. \tag{3.7}$$

where $\overline{S_k(f)}$ was the peaked-conditioned averaged spectrum and k represented the time instant (every 5 seconds). This ratio aimed to quantify how much power related to the respiratory component appeared in each PDR signal in each stage, assuming than a higher relative power means more respiratory signal-to-noise ratio.

As PPG sensor location could change PPG morphology and therefore vary respiratory information in the PDR signals [39, 93], also the width and the rate were analysed for each pulse (subscript i) of the PPG signal recorded in the finger and the forehead:

- Width: reflected the pulse width of each wave.

$$PW_i = n_{Ei} - n_{Oi}. \tag{3.8}$$

- Rate: reflected the difference between adjacent medium points.

$$PR_i = \frac{1}{n_{Mi} - n_{Mi-1}}. \tag{3.9}$$

Figure 3.3 shows an example of how the rate and the width are extracted from finger and forehead PPG signals.
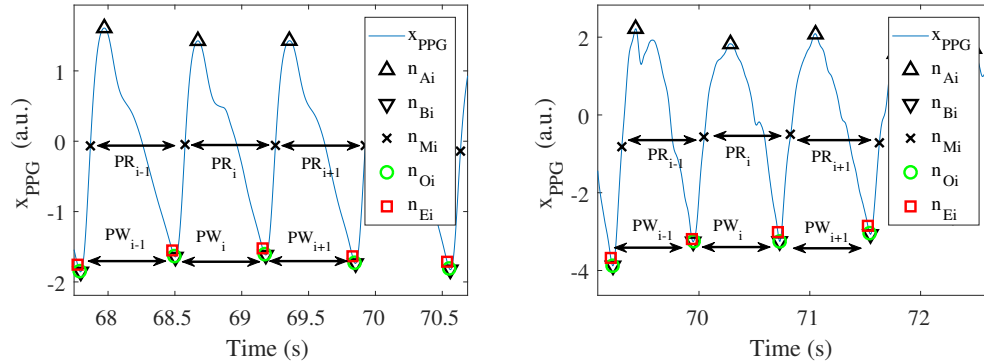
Figure 3.3: Extraction of the rate and width from finger (left) and forehead (right) PPG signals.

Finally, an statistical analysis was made to compare all these results from the PPG signal registered in the finger and the forehead. First, a Shapiro-Wilk test was applied to verify the normal distribution of the data. The t-Student test was applied if the distribution was normal, otherwise, the Wilcoxon paired test was the one applied. In both methods, p-value ≤ 0.05 defined the significance.

3.4 Results

Figure 3.4 shows an example of 8 different PDR signals spectra during the controlled breathing stage at a respiratory rate of 0.4 Hz. Each column represents one different PPG signal (finger and forehead) and each row corresponds with one different PDR signal (PRV, PWV, PAV and RIIV). It can be seen that there is a high spectral power component (yellow zone) around the expected respiratory rate (red line) in six out of eight PDR signals. In the other two, (RIIV extracted in finger and forehead), the main frequency component is located between 0.1 and 0.2 Hz and no related to respiration.

Table 3.2 shows the respiratory rate estimation success rate in each stage using a single PDR signal and with all the possible combinations of them, for both possible PPG sensor locations. Results showed a better performance of the algorithm at low respiratory rates and when the sensor was located in the finger. When only one PDR signal was used, PRV obtained the best results at lower frequencies, but when the frequency was above 0.2 Hz PAV reached the best results in finger and
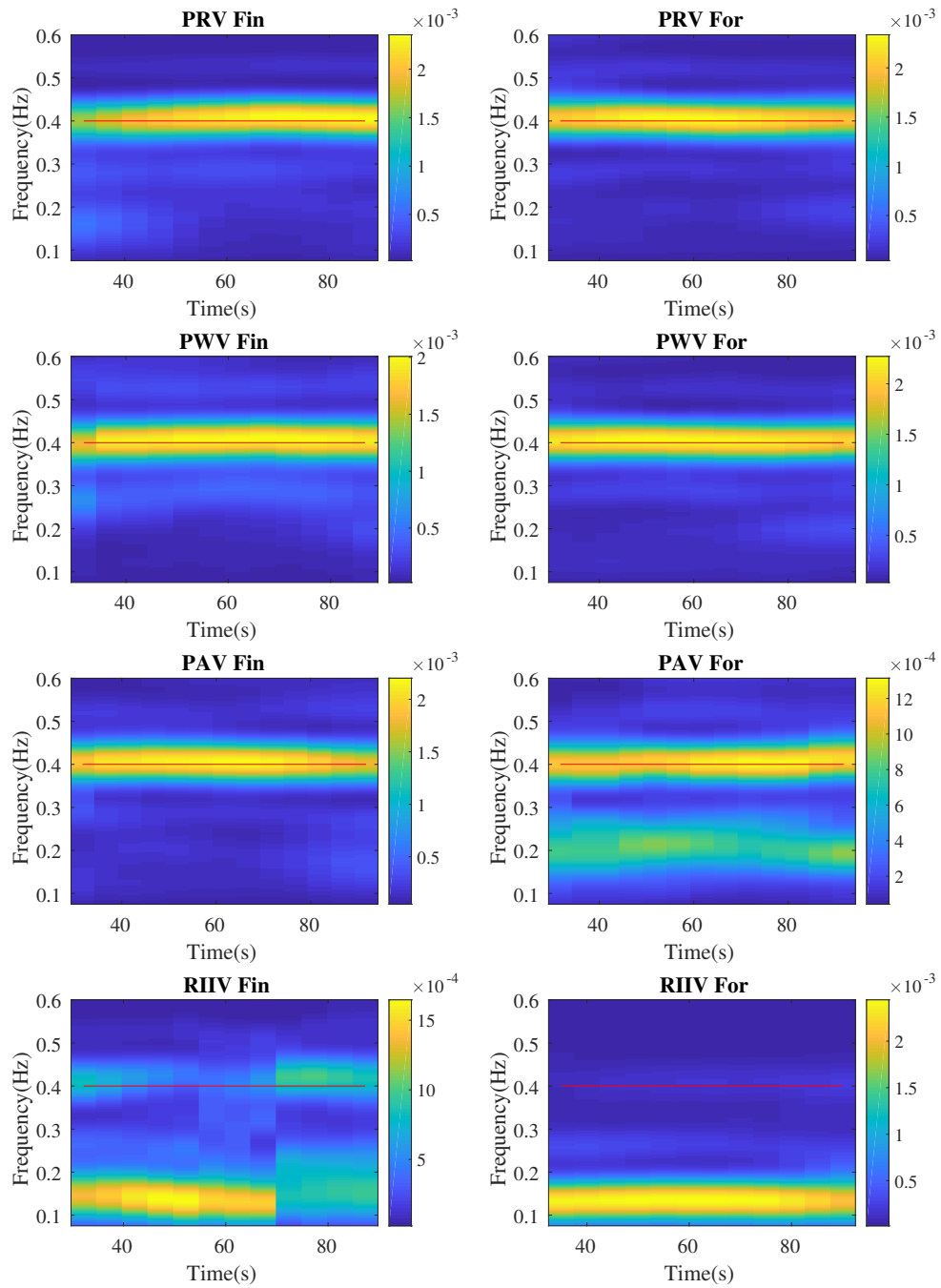
Figure 3.4: Time-frequency maps of the respiratory rate estimation using the finger (left column) and the forehead (right column) PPG signal with different PDR signals: PRV (first row); PAV (second row); PWV (third row); and RIIV (last row). Red line represents the chest-band respiratory rate estimation.

PWV in forehead. Good results were found when several signals were combined, specially with PRV-PWV, PWV-PAV and PRV-PWV-PAV. The worst results were found with RIIV signal (and all its combinations) except in 0.1 Hz stage. It must be noticed that combining PDR signals did not imply an increase in success rate.

Table 3.3 shows the relative error of each single PDR signal and with all the possible combinations of them for both possible PPG sensor locations. It must be noticed that the error was usually negative (except in 0.1 Hz stage). This indicates that the estimated respiratory rate was lower than the real respiratory rate. Results showed lower error when the sensor was located in the finger and when the respiratory rate was low. Similar to Table 3.2, the lower error was found in PAV in finger and in PWV in forehead when only one PDR signal was used. Also, combinations that showed a low error were PWV-PAV and PRV-PWV-PAV.

Due to the differences found in the respiratory rate estimation of every PDR signal, a study of the four PDR signals separately was done to analyse the causes of the differences between both locations of the PPG sensor. Table 3.4 shows 4 confusion matrix where all the estimations of each single PDR signal were compared with respect to the reference respiratory rate given by the chest band for both possible PPG sensor locations. Results show higher accuracy in lower frequencies and in finger with respect to forehead estimations. In PRV, PWV and PAV the diagonal presents the highest values (this indicates than the estimation matched with the reference) except from 0.6 Hz stage in PRV and PAV. In RIIV, in all the stages except in 0.2 Hz, the highest percentage of estimations was found in the 0.1 Hz stage in finger and in 0.1 and 0.2 Hz stages in forehead. This means that, when an error occurred, the respiratory rate estimation was 0.1 or 0.2 Hz in most of the cases. This result is in agreement with the poor success rate showed in Table 3.2 and with the large negative error in Table 3.3.

Figure 3.5 shows the mean of the relative power in each stage for finger and forehead. For the four PDR signals, $\overline{P_R}$ was higher in the finger than in the forehead and it decreased when the frequency increased. PWV is the one with less significant differences in both locations, only in 0.2 and 0.3 Hz stages.

Table 3.2: Mean ± std of the respiratory rate estimation success rate (SR) using the PDR signals separately and all the possible combinations of them, in both locations (Fin for finger and For for forehead). Best results of each stage (single, double or triple combination) are highlighted in bold. Significant differences between finger and forehead values are indicated with an * ($p < 0.01$) or with a ** ($p < 0.001$).

SR (%)	Zone	PRV	PWV	PAV	RIIV	PRV PWV	PRV PAV	PRV RIIV	PWV PAV	PWV RIIV	PAV RIIV	PRV PWV PAV	PRV PWV RIIV	PRV PAV RIIV	PWV PAV RIIV	PRV PWV PAV RIIV
Spt	Fin	70.4±38.5	69.0±40.7	**77.1**±40.3	31.2±43.5	**76.8**±36.9	68.3±40.3	37.4±43.1	68.8±39.7	36.6±42.7	36.1±42.9	**66.7**±40.9	37.9±43.5	37.4±43.6	36.6±42.9	37.4±43.6
	For	51.5±46.3*	58.4±41.8	**63.4**±42.6	33.8±42.6	57.5±45.7*	60.9±43.0	37.2±46.5	**72.5**±36.7	43.7±43.4	40.1±42.8	**59.0**±44.7	38.5±46.2	39.0±46.5	45.0±43.3	39.2±46.0
0.1	Fin	**97.4**±15.2	79.9±34.4	85.5±33.5	94.6±22.4	**97.4**±15.2	**97.4**±15.2	**97.4**±15.2	91.9±24.6	94.0±22.5	**97.4**±15.2	**97.4**±15.2	**97.4**±15.2	**97.4**±15.2	**97.4**±15.2	**97.4**±15.2
	For	**97.1**±14.1	76.2±38.6	43.6±43.4**	78.7±38.8	94.5±20.5	**97.1**±14.1	95.3±17.4	65.2±42.0*	86.8±26.3	78.4±38.9*	**97.1**±14.1	95.6±16.5	95.3±17.4	87.6±26.7*	95.6±16.5
0.2	Fin	**91.0**±25.9	90.0±26.2	86.3±30.9	56.5±45.0	89.0±28.1	90.0±26.9	64.7±44.6	**91.1**±24.4	57.5±44.7	57.1±46.5	**87.4**±30.0	63.8±43.8	62.3±45.2	56.0±45.9	61.4±44.5
	For	**77.3**±32.8	76.6±35.1	54.9±44.4	59.8±44.4	**80.1**±31.8	69.1±38.5*	59.2±44.9	70.1±39.8	65.2±41.6	59.3±43.4	**75.1**±36.0	56.0±45.7	58.9±44.6	64.3±43.0	56.0±45.7
0.3	Fin	83.1±34.2	77.7±38.0	**89.3**±24.7	30.6±44.1	81.8±37.1	82.1±35.5	43.5±45.8	**86.8**±31.4	39.7±45.0	38.2±47.1	**80.0**±37.4	46.3±45.3	44.9±46.1	41.3±45.9	45.4±45.9
	For	58.0±45.0**	**72.4**±39.5	63.3±46.7	2.9±16.9**	64.5±42.1	63.7±41.0	10.1±24.5**	**73.4**±37.9	12.4±29.3**	15.4±30.8*	**63.6**±41.7	12.6±27.5**	15.7±28.7**	18.6±33.3**	16.2±30.7**
0.4	Fin	68.3±45.8	58.7±46.9	**78.6**±39.4	30.4±45.9	58.4±48.2	**66.0**±46.4	35.9±45.2	61.2±43.8	26.0±43.3	39.0±44.5	**57.4**±47.3	29.1±44.0	38.3±44.0	28.6±42.4	28.6±42.4
	For	45.1±47.4	**60.0**±42.7	55.1±43.6	1.3±7.7**	**54.0**±46.9	44.9±46.1	2.6±13.9**	51.6±44.3	8.3±23.8*	5.3±17.2**	**44.6**±46.0	4.7±17.4	4.2±15.2**	9.6±23.4*	5.7±18.2*
0.5	Fin	57.7±49.6	51.1±47.3	**75.8**±40.7	17.4±36.5	53.9±48.8	57.4±49.1	17.4±36.5	**61.3**±45.1	17.9±36.9	21.8±38.8	**55.8**±47.6	17.7±36.8	20.3±38.5	22.1±39.5	20.0±38.6
	For	40.0±41.3	**45.2**±46.5	40.3±47.2	0.0±0.0*	37.4±44.2	**40.2**±43.7	2.9±16.9*	37.8±46.1*	0.0±0.0*	3.9±16.4*	**33.7**±42.3	1.8±10.7*	2.9±16.9*	1.6±9.2*	1.8±10.8*
0.6	Fin	36.4±47.2	45.4±48.7	**46.5**±48.0	10.1±29.4	32.2±45.9	34.0±46.3	8.6±28.4	**43.4**±46.2	8.6±28.4	8.6±28.4	**34.0**±46.3	8.6±28.4	8.6±28.4	8.6±28.4	8.6±28.4
	For	27.8±41.4	**33.5**±45.3	20.5±37.0*	0.0±0.0	**26.5**±42.7	15.3±31.3	0.8±3.4	14.5±32.0**	0.8±4.6	1.8±8.2	**17.9**±33.5	0.0±0.0	0.8±3.4	1.6±6.8	0.5±3.1

Table 3.3: Mean ± std of the percentage of the relative error (e_r) committed in the respiratory rate estimation by each PDR signal separately and with all the possible combinations of them, in both locations (Fin for finger and For for forehead). Best results of each stage (single, double or triple combination) are highlighted in bold. Significant differences between finger and forehead values are indicated with an * ($p < 0.01$) or with a ** ($p < 0.001$).

e_r (%)	Zone	PRV	PWV	PAV	RIIV	PRV PWV	PRV PAV	PRV RIIV	PWV PAV	PWV RIIV	PAV RIIV	PRV PWV PAV	PRV PWV RIIV	PRV PAV RIIV	PWV PAV RIIV	PRV PWV PAV RIIV
Spt	Fin	-17.3±22.3	**-8.2**±**27.9**	-9.3±19.1	-40.4±23.7	**-14.7**±**22.3**	-17.5±22.2	-36.8±23.5	-15.2±21.2	-36.7±23.6	-37.4±23.3	**-17.6**±**22.6**	-36.5±23.7	-36.7±23.7	-37.2±23.3	-36.7±23.7
	For	-21.8±34.0	**1.9**±**43.3**	17.0±41.4	-29.3±24.1**	-23.5±23.7	-20.0±23.7	-33.6±23.0	**2.7**±**34.9***	-24.4±23.0*	-22.7±28.7**	**-20.3**±**25.2**	-32.6±22.3	-32.7±22.0	-24.6±21.9**	-32.4±22.1
0.1	Fin	**-1.1**±**7.7**	14.8±30.1	11.3±33.6	1.3±16.8	**-1.1**±**7.7**	-1.3±7.6	-1.9±7.5	3.3±18.9	1.6±16.9	-1.5±7.7	**-1.4**±**7.6**	-1.9±7.5	-1.9±7.5	-1.5±7.7	-2.0±7.5
	For	**0.4**±**8.8**	-34.8±72.3	94.4±95.7**	19.2±27.1**	-2.3±14.7	**0.9**±**9.3**	1.6±11.3	56.5±87.3**	8.4±18.1*	19.2±27.3**	**0.8**±**9.3**	1.4±11.0	1.6±11.3	8.4±19.0**	-1.4±11.0
0.2	Fin	-4.3±11.6	-4.6±10.8	**-1.6**±**15.4**	-20.4±20.6	-5.5±12.9	-4.9±12.4	-16.9±20.6	**-4.5**±**11.4**	-20.1±20.4	-20.2±21.3	**-6.4**±**13.9**	-17.4±20.3	-18.0±21.0	-20.8±20.9	-18.5±20.6
	For	**-4.2**±**22.6**	6.3±19.8*	31.4±50.4**	-19.6±16.0	-7.4±15.5	**2.2**±**33.4**	-20.4±15.5	16.2±32.2*	-13.8±18.6	-12.7±24.4	**-4.2**±**23.4**	-17.9±22.9	-20.2±15.7	-12.9±22.7	-17.9±22.9
0.3	Fin	-9.8±20.9	-10.5±20.7	**-5.5**±**14.3**	-42.6±28.4	-10.9±22.5	-10.3±21.3	-34.4±28.7	**-7.6**±**18.4**	-36.7±28.4	-38.2±29.6	**-11.8**±**22.3**	-32.7±28.6	-33.7±29.2	-35.9±28.7	-33.4±29.0
	For	-18.3±28.6	**-7.3**±**21.3**	-10.8±25.5	-49.1±11.2	-14.3±28.2	-18.6±23.0	-46.7±16.5*	**-12.6**±**20.2**	-44.6±17.0	-41.7±18.0	**-19.5**±**23.7**	-46.5±16.3*	-44.5±17.3	-41.0±18.9	-44.7±18.4
0.4	Fin	-22.6±32.7	-24.1±28.7	**-15.4**±**28.2**	-50.2±33.5	-27.9±33.3	**-24.2**±**33.5**	-45.2±32.8	-24.9±30.1	-51.4±31.4	-43.0±32.8	**-29.2**±**33.7**	-49.4±31.8	-43.7±32.5	-49.8±31.0	-49.7±30.9
	For	-34.6±32.1	**-17.3**±**20.7**	-22.3±27.4	-62.7±7.3	-28.6±30.7	-32.2±28.9	-61.5±10.5*	-24.4±25.7	-57.3±15.7	-58.7±14.0*	**-32.4**±**28.3**	-60.4±12.4	-60.4±11.6*	-56.1±16.7	-59.5±13.3
0.5	Fin	-30.6±37.1	-29.9±31.7	**-16.4**±**29.5**	63.9±28.7	-34.1±37.1	-31.3±37.0	-64.0±28.6	-25.0±31.1	-61.9±29.4	-59.7±30.8	**-31.5**±**35.5**	-63.4±28.8	-61.4±30.3	-58.8±31.0	-61.5±30.3
	For	-35.5±31.5	**-30.7**±**29.8**	-31.0±27.5*	-70.3±4.4	-37.3±31.8	-35.3±30.3	-69.1±12.8	-34.4±29.4	-69.7±5.2	-65.6±14.0	**-39.1**±**29.6**	-68.9±9.5	-67.9±13.1	-67.7±10.1	-68.5±9.7
0.6	Fin	-44.3±36.1	-36.6±34.8	**-28.6**±**31.7**	-70.7±25.8	-51.1±37.3	-43.9±35.7	-72.4±23.7	-37.4±34.7	-71.8±24.0	-72.1±23.9	**-49.6**±**37.2**	-72.8±23.6	-72.3±23.8	-72.5±23.8	-72.5±23.9
	For	-45.1±33.5	**-40.1**±**31.9**	-45.7±28.5*	-75.2±4.1	-47.9±33.0	-55.0±26.6	-74.0±8.9	-54.4±25.8*	-73.7±9.6	-72.4±9.9	**-54.9**±**27.7**	-74.3±7.9	-72.6±12.2	-72.3±11.0	-74.1±8.2

Table 3.4: Confusion matrix by each PDR signal comparing each respiratory rate estimation (vertical axis) with the reference given by the chest band (horizontal axis), in both locations (Fin for finger and For for forehead). Best results of each stage are highlighted in bold.

PRV	Zone	Spt	0.1	0.2	0.3	0.4	0.5	0.6	PWV	Zone	Spt	0.1	0.2	0.3	0.4	0.5	0.6
Spt	Fin	**267**	0	0	0	0	0	0	Spt	Fin	**262**	0	0	0	0	0	0
	For	**196**	0	0	0	0	0	0		For	**221**	0	0	0	0	0	0
0.1	Fin	91	**371**	34	55	119	144	**177**	0.1	Fin	75	**305**	34	48	90	88	98
	For	152	**377**	65	114	150	125	**147**		For	55	**301**	27	41	44	72	101
0.2	Fin	18	0	**348**	8	0	5	11	0.2	Fin	17	66	**346**	30	34	45	56
	For	12	2	**292**	19	18	24	32		For	45	32	**289**	40	18	41	51
0.3	Fin	1	0	0	**317**	2	4	16	0.3	Fin	21	0	2	**298**	30	36	20
	For	1	0	9	**220**	30	22	13		For	38	36	42	**276**	86	63	35
0.4	Fin	2	0	0	0	**259**	8	11	0.4	Fin	4	0	0	4	**226**	18	29
	For	14	0	9	24	**174**	49	39		For	2	6	18	21	**224**	26	23
0.5	Fin	0	0	0	0	0	**220**	26	0.5	Fin	0	0	0	0	0	**194**	3
	For	2	0	1	3	0	**152**	39		For	5	4	0	2	0	**172**	38
0.6	Fin	0	0	0	0	0	0	140	0.6	Fin	0	0	0	0	0	0	**175**
	For	0	0	0	0	0	2	107		For	11	0	0	0	0	0	**129**

PAV	Zone	Spt	0.1	0.2	0.3	0.4	0.5	0.6	RIIV	Zone	Spt	0.1	0.2	0.3	0.4	0.5	0.6
Spt	Fin	**291**	0	0	0	0	0	0	Spt	Fin	117	0	0	0	0	0	0
	For	**243**	0	0	0	0	0	0		For	130	0	0	0	0	0	0
0.1	Fin	84	**326**	40	30	79	74	92	0.1	Fin	**255**	**361**	166	**254**	**264**	**310**	**320**
	For	5	**169**	19	45	65	34	63		For	**162**	**298**	145	198	203	192	203
0.2	Fin	0	38	**330**	11	0	0	7	0.2	Fin	17	10	**216**	10	1	2	0
	For	35	89	**208**	64	64	100	**119**		For	79	81	**229**	171	163	182	172
0.3	Fin	2	7	2	**339**	3	0	24	0.3	Fin	0	0	0	116	1	0	13
	For	26	41	42	**240**	22	47	30		For	6	0	0	11	1	0	1
0.4	Fin	2	0	10	0	**298**	17	18	0.4	Fin	0	0	0	0	114	2	7
	For	60	76	83	27	**214**	45	48		For	0	0	2	0	5	0	0
0.5	Fin	0	0	0	0	0	**290**	60	0.5	Fin	0	0	0	0	0	67	1
	For	6	4	22	4	7	**148**	39		For	0	0	0	0	0	0	1
0.6	Fin	0	0	0	0	0	0	**180**	0.6	Fin	0	0	0	0	0	0	40
	For	2	0	2	0	0	0	78		For	0	0	0	0	0	0	0

Not only differences in the power distribution, but also morphological differences between the two PPG signals extracted in the finger and the forehead have been found. Figure 3.6 shows the width and rate of the PPG signal in both locations. The width was higher in the forehead than in the finger but the rate remained nearly equal for both signals.
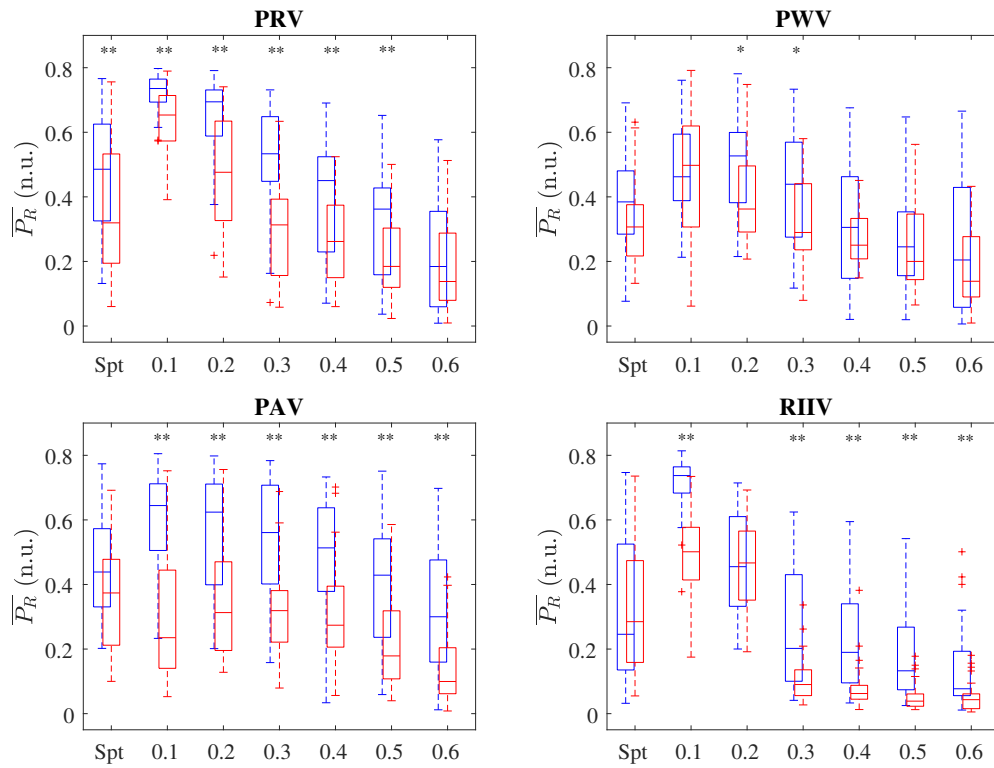
Figure 3.5: Boxplots of $\overline{P_R}$ from finger (blue) and forehead (red) PPG using PRV (top left), PWV (top right), PAV (bottom left) and RIIV (bottom right). Significant differences between finger and forehead values are indicated with an $*$ ($p < 0.01$) or with a $**$ ($p < 0.001$).
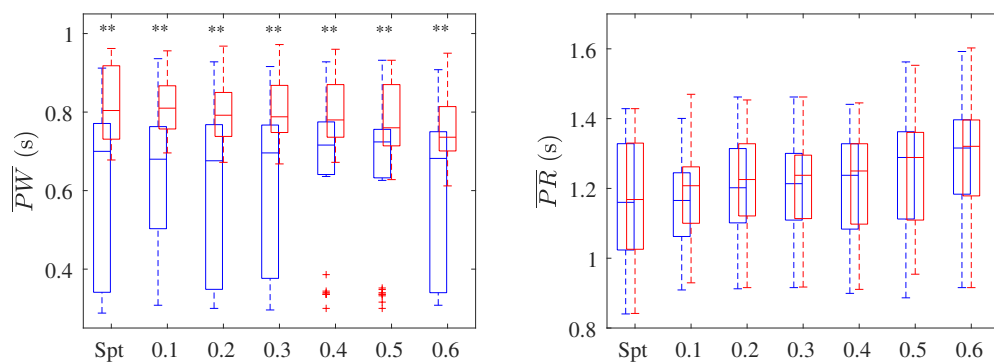

Figure 3.6: Boxplots of the morphological parameters extracted from PPG signals recorded in the finger (blue) and the forehead (red). Significant differences between finger and forehead values are indicated with an $*$ ($p < 0.01$) or with a $**$ ($p < 0.001$).

3.5 Discussion

In this Chapter, an evaluation of how the location of the PPG sensor affects the respiratory rate estimation and which PDR signals are more appropriated to this purpose is performed. PPG signals have been recorded in finger and forehead from subjects breathing spontaneously and at different controlled respiratory rates. 4 PDR signals (PRV, PWV, PAV and RIIV) have been extracted to both locations of the PPG signals, obtaining one respiratory rate estimation per PDR signal. In addition, respiratory rate have been also estimated from all the possible combinations of these 4 PDR signals. The estimations have been compared with the respiratory rate estimated from chest-band, which was taken as reference. The respiratory estimation has been considered accurate if it differs less than 0.05 Hz (0.3 bpm) from the reference, based on the errors reported in previous works [73]. The success rate and the relative error of the estimated respiratory rate from both locations are presented, as well as a confusion matrix for each PDR signal to evaluate their performance. Also, the power distribution of the respiratory information in the averaged spectrum and the rate and the width of the pulse wave in finger and forehead PPG signals are analyzed trying to explain the differences between both sensor locations.

Finger and forehead were the selected parts of the body since they are the most extended locations of PPG sensor in the bibliography [38, 65, 69, 70, 71, 72, 73, 74, 95]. In fact, one of the conclusions in [38] was that finger and forehead were the best sites to place PPG sensor for respiratory rate estimation, compared to other four possible locations. The change in the place where PPG signal is registered involves some variations that should be considered: different locations imply different configurations in signal acquisition, as light-transmission configuration can be used in the finger but not in the forehead, where light-reflection is the only possible configuration; the optical features of the skin are not the same in the finger than in the forehead; also the peripheral blood flow varies from one location to another because different capillary vessels irrigate the different zones. These changes affect the PPG morphology, obtaining a smoother waveform when the signal is recorded in forehead than in finger [39, 93]. This change in the waveform may affect respiratory information in the PDR signals, with a possible variation in the modulation that respiration induces

over these signals, and therefore affecting respiratory rate estimation. In fact, an important conclusion of this study is that respiratory rate estimation is more accurate when PPG signal is recorded in the finger than in the forehead. The success rate is higher and the relative error is lower in finger than in forehead for all the stages and all the PDR signals. In addition, the diagonal of the confusion matrix shows higher number of correct estimations in finger than in forehead. One possible explanation of this best results in finger lies in the relative power of the respiratory band, represented in Figure 3.5. In finger, a higher $\overline{P_R}$ was calculated, which means that the respiratory component is easier to be identified, and therefore, the respiratory rate estimator has more chances to give a correct result. In forehead (specially in the high frequencies) a lower value of $\overline{P_R}$ was calculated, which implies that is easier to mislead the respiratory component and consequently getting a wrong estimation. This result is in contrast with [93], where the frequency component analysis shows lower power of the respiratory component in the finger compared to other sensor locations. It is worth noting that in that study signals were recorded in supine position where parasympathetic activity is enhanced and the methodology used was based in the analysis of the PPG signal spectrum, while our recordings were in sitting position and the analysed spectral power is extracted from PDR signals. Therefore the counterbalance of respiratory related and unrelated components of PDR signals seems to be essential, at least for frequency based methods.

Another important conclusion of this work is the best performance of the respiratory rate estimation in lower frequencies than in higher ones. As Table 3.2 shows, the success rate decreases 30% from 0.2 to 0.5 Hz stages in almost all the PDR signals (except in PAV) and for both body locations. Consequently, the error committed is higher in 0.5 Hz stage (more than a 25% with respect to the 0.2 Hz stage). Spontaneous respiratory stage also shows good results because respiratory rate during rest usually is in the lower frequencies range, with a mean value of 0.23 Hz in this dataset. The relative error in spontaneous breathing is slightly higher than in 0.3 Hz stage because 6 subjects have a respiratory rate above 0.3 Hz, being more difficult to properly estimate respiratory rate in these cases. The best performance of the respiratory estimation in lower frequencies than in higher ones has also been reported in other studies [65, 91, 92]. A possible explanation to this could be a decrease in

the power of the respiratory component when the respiratory rate increases, for the 4 PDR signals, as Figure 3.5 shows. This could happen due to a low respiration-related modulation [96], since respiratory rate was the only difference in the setup of the different stages. In case of PRV, this is coherent with the well-known decrease of respiratory sinus arrhythmia as respiratory rate increases [97, 98]. A possible reason of this observation is that autonomic nervous system may act as a physiological low-pass filter. That would explain also the effect in PAV and PWV. Even more, PRV and PWV could be affected also by the mechanical effect of respiration on the intrathoracic blood pressure, which may have also a low-pass behaviour [96]. The decrease of the power of the respiratory spectral component at high breathing rates also causes that other spectral components non-related with respiration become relevant and act as a confound. Our results suggest the presence of a non-respiratory related spectral component around 0.1 and 0.2 Hz (see Figure 3.4, specially in RIIV). When an error occurred, respiratory rate estimation was usually around 0.15 Hz. In fact, in Table 3.4 the higher values of the confusion matrix are found either in the expected stage or in 0.1-0.2 Hz. This component is probably related to Mayer waves [99, 100] and the problems that may cause for respiratory rate estimation has been pointed out in others works [60]. In this dataset, this problem seems to significantly influence PPG signal, specially when it is registered in forehead. If the respiratory rate of one specific application is expected to be higher than 0.15 Hz, a more restrictive filter with a higher value of the low cut-off frequency could be applied trying to overcome this non-respiratory related component. In this work, a trial with 0.15 Hz as the low cut-off frequency of the filter that isolate respiratory components was implemented and results showed an increase higher than 20% in the success rate for all the single PDR signals when the PPG was registered in the finger and an increase of 10% in the forehead.

Concerning which PDR signal is the best to estimate the respiratory rate, PRV showed the best results for lower frequencies (below 0.3 Hz), with the higher success rate, the lower relative error and the higher number of correct estimations. However, its performance was not so good for higher frequencies. Above 0.3 Hz, PAV was the one with the best results when PPG was registered in finger, although results in lower frequencies were quite acceptable too. However, PAV results were not so good

in forehead, with significant differences in the success rate and the power around the respiratory component between both locations. This difference in PAV between finger and forehead measurements have been already noticed in [101], with better values in finger. In that study, removing the baseline modulation helped to reduce the variability between the two places, but in our study this type of filtering did not change the results. On the other hand, PWV was the one with best results in the forehead, specially in frequencies above 0.3 Hz. PWV was the only PDR signal whose results in finger were quite similar to the forehead ones. This could be explained by the similar distribution of the power related to the respiratory component in both locations, with no significant differences between both sites. Although RIIV was used in previous studies to estimate respiratory rate [60, 63, 64, 65, 74], it was the one which obtained the worst results both for finger and specially for forehead. This could be explained by the low power in the spectra at the expected respiratory rate, thus leading to a selection of a component non-related to respiration as the given estimation. Finally, the combination of PDR signals did not give the method more robustness, even more, results with a combination of PDR signals were worse in the higher frequency stages. This result is in contrast with the conclusion extracted in several works [60, 65, 73, 74], where the PDR signal combination offered more accurate estimations. Probably, the combination of several PDR signals is a good method if each PDR signal by itself provide good results (an accuracy of more than 85%-90%), but this was not the case in this study. Also, the final aim of the dataset must be considered for PDR signals combination: these 4 PDR signals have been studied in this specific dataset, conformed by healthy subjects with a mean age of 35.1 ± 6.5 years, however, in the study of a different dataset with different subjects, maybe some of these PDR signals could be eliminated as they could not provide faithful respiratory information. For example, while in this dataset PAV seems to be the one with the best performance, in a different dataset conformed by patients with a fluid overload PAV may not provide valid information [102]. Otherwise, in an elderly dataset where respiratory sinus arrhythmia will be not so significant [103], PRV performance should decrease. Therefore, the inclusion of each PDR signal in the respiratory rate estimation method should be considered depending on the final application.

Finally, an analysis of the morphology of PPG waveform was also presented in order to study how different the finger and forehead waves are, and whether PPG morphology is affected by the respiratory rate or not. Results show higher width when the PPG was registered in the forehead in comparison with the finger, independently of the respiratory rate. These differences imply morphological changes between both locations, as other studies in the bibliography show [39, 93]. However, the results do not show that these morphological changes cause restrictions in the respiratory rate estimation. In the case of the width of the pulses, a higher width does not imply a decrease in the modulation that the respiration induces over the PWV signal. In fact, PWV is the PDR signal with lower differences between finger and forehead recordings, despite of these change in the pulse width. Therefore, respiratory rate estimation is apparently more affected by the ratio between the respiratory power with respect to the power of the entire spectrum that could mask the respiratory information than by morphological factors.

3.6 Conclusion

It has been shown that differences in the respiratory rate estimation and changes in morphological features are found when the PPG signal is recorded in the finger and in the forehead. General results for respiratory rate estimation are characterized by a better performance in the low frequencies and when the sensor is located in the finger when compared to the forehead. Also, RIIV showed a poor performance and it affected negatively to the accuracy of the estimation when RIIV was combined with other PDR signals. Therefore, finger is the recommended location for PPG signal acquisition and RIIV signal is not recommended, specially when respiratory rate could increase to higher values. For this specific dataset, although PRV in finger obtain good results in lower frequencies, the use of PAV in finger would be preferable because it also obtains good results at lower frequencies (above 85% of success rate at 0.1 and 0.2 Hz) and the best results at higher frequencies (almost 90% of success rate at 0.3 Hz and above 75% at 0.4 and 0.5 Hz) and during spontaneous breathing (almost 80% of success rate). The inclusion of each PDR signal in the fusion algorithm should be analysed for each specific application considering both

the subject population and the breathing pattern, taking into account the effect of these factors on the respiratory modulation of the PPG.

Chapter 4

Changes in PPG morphology in hyperbaric environments

4.1 Introduction

As it was probed in Chapter 2, PRV is an efficient tool to measure ANS activity inside a hyperbaric chamber. Furthermore, not only PRV contains information about the ANS response. Also, PPG morphology can provide a great amount of information about vascular assessment or arterial compliance, since pulse pressure propagation in arteries causes alterations in blood volume and therefore changes in the PPG pulse shape [39, 50]. As mentioned in Section 1.4.2, the amplitude [51], the width [56], the areas[55] or some ratios [40, 52, 53, 54] could give information about the systemic vascular resistance controlled by the ANS system. All these PPG morphological parameters allows to identify low stress states [104] or distinguish between different types of exercise [9, 105] or even differentiate postural changes [106].

These parameters are extracted from the original PPG waveform or from its first or second derivatives. In other works, those parameters are extracted from PPG pulses modelled by a linear combination of several waves. This methodology is called Pulse Decomposition Analysis (PDA). The premise of the PDA model is that the peripheral arterial pressure pulse is a superposition of individual component pressure pulses, the first of which is due to the left ventricular ejection from the heart while the remaining component pressure pulses are reflections and re-reflections [107].

Most of the PDA techniques try to fit a model based on a superposition of waves at once, based on different shapes including gaussians [107, 108, 109], lognormals [110], rayleights [111] or a combination of them [112, 113]. Some works decompose the PPG pulse in systole and diastole and then modelled each part separately [114]. Another type of approach is to extract the waves one-by-one, as in [115, 116] instead of fitting a several-waves-model at once.

In this Chapter, a new algorithm is proposed to extract systolic and diastolic information. A first wave related to the systole is extracted directly from the PPG pulse concatenating the up-slope (from the beginning till the absolute maximum) with itself horizontally flipped. Then a second wave related with the diastole is modelled by a lognormal wave. From these two waves, the amplitude, the time instant, the width, the area and some ratios are extracted with the aim of identifying parameters that show significant changes in the ANS response of subjects exposed to variable hyperbaric environments.

4.2 Materials

PPG signal of 23 subjects (22 males and 1 female), with a mean age of 27.74 ± 5.15 years, from the hyperbaric chamber dataset presented in Section 2.2 were used. In this case, only the stages of five different pressures (S1D, S3D, S5, S3A and S1A) were analyzed. More details of this protocol can be consulted in Section 2.2.

4.3 Methods

4.3.1 PPG preprocessing

A low-pass FIR filter with a cut-off frequency of 10 Hz was applied to the PPG in order to attenuate noise [73]. Artefactual pulses were suppressed by using the artefact detector described in [83]. Later, the PPG pulses were automatically detected and the basal points, n_{Bi}, of each pulse were obtained using an algorithm based on a low-pass differentiator filter [46]. Finally, the baseline of the PPG signal was estimated by cubic-spline-interpolation of n_{Bi} and subsequently subtracted to ensure that each

PPG pulse begins and ends with zero amplitude. The resulting PPG signal was called $x_{PPG}(n)$.

4.3.2 Pulse decomposition analysis

Once each pulse was isolated, the new algorithm is applied, extracting two main waves, the first one related with the systole and the second one related with the diastole, trying to match the maximum of each wave with the two peaks. To do that, the algorithm explained in [115] was applied to extract the first wave related to the systole part of the *i-th* pulse as follows:

1. Set the beginning of the up-slope wave as the previous to the first non-zero-amplitude sample (in this case, n_{Bi}).

2. Set the end of the up-slope wave as the time instant of the absolute maximum (n_{Ai}).

3. Estimate the systolic wave $(y_{S,i}(n))$ by concatenating the up-slope with itself horizontally flipped, as it is shown in Eq. 4.1, assuming that it is symmetric.

$$y_{S,i}(n) = \begin{cases} x_{PPG}(n), & n \in [n_{Bi}, n_{Ai}] \\ x_{PPG}(-n + 2n_{Ai}), & n \in [n_{Ai}, 2n_{Ai} - n_{Bi}] \\ 0, & otherwise \end{cases} \quad (4.1)$$

Therefore, this first wave represents the part of the PPG associated with the systolic peak. Then, this wave was subtracted from the original PPG waveform to characterize the diastolic part, obtaining the residual pulse waveform $(r_{PPG}^1(n))$. Usually, as the systolic up-slope is more abrupt than the down-slope, the new maximum is found at the beginning of $r_{PPG}^1(n)$ instead of being in the diastolic peak. If this happens, the same algorithm explained for the first wave was repeated one more time, obtaining a transition second wave that was not used. The way to determine if this maximum belongs to the diastolic peak or not was by setting a temporal threshold: if the temporal location of the maximum is higher than the 35% of the pulse wave duration, this peak belongs to the diastolic part; if not, a transition wave $(y_{T,i}(n))$ is obtained concatenating the up-slope with itself horizontally flipped again

and subtracted from $\mathrm{r}_{\mathrm{PPG}}^1(n)$, obtaining another residual pulse waveform $(\mathrm{r}_{\mathrm{PPG}}^2(n))$. Finally, when the residual waveform related to the diastolic part was found $(\mathrm{r}_{\mathrm{PPG}}^1(n)$ or $\mathrm{r}_{\mathrm{PPG}}^2(n))$, it was modelled as a lognormal wave in order to be able to extract some characteristics as the amplitude, the width and the area under the curve. To do this modelling, first the residual waveform was normalized to the unit in amplitude and to 1000 samples in time by spline interpolation. Once normalized, a lognormal wave was created as in Eq. 4.2:

$$f(x) = \frac{1}{x \cdot \sigma \cdot \sqrt{2\pi}} \exp{-\frac{(\ln x - \mu)^2}{2\sigma^2}}, \tag{4.2}$$

with μ varying from μ_0-100 to μ_0+300 in steps of 25 (where μ_0 is the time location of the maximum) and σ varying from 0.2 to 1 in steps of 0.1. The values of μ and σ that minimize the mean-squared error between the lognormal wave and the residual pulse waveform were selected and the lognormal wave obtained was now reconverted to the original values of amplitude and time $(\mathrm{y}_{\mathrm{D,i}}(n))$. All the entire process is illustrated in Figures 4.1 and 4.2, with an example of the PPG pulse decomposition with three waves and with only two waves, respectively.

4.3.3 Pulse waveform characteristics

From the first wave associated with the systolic peak $(y_{S,i}(n))$ and from the lognormal associated with the diastolic peak $(y_{D,i}(n))$, several morphological features were extracted. The amplitude (A1 and A2) and the position of the maximum (T1 and T2) of the two waves were defined. The width (W1 and W2) was estimated as the full-width at half maximum since the end of the lognormal down-slope did not finish in the zero value. Also the area under the curve from the top until the half maximum (D1 and D2) was computed. An example of these parameters can be seen in Figure 4.3. The time delay between both waves (T12 = T2-T1), the reflection index (RI = A2/A1), the ratio between the widths (W2/W1), the ratio between the areas (D2/D1), the index of large artery stiffness (SI = h/T12, where h is the subject age) and the pulse-to-pulse interval $(\mathrm{T_{BB}})$, measured as the difference between consecutive n_{Bi}, were also calculated. These parameters were extracted from the five stages of the hyperbaric chamber dataset to see differences between the stages.
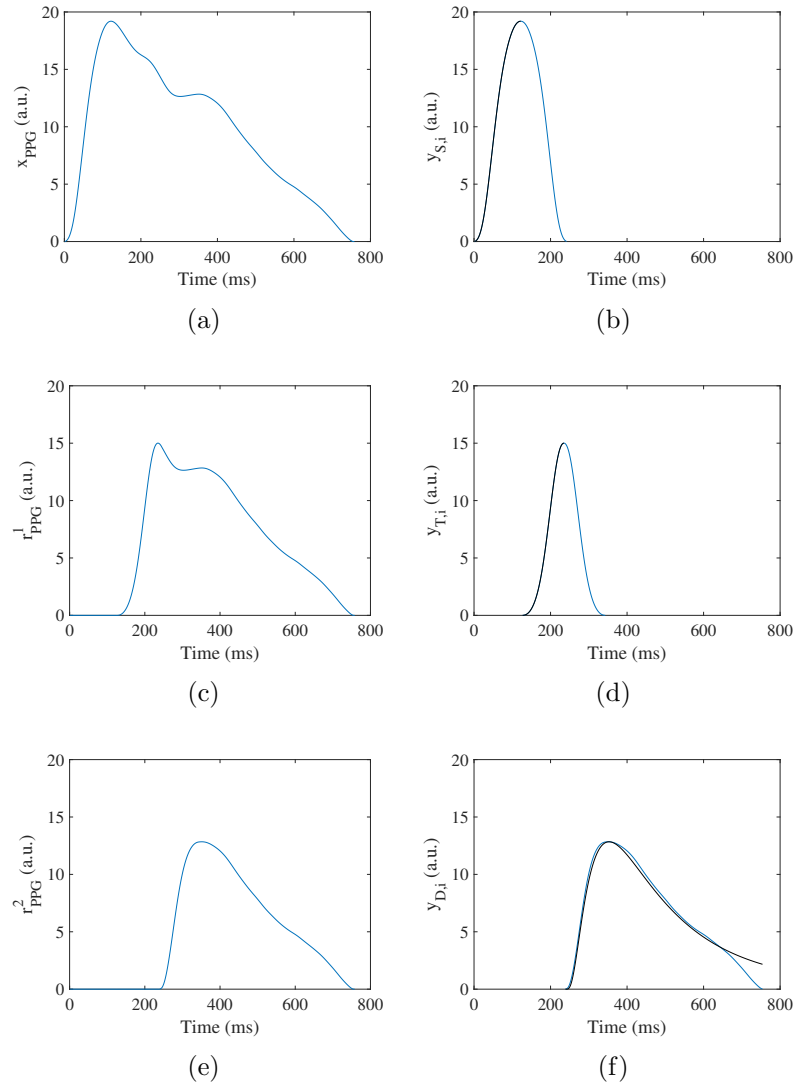
Figure 4.1: Example of the entire algorithm with three waves. Firstly, a) represents the original PPG pulse ($x_{\mathrm{PPG}}(n)$); b) represents the extraction of the wave related to the systolic peak ($y_{\mathrm{S,i}}(n)$), with the up-slope (that it was horizontally flipped) highlighted in black. Secondly, c) represents the first residual pulse waveform ($r^1_{\mathrm{PPG}}(n)$), obtained as the subtraction of $y_{\mathrm{S,i}}(n)$ from $x_{\mathrm{PPG}}(n)$, with the time duration of its maximum being shorter than the 35% of the complete pulse time duration; d) represents the extraction of the transition wave ($y_{\mathrm{T,i}}(n)$) not related with the diastolic peak, with the up-slope (that it was horizontally flipped) highlighted in black. Finally, e) represents the second residual pulse waveform ($r^2_{\mathrm{PPG}}(n)$), obtained as the subtraction of $y_{\mathrm{T,i}}(n)$ from $r^1_{\mathrm{PPG}}(n)$; f) represents the extraction of the wave related with the diastolic peak ($y_{\mathrm{D,i}}(n)$), modelled as a lognormal wave (in black).
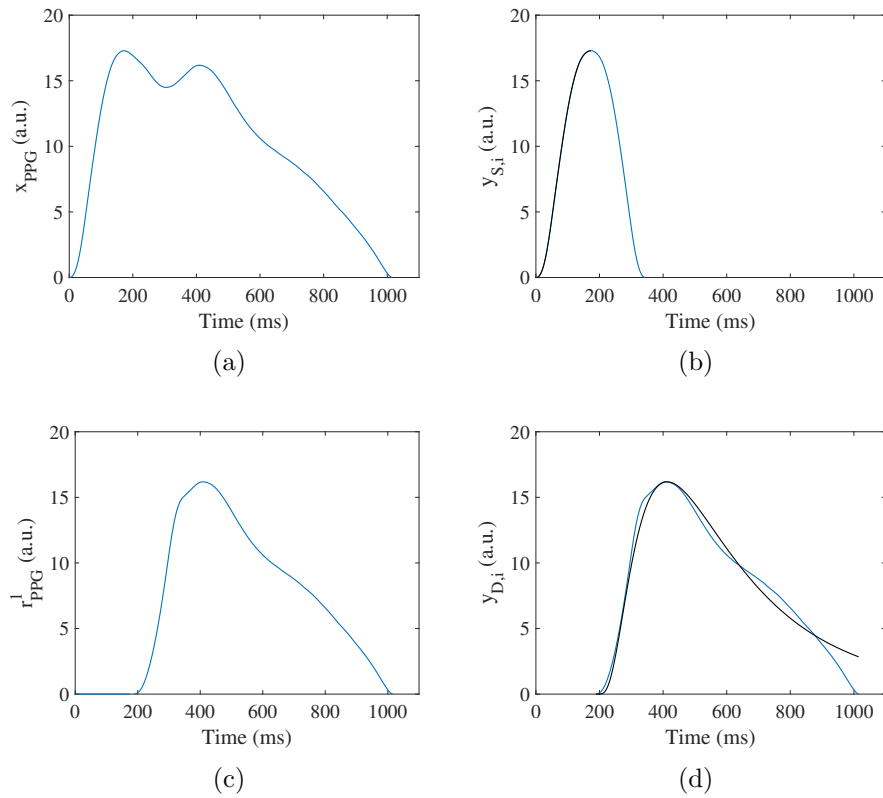
Figure 4.2: Example of the entire algorithm with two waves. Firstly, a) represents the original PPG pulse ($x_{PPG}(n)$); b) represents the extraction of the wave related to the systolic peak ($y_{S,i}(n)$), with the up-slope (that it was horizontally flipped) highlighted in black. Secondly, c) represents the first residual pulse waveform ($r^1_{PPG}(n)$), obtained as the subtraction of $y_{S,i}(n)$ from $x_{PPG}(n)$, with the time duration of its maximum being longer than the 35% of the complete pulse time duration; d) represents the extraction of the wave related to the diastolic peak ($y_{D,i}(n)$), modelled as a lognormal wave (in black).

4.3.4 Statistical analysis

A Shapiro-Wilk test was applied to check the normal distribution of each parameter, with paired Student's t-test being applied to every pair of stages if the distribution was normal and the Wilcoxon paired test if not. In both methods, a *p*-value $\leq \alpha$ defined significance, where α could be 0.05, 0.01 or 0.001.
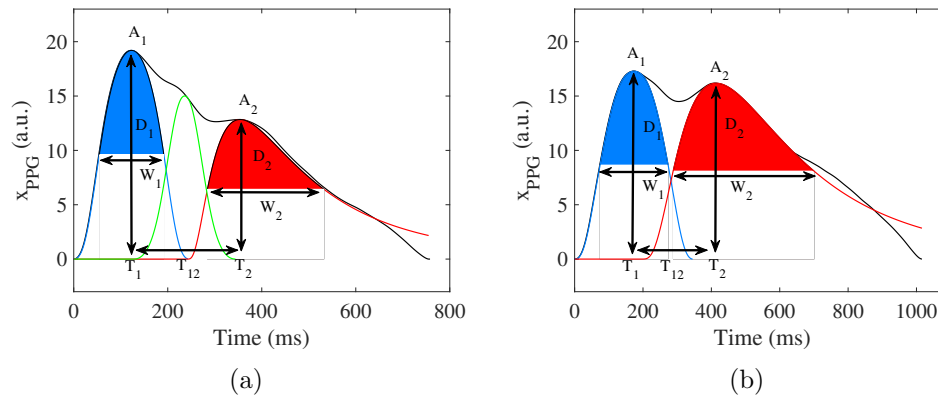
Figure 4.3: Example of the amplitude (A1 and A2), position (T1 and T2), width (W1 and W2), area (D1 and D2) and time delay (T12) in two PPG pulses, the first one decomposed with three waves (a) and the second one decomposed with two waves (b).

4.4 Results

It must be noticed than some subjects could not be recorded properly in all the stages due to a poor PPG signal quality because the PPG sensor was moved during the recording. Then, there were 23 subjects in S1D and S3D, 18 in S5, 19 in S3A and 17 in S1A. For the stages comparison, 23 subjects were compared in S1D vs. S3D; 18 in S1D vs. S5 and in S3D vs. S5; 19 in S1D vs. S3A and in S3D vs. S3A; 17 in S1D vs. S1A, in S3D vs. S1A and in S3A vs. S1A; 16 in S5 vs. S3A; and 13 in S5 vs. S1A.

Figure 4.4 shows the amplitude (A1 and A2), the position (T1 and T2), the width (W1 and W2) and the area (D1 and D2) of the first and second waves of the PPG pulse associated with the systolic and the diastolic peak. The pulse-to-pulse interval (T_{BB}), the time delay between both waves (T12), the large artery stiffness (SI), the reflection index (RI), the ratio between the width (W2/W1), and the ratio between the areas (D2/D1) are also shown. Results showed three different trends: i) A1, A2, D1 and D2 did not show significant changes among stages; ii) T_{BB}, T2, T12, SI, RI, W2, W2/W1 and D2/D1 showed significant differences between the initial stages with the final stages, increasing or decreasing their value during the entire protocol; iii) T1 and W1 increased their value from S1D to S5 stages and then decreased till S1A, with significant differences between stages of 1 and 5 atm.
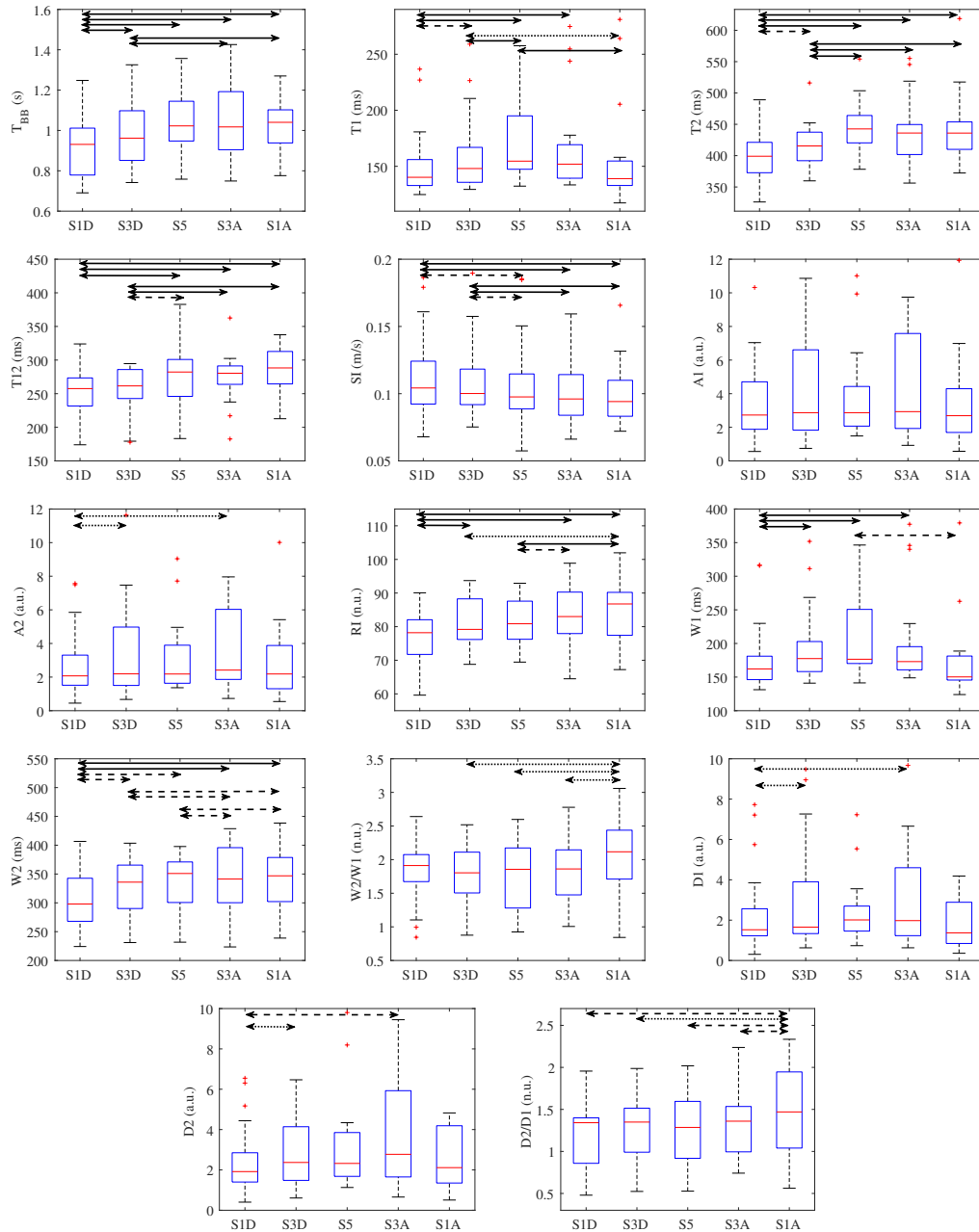
Figure 4.4: Boxplots of the pulse-to-pulse interval, T_{BB}, the time instant of the first peak and the second peak and the difference among them, T1, T2, and T12, the large artery stiffness index, SI, the amplitude of the first peak and the second peak and the reflection index, A1, A2 and RI, the width of the first and second peak and the ratio between them, W1, W2 and W2/W1, and the area under the curve of the first and second peak and the ratio between them, D1, D2 and D2/D1. Significant differences between stages are represented by a double arrow (dotted if $p-$value$\leq$0.05, dashed if $p-$value$\leq$0.01 and solid if $p-$value$\leq$0.001).

4.5 Discussion

In this Chapter, 14 morphological parameters extracted from the PPG pulse wave were analyzed to find differences due to the effect of the pressure in a dataset recorded inside a hyperbaric chamber. To do that, five different stages with three different pressures (1, 3 and 5 atm) were analyzed and the PPG signal was recorded in each of these stages. Each PPG pulse was isolated and two waves were extracted from them. The first one, related to the systole, was extracted directly from the pulse, by concatenating the up-slope from the beginning to the maximum with itself flipped horizontally. The second wave was modelled by a lognormal wave whose maximum matched with the maximum associate with the diastolic peak. From these two waves, the amplitude, the time of their maximum, the width and the area under these curves were calculated, together with some ratios and other parameters extracted from the literature as the large artery stiffness index, to find out if there were changes in these parameters due to the pressure.

The main novelty of this Chapter is the algorithm to extract the two waves. The idea issues from the necessity of having two waves whose peaks match with the systolic and the diastolic peaks. One option was applying a pulse decomposition analysis that models the PPG pulse as a main wave superposed with several reflected waves. Several models can be found in the literature, based on different shapes including gaussians [107, 108, 109], lognormals [110], rayleights [111] or a combination of them [112, 113]. The main problems of this approximation are that not always the decomposed waves match with the systolic and diastolic peaks and that the amplitude of the waves can be not higher enough to extract some parameters as the amplitude or the reflection index, therefore this strategy was discarded. Other option was using a pulse decomposition analysis based on extracting the waves one-by-one, as in [115, 116]. This was the strategy selected here, following the same algorithm that in these works: first, the beginning of the up-slope of each wave is set as the previous to the first non-zero-amplitude sample; secondly, the end of the up-slope is set as the first relative maximum; then, each wave is estimated by concatenating the up-slope with itself horizontally flipped, assuming that it is symmetric; finally each wave is subtracted to the original PPG waveform to obtain the residual PPG

waveform that has to be decomposed. The algorithm assumes than each wave can be modelled as a gaussian, so the amplitude, the mean and the standard deviation can be computed. This algorithm fits with the first peak and is able to characterize the systolic peak, however, when the first wave is subtracted and the residual PPG waveform is obtained, the up-slope of this new pulse is usually more abrupt than the down-slope. This caused a problem, since with the use of three waves as in [115, 116] it was impossible to decompose the entire pulse. Therefore, the alternative that we propose in this work is using a lognormal wave to characterize the diastolic part of the PPG pulse, since its down-slope is smoother than its up-slope and this type of curve fits better with the rest of the PPG pulse wave.

In fact, the approximation of modelling each part of the PPG pulse separately is not new in the literature, for example in [114] the anacrotic and catatrotic phases were modelled separately. Once the type of wave to model the diastolic phase was established, it was necessary that the maximum peak of the residual PPG waveform matched with the diastolic peak. It must be noticed than when the wave associated to the systolic part is subtracted from the original PPG pulse, then the new maximum of the residual PPG waveform is usually found at the beginning of the new waveform instead of being in the diastolic peak. If this happens, the same algorithm explained for the first wave is repeated one more time, obtaining a transition second wave that it is not used for extracting parameters, but it is subtracted from the PPG pulse. Again, the new maximum of the residual PPG pulse (with the subtraction of one or two waves if necessary) is located, and this value do match with the diastolic peak, so this part can be modelled as the diastolic part. The way to determine if this maximum belongs to the diastolic peak or not (in other words, if the second wave extracted only for subtraction is needed) is by setting a temporal threshold: if the temporal location of the maximum is higher than the 35% of the pulse wave duration, this peak belongs to the diastolic part; if not, the maximum is located in the transition part and the second wave is obtained and subtracted from the resultant pulse waveform. This temporal threshold of 35% has been determined experimentally. Other way to determine if the maximum belongs to the diastolic part could be the maximum after the dicrotic notch. However, this point is not easy to identify in all pulses, so this was the reason to establish a temporal threshold.

Once the rest of the PPG pulse related to the diastolic part is determined, the resultant pulse can be modelled as a lognormal wave, whose amplitude, width and area characterize the diastolic part of the PPG pulse. Therefore, the resultant pulse is modelled as a lognormal wave, fitting μ and σ in order to minimize the mean-squared error between the lognormal wave and the resulting pulse waveform. The main problem of this type of wave is that the end part of the down-slope do not return to the zero value, therefore the width and the area under the curve were calculated using the 50% of amplitude instead of the 100%.

Morphological parameters were extracted from the systolic and diastolic waves. The first parameters to analyze are the ones associated with time. First of all, there was a significant increase in the pulse-to-pulse interval, T_{BB}, from the first stages (S1D and S3D) to the last ones (S5, S3A and S1A). In fact, the increase in the pulse-to-pulse interval, implies a decrease in the heart rate, which had been reported previously in hyperbaric chamber studies [1, 15, 16, 17, 117] and in immersion data [12, 14]. Results from the time instant of the peaks revealed two different trends: while the value of T1 increased when the pressure increased, from its minimum in S1D to its maximum in S5 and then decreasing till another minimum in S1A, the value of T2 increased from the two first stages to the last three ones. This mean that T1, which is related with the systolic peak and only reflect the heart pumping, was affected by pressure, but T2, which is related with the diastolic peak and reflects both the heart pumping and wave reflections from the periphery, was affected by the pressure and the time spent inside the hyperbaric chamber. The increase of T1 when the pressure increased may be explained by an increased vascular resistance, which could be attributable to a vasoconstriction [56]. This vasoconstriction could be related to an activation of the sympathetic system of the subject [51]. The relationship with the time spent inside the hyperbaric environment showed in T2 was also reflected in T12, that increased its value in each stage, as it was logical seeing the values of T1 and T2. The variation in T12 was reflected in the large artery stiffness index (SI), since it depends on the age of the subject (that did not vary) and the time between the two peaks [54]. This index is based on the time difference between systolic and diastolic peaks, that can be used to infer the transit time taken for the PPG wave to propagate along the aorta and large arteries to the major sites

of reflection in the lower body and back to the root of the subclavian artery [118]. Therefore, the decrease in SI could mean a change in PPG pulse contour due to a decrease in large artery stiffness when subjects are inside the hyperbaric environment. Other parameter related with the large artery stiffness is the ratio between the two amplitudes (RI) [40, 53, 114, 119], that showed an increase in its value during the entire protocol. Although both SI and RI had a similar trend, varying when most time was spent inside the chamber, these parameters are usually related with the subject age, so their interpretation as markers of the cardiovascular response of the body in hyperbaric environments should be taken into account carefully. Related to RI, the amplitude of the two peaks did not show significant differences between stages.

About the widths, W1 increased its value from the first stage to the deepest stage and then decreased until the last stage, however W2 increased from the two first stages to the last three ones. It must be noticed than these trends were the same that the trends of T1 and T2 respectively, so W1 was affected by pressure and W2 was affected by pressure and the time spent into the hyperbaric chamber. A possible explanation of these behaviours is that the width of the first wave depends only on the systemic vascular resistance, while the width of the second wave depends on the systemic vascular resistance and on the heart rate. When the heart rate decreases (as it did during the protocol), the heart beat had more time to recover and therefore the down-slope of the pulse was larger (as T12 showed), thus increasing the width of the diastolic part. Then, the increase of W1 due to pressure could reflect only the vasoconstriction, which could be related to an activation of the sympathetic system [51], since the reduction in the arterial diameter could mean that more time is required to the blood to circulate, and therefore the up-slope of the pulse wave was enlarged. The ratio between the two widths only showed significant differences among S1A and the rest of stages, however no physiological interpretation of this ratio had been found in the literature. The areas showed significant differences between S1D with S3D and S3A, but not with S5. Maybe, as they depend on the amplitude (which did not show differences among stages) and on the width, the area at half the amplitude did not have power enough to discriminate between stages. The ratio between the two subareas (D2/D1) also showed the difference among S1A and

the rest of the stages, as the ratio of the two widths. This parameter was linked with an increase in the total peripheral resistance and therefore with a vasoconstriction in other work [55], however in this dataset this ratio does not follow the same trend than the time and width parameters, which also pointed out to a vasoconstriction.

To summarize, time and width parameters extracted with the decomposition of the PPG pulse using this new algorithm showed a dependency with pressure of the parameters of the systolic wave and a dependency with the time spent in the hyperbaric chamber of the parameters of the diastolic wave. On the one hand, the systolic part reflects a vasoconstriction related with an increase in pressure, probably due to an activation of the sympathetic system on the blood vessels that increases the systemic vascular resistance [51]. On the other hand, the diastolic part depends on the systemic vascular resistance and on an increase in the pulse-to-pulse interval during the entire protocol. The ratio of the amplitudes did show this last behaviour, although the amplitudes by theirselves did not show changes between stages. The parameters related with the area did not show the same differences as the others.

Based on our knowledge, the most similar work to this was the one in [120], where alterations in the morphology of the PPG were studied inside a hyperbaric chamber. One difference among the two studies lies in the separation of the pulses: while in [120] the pulse was divided into the anacrotic and the catatrotic phases, with the maximum of the PPG pulse being the separation of both phases, in this work two waves representing the systolic and diastolic peaks were obtained. In fact, in [120] the difficulty to estimate the location of the dicrotic notch and the diastolic peak was pointed out, so the algorithm presented in this work proposed a robust method to overcome these difficulties and this methodology gives us the opportunity to study some parameters than in the other study were impossible to measure, as the amplitude and the time instant of the peaks, and the time instant difference or the amplitude ratio. Other difference among the studies resides in the way to extract the morphological parameters: while in [120] they were extracted directly from the pulse, in this study they were extracted from the pulse in the first wave and also from the lognormal curve than approximates the diastolic wave. This change in the form to extract the PPG parameters made that they could be computed only at half the maximum in this work, while in [120] the were computed both at half the maximum

and at the base. Looking at the results, in [120] the width of the up-slope (similar to W1 here) had a maximum in S3A instead of S5, so the dependency with the pressure was not found with this parameter, however in the area of the up-slope (similar to D1 here) there was an increase with the increase of the pressure, which matches with our findings. Independently of the methodology used, results of both works point out to a vasoconstriction when the pressure increases, with an increased vascular resistance. This vasoconstriction could be produced by the increase in partial pressure of oxygen that occurs inside the hyperbaric environments [121].

4.6 Conclusion

In this Chapter, a new methodology to decompose the PPG pulse into two waves related with the systolic and the diastolic peaks was presented. The first wave was obtained concatenating the up-slope from the beginning to the first maximum with itself flipped horizontally. The second wave was modelled by a lognormal curve, adjusting its maximum to the diastolic peak (this happened only if the temporal location of the maximum is higher than the 35% of the pulse wave duration) and varying μ and σ in order to minimize the difference between the lognormal wave and the resulting pulse waveform. This methodology was applied in a hyperbaric chamber dataset. Results of the time and width of the wave related with the systolic peak pointed out to a vasoconstriction, probably due to an activation of the sympathetic system on the blood vessels, when the pressure increased. Results of the time and width of the wave related with the diastolic peak reflected the vasoconstriction but also a dependency with the pulse-to-pulse interval. Therefore this methodology offers an alternative to extract parameters related to PPG morphology that are able to distinguish changes in its waveform, at least in hyperbaric environments.

Chapter 5

ANS response in different hyperbaric environments

5.1 Introduction

In Chapter 2, a study of the ANS response inside a hyperbaric chamber allowed us to evaluate the ANS response changes due to the pressure. However, there are more variables that could affect the body's cardiovascular response during diving, such as diver body position, diver equipment, visibility, physical activity, water temperature, breathing with a scuba mouthpieces and more [122, 123, 124]. This is the reason why in this Chapter, the ANS response in three different hyperbaric environments, including two real dives, is analyzed. There are only a few studies analyzing ANS response during immersion and they show dominance of the parasympathetic activity [10, 12, 13, 14]. However, these studies involved lower depths in a pool [10], or only linear relationships were considered in their analysis [10, 12], or they analyzed divers that remained static during the immersion [13, 14].

Also in Chapter 2, the ANS response inside a hyperbaric chamber was characterized using classic time and frequency domain parameters. However, although PSD methods are widely used in the literature, its true efficacy as an accurate ANS index has been questioned [125, 126, 127]. Among PSD limitations, the two more highlighted are: i) PSD is a linear technique, so it fails to account for non-linear properties of HRV; ii) PSD overestimates the power in the LF band (and consequently

underestimates the power in the HF band) when the respiratory rate falls into the LF band. To overcome them, two different analyses are presented in this Chapter: i) PDM method, which is able to extract and separate sympathetic and parasympathetic dynamics and handles linear and non-linear relationships [34], as results from human studies have shown [14, 128, 129]; ii) The OSP method, which is able to separate the linearly related respiratory influences from the heart rate variability, providing information about how much of the respiratory component is reflected in the HRV and therefore leading to a more accurate estimation of the sympathovagal balance [79, 130].

Other factor that has been questioned recently is the time duration of the recordings: while the Task Force indicates that 2 minutes are needed to address the LF and HF components [27], some recent studies suggest that less than 5 minutes recordings may not be sufficient to assess HRV parameters accurately [131, 132].

In light of the above, three different aims are studied in this Chapter. Firstly, a comparison between PSD, OSP and PDM methods has been performed for data obtained in a hyperbaric chamber, to examine if OSP and PDM can overcome the aforementioned limitations of PSD. Secondly, comparison between time domain, frequency domain, PDM and OSP parameters from 5 minutes and 3 minutes recordings has been done in this same dataset to examine the appropriateness of these two time durations. Finally, to complete the analysis of ANS response in hyperbaric environments, time domain, PDM and OSP parameters have been studied in two additional datasets: the first dataset involves a controlled water immersion, where divers remained static in order to minimize the effects of different variables; the second dataset consists in an uncontrolled water immersion, where divers performed physical activities during the immersion, which is expected to alter ANS dynamics.

5.2 Materials

Three different datasets were analyzed in this Chapter. The first dataset is comprised of data collected in the hyperbaric chamber presented in Section 2.2. This dataset was used to compare the PSD method against both, OSP and PDM. In addition, the two different data lengths (5 and 3 minutes) were compared. For the other two

water immersion datasets, the ANS response during real immersions with similar depths (around 20 m or 66 ft) were investigated and compared with the hyperbaric chamber dataset. Subjects in the three datasets were different, but they shared to be military personnel, to be physically active (at least one hour of exercise daily), to be experienced scuba divers (more than 10 dives in the last year) and to have not taken caffeinated beverages prior to the study.

5.2.1 Datasets

1. Hyperbaric Chamber (HC): 28 subjects (24 males and 4 females) with a mean age of 28.73 ± 6.39 years were recorded inside the hyperbaric chamber of the Hospital General de la Defensa de Zaragoza. This dataset was the same presented in Section 2.2, so more details could be consulted there. In this case, only ECG (f_s=2000 Hz) and pressure (f_s=250 Hz) recordings were studied during the 5 minutes stops at 1 atm (which is the pressure at sea level), at 3 atm (simulating 20 meters or 66 feet depth), at 5 atm (simulating 40 meters or 131 feet depth), and then coming back to 3 and 1 atm. These stages were named S1D, S3D, S5, S3A and S1A (S from stage; the number reflects the pressure, n atm; the letter D or A refers to descent or ascent).

2. Controlled Dive (CD): 11 experienced scuba divers (all men) with a mean age of 41.13 ± 2.03 years were recorded during an immersion in the sea, with the approval of the Worcester Polytechnic Institute's Institutional Review Board. Only two stages have been analyzed in this work, although there are multiple stages in the data (this is a longer dataset, see details in [14]). In the baseline stage, the divers floated on the surface for 10 minutes with minimal movement, in the supine position, with their faces out of water and breathing through their scuba masks. In the immersion stage, divers remained at 66 feet (20 m) in a prone body position with minimal movement for 30 minutes, breathing air through their scuba masks. Water temperature at the bottom depth was 12.78 ± 0.57°C and divers wore a dry suit. With this dataset, the effect of the change of pressure in a semi-controlled real immersion can be analyzed, trying to minimize the influence of the rest of the variables. Recordings

were performed using a 5 lead digital Holter ECG monitor (RZ153+, Rozinn Electronics, Cleveland, OH), f_s=180 Hz. A diving data logger (GEO, Oceanic, San Leandro, CA) was used to record each diver's dive profile including the dive duration, depth, and water temperature.

3. Uncontrolled Dive (UD): 15 experienced scuba divers (all men) with a mean age of 28.40 ± 4.95 years were recorded in a real dive in a reservoir, with the approval of "Comité de ética de la investigación con medicamentos de la inspección general de sanidad de la Defensa", the hospital Review Board. Two different stages were analyzed. In the baseline stage, divers remained relaxed and sitting comfortably in silence without moving during 5 minutes outside the water. In the immersion stage, divers immersed for variable duration, but with a 3 minutes stay between 15 and 25 m (49 to 82 ft), breathing air through a scuba mouthpiece, performing physical tasks under low visibility. Water temperature on the surface was 8°C and divers wore dry suits. In this dataset, several factors such as body position, the type of activity, the surroundings during immersion and the way of breathing varied. Therefore, results needed to be carefully analyzed taking into account all these factors. Similar to the hyperbaric chamber dataset, recordings were performed using the Nautilus device [80], so signals from 3 lead ECG (f_s=2000 Hz) and the atmospheric pressure (f_s=250 Hz) were obtained.

A schematic representation of the three datasets comparison is shown in Table 5.1. From the HC dataset, stages S1D (as baseline) and S3D (as immersion) were selected to study the effect of pressure change, since the rest of variables remained equal.

Table 5.1: Explanation of the comparison of the three datasets, with the differences between them.

Immersion factors	Hyperbaric chamber (HC)		Controlled dive (CD) (sea immersion)		Uncontrolled dive (UD) (reservoir immersion)	
Stages	Baseline	Immersion	Baseline	Immersion	Baseline	Immersion
Pressure	1 atm	3 atm	1 atm	3 atm	1 atm	3 atm
Location	Chamber	Chamber	On water surface	Inside the water	Outside the water	Inside the water
Position	Sitting	Sitting	Supine	Prone	Sitting	Activity
Environment	Controlled	Controlled	Controlled	Semi-controlled	Controlled	Challenging
Breathing	Normal	Normal	Diver mask	Diver mask	Normal	Diver mask

5.2.2 Data extraction

The 5 minutes stops of each stage in the HC dataset were chosen in order to compare PSD vs. PDM and OSP methods. Then, the first 3 minutes of each stage were selected to compare the parameters extracted with the 5 minutes recordings, to see if the HRV parameters were reliable and did not change significantly from different signal duration. Finally, the first 3 minutes of each stage in the HC, CD and UD datasets were chosen, in order to be able to compare the ANS response between the three datasets. These 3 minutes segments were selected because it was the time that divers remained at the maximum depth during the reservoir immersion.

5.2.3 Respiration analysis

In order to better characterize the effect of the way of breathing through a scuba mouthpiece (breath is exaggerated, which can affect the parasympathetic system), an extra dataset was studied. In this fourth dataset, 12 subjects (6 men and 6 women) with a mean age of 27.17 ± 5.22 years were recorded while breathing in a spontaneous way and then while simulating respiration with a scuba mask, breathing deeply and rapidly, with pursed lips. Both stages (breathing styles) had a duration of 3 minutes and subjects remained sitting and relaxed during the entire test. One lead ECG recordings were taken using an HP 78354A ECG (Hewlett-Packard) and signals were digitized using a PowerLab system at 1000 Hz.

5.3 Methods

5.3.1 ECG Analysis

For HC and UD datasets, a similar preprocessing to the one applied in Section 2.3 was done. A FIR low-pass filter was applied to the ECG signal to estimate the baseline and then to remove baseline wandering (cut-off frequency of 0.03 Hz) [26]. Heartbeats were detected using a wavelet-based algorithm on the second lead of the recorded ECG signal [81]. In addition, ectopic beats and missed and false detections were identified and corrected [82]. As a result, the QRS complexes could be located

in the ECG, and the difference between consecutive R waves was used to generate the RR time series.

For the CD dataset, R waves in the ECG recordings were detected using automated software developed for the Rozinn monitor (Holter for Windows+). Any incorrectly recognized R waves were manually corrected.

Then, for the three datasets, the TVIPFM model was applied to determine the influence of the ANS on the beat occurrence time series [30]. More information about this model can be consulted in Section 2.3.1. Using this model, the instantaneous heart rate signal (d_{HR}) was created at a sampling rate of 4 Hz. The mean heart rate (d_{HRM}) was obtained by low-pass filtering the d_{HR} with a cut-off frequency of 0.03 Hz. Finally, the heart rate variability (d_{HRV}) was obtained as the difference between these two terms: $d_{HRV} = d_{HR} - d_{HRM}$.

5.3.2   Time Domain Parameters

Four time domain parameters were computed from the beat-to-beat time series:

- $mHR(b.p.m.)$: mean of the mean heart rate, measured in beats per minute (b.p.m.).

- $SDNN(s)$: standard deviation of the Normal-to-Normal (NN) intervals, as a measure of statistical dispersion. This parameter could be interpreted as an indicator of overall ANS activity [27].

- $RMSSD(s)$: Root mean Square of the successive differences between adjacent NN intervals. This parameter mainly reflects the parasympathetic tone [27].

- $pNN50(\%)$: number of pairs of successive NNs that differ by more than 50 ms divided by the total number of NN intervals.

5.3.3   Frequency Domain Parameters

As the recordings in the hyperbaric chamber were considered stationary, four frequency domain parameters were calculated based on the PSD analysis of the d_{HRV} signal, using Welch's power spectral density estimation. The parameters computed were:

- $P_{LF}(a.u.)$: power inside the LF band (0.04-0.15 Hz).

- $P_{HF}(a.u.)$: power inside the HF band (0.15-0.4 Hz).

- $P_{LFn}(n.u.)$: power in LF band normalized with respect to those of the LF and HF bands.

- $R_{LF/HF}(n.u.)$: ratio between LF and HF powers.

5.3.4 Respiratory information extracted from ECG

As it was announced in Section 1.4.3, the relationship between respiratory rate and the parasympathetic system must be taken into consideration during the analysis of ANS response. The method presented in Section 2.3.2, which consists of estimating the respiratory rate from peaked-conditioned averaged spectra, is used. As a sum up, this method exploits respiration-induced morphology variations in the ECG signal based on three EDR signals, namely the R-wave angle, and upwards and downwards of the R wave slope [85]. For each EDR signal, PSD was estimated every 5 seconds and the location of the largest peak closest to the previous respiratory rate estimation inside a reference interval was selected. A measure of peakness was subsequently obtained as the percentage of power around this peak with respect to the reference interval. Only if this measure was higher than a threshold (if it was peaked enough) the respiratory component was considered clear. Then, a peaked-conditioned average spectra was obtained by averaging those spectra (5 at maximum) which were peaked enough. Finally, the respiratory rate (F_R) was estimated as the maximum of the averaged spectra. Those subjects with F_R lower than 0.15 Hz (upper limit of the LF band) were discarded from the classic PSD analysis of the ANS response to avoid possible misinterpretations [78].

5.3.5 Analysis of HRV using Principal Dynamic Mode

The PDM is a method based on extracting only the principal dynamic components of the signal via eigen decomposition. The PDMs were calculated using Volterra-Wiener kernels based on expansion of Laguerre polynomials [133]. A minimum set of basis functions was determined by using principal component analysis, in which

the dominant eigenvectors were retained, as they relate more closely to the true characteristics of the signal. In the case of HRV signal, the dominant eigenvectors should reflect the dynamics of the sympathetic and parasympathetic systems. The non-dominant eigenvectors represent noise or non-essential characteristics.

The first step of the PDM method is to obtain a signal with broadband spectral characteristics in order to accurately estimate the Volterra-Wiener kernel. In many instances, significant power in HRV exists in the VLF band (0-0.04 Hz) compared to the LF and HF bands. Consequently, the method introduced by Tarvainen et al [134] was used with the aim of reducing VLF power to the level of the LF and HF bands so that the overall spectral characteristics are broadband. The result of this process was labeled as d_{HRC} [34].

The PDM method requires both the input and output data, but we had only the output signal (d_{HRC}), so it was necessary to create an input signal with broadband spectral characteristics and with a correlation to the dynamics of the heart rate. The Time Variant-Optimal Parameter Search (TV-OPS) algorithm, explained in [135], was used to create the input signal. This procedure was represented as an autoregressive (AR) model where the output signal (d_{HRC}) could be estimated through past samples of this signal (delayed d_{HRC}):

$$d_{HRC}(n) = \sum_{i=1}^{P} a(i,n) \cdot d_{HRC}(n-i) + e(n), \tag{5.1}$$

where $a(i,n)$ represents the time-varying AR coefficients, P is the maximum order of the AR model (established in 8 as in [135]) and $e(n)$ is the prediction error.

These $a(i,n)$ coefficients are expanded onto a set of eight (V = 0...7) Legendre polynomials basis functions ($\pi_k(n)$):

$$a(i,n) = \sum_{k=0}^{V} \alpha(i,k) \cdot \pi_k(n). \tag{5.2}$$

Legendre polynomials are selected because they are more appropriate for smoothly changing dynamics. An example of the first eight orders of Legendre functions can be seen in Figure 5.1.
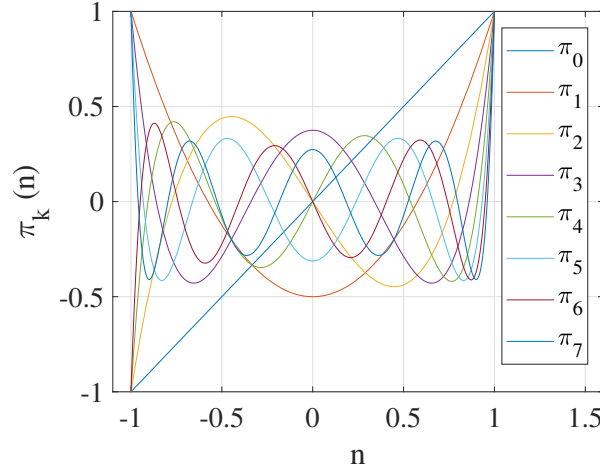
Figure 5.1: Dynamic characteristics of the first eight orders of Legendre functions.

Then, the projection of the past samples of the signal over the Legendre basis functions can be formulated as:

$$d_{HRK}(k, n-i) = \pi_k(n) \cdot d_{HRC}(n-i). \tag{5.3}$$

Substituting Eq 5.2 and Eq 5.3 into Eq 5.1, the following expression can be obtained:

$$d_{HRC}(n) = \sum_{i=1}^{P} \sum_{k=0}^{V} \alpha(i, k) \cdot d_{HRK}(k, n-i) + e(n). \tag{5.4}$$

Then, a pool of linear independent candidates was selected to estimate the projected coefficients. Between all the candidates, the first candidate vector $(d_{HRK}(0, n-1))$ and the second one $(d_{HRK}(1, n-1))$ are used to determine whether they are linearly independent by the least-square analysis and calculate the residual of the fit. If this residual is larger than a preset threshold, then $d_{HRK}(1, n-1)$ is considered independent from $d_{HRK}(0, n-1)$ and if not is discarded. This procedure is repeated with all the candidates, until all of the linearly independent candidate vectors are selected (W):

$$W = (w_1, w_2, ..., w_s), \tag{5.5}$$

being S the number of the linearly independent candidate vectors.

With this new matrix of linearly independent vector, the reconstructed output signal (d_{HRR}) can be formulated as:

$$d_{HRR}(n) = \Theta^T \cdot W + e(n), \tag{5.6}$$

being $\Theta = [\alpha(1), \alpha(2), ..., \alpha(S)]$.

As the objective is to minimize the error, a least-square criterion function is applied, defined as follows:

$$J_N(\Theta) = \sum_{n=1}^{N} [d_{HRR}(n) - \Theta^T \cdot W]^2. \tag{5.7}$$

The last mean-square error criterion is quadratic in Θ, so the projected coefficients can be estimated as:

$$\Theta = [W \cdot W^T]^{-1} \cdot W \cdot d_{HRC} \tag{5.8}$$

Therefore, substituting this equation into Eq. 5.6, the output signal of TV-OPS algorithm can be obtained. This signal was subtracted from the original output signal to obtain the estimation error signal, labeled d_{HRE}: $d_{HRE} = d_{HRC} - d_{HRR}$.

This error signal, normalized to a unit variance (d_{HRN}), had the broadband characteristics needed for accurate estimation of PDMs. Therefore, d_{HRN} was used as the input signal and d_{HRC} was used as the output signal of PDM model to estimate the Volterra-Wiener kernel, as was used in previous studies [14, 34, 128]. In fact, the general input-output relation of a stable non-linear time invariant dynamic system is given by the discrete time Volterra series as:

$$d_{HRC}(n) = k_0 + \sum_{m=0}^{M-1} k_1(m) \cdot d_{HRN}(n - m) +$$
$$\sum_{m_1=0}^{M-1} \sum_{m_2=0}^{M-1} k_2(m_1, m_2) \cdot d_{HRN}(n - m_1) \cdot d_{HRN}(n - m_2) + ... \tag{5.9}$$

where d_{HRN} is the input, d_{HRC} is the output, M is the memory of the system (limited to 60) and $k_0, k_1, k_2...$ are the Volterra kernels, which describe the dynamics of the system from a hierarchy of system non-linearities.

The kernel values are combined to form a real symmetric (M+1)x(M+1) square matrix, that allow to express the second order Volterra model response in a quadratic form:

$$
Q =
\begin{bmatrix}
k_0 & \frac{1}{2}k_1(0) & \frac{1}{2}k_1(1) & \cdots & \frac{1}{2}k_1(M-1) \\
\frac{1}{2}k_1(0) & k_2(0,0) & k_2(0,1) & \cdots & k_2(0,M-1) \\
\frac{1}{2}k_1(1) & k_2(1,0) & k_2(1,1) & \cdots & k_2(1,M-1) \\
\vdots & \vdots & \vdots & \ddots & \vdots \\
\frac{1}{2}k_1(M-1) & k_2(M-1,0) & k_2(M-1,1) & \cdots & k_2(M-1,M-1)
\end{bmatrix},
\quad (5.10)
$$

$$
d_{HRC}(n) = d_{HRN}^T(n) \cdot Q \cdot d_{HRN}(n). \tag{5.11}
$$

Expansion of the Volterra kernels on a complete basis using a maximum of 6 (L) Laguerre functions ($b_j(m)$) transforms Eq. 5.9 in:

$$
d_{HRC}(n) = c_0 + \sum_{j=0}^{L-1} c_1(j) \cdot v_j(n) + \sum_{j_1=0}^{L-1}\sum_{j_2=0}^{L-1} c_2(j_1,j_2) \cdot v_{j_1}(n) \cdot v_{j_2}(n) + ..., \tag{5.12}
$$

with

$$
v_j(n) = \sum_{m=0}^{M-1} b_j(m) \cdot d_{HRN}(n-m). \tag{5.13}
$$

In the same way, Q can be constructed with the estimated kernels ($c_0, c_1, c_2...$) in the following way:

$$
Q =
\begin{bmatrix}
c_0 & \frac{1}{2}c_1^T \cdot B^T \\
\frac{1}{2}B \cdot c_1 & B^T \cdot c_2 \cdot B
\end{bmatrix}
\tag{5.14}
$$

with $B = [b_0^T, b_1^T, ..., b_{L-1}^T]$.

Laguerre functions are selected because they are an orthogonal basis, meaning than now Q is a real symmetric square matrix that can be decomposed as:

$$
Q = R \cdot \Lambda \cdot R^T, \tag{5.15}
$$

where R is the eigenvector matrix and Λ is the diagonal eigenvalue matrix.

For each significant eigenvalue λ_s, the values of the corresponding eigenvector $\mu_s^T = [\mu_{s,0}, \mu_{s,1}, ..., \mu_{s,M}]$ (except of $\mu_{s,0}$) defines the *sth* PDM. In the case of HRV signal, the dominant eigenvectors and eigenvalues should reflect the dynamics of the sympathetic and parasympathetic systems. While the obtained PDMs were in time domain representation, the Fast Fourier Transform (FFT) transform was used to convert them to the frequency domain. The PDM with the highest power in the HF band was selected to represent the dynamics corresponding to the parasympathetic nervous activity. The power in 0.04 Hz to 0.4 Hz range was computed for this mode ($PDMpara$) since parasympathetic component is reflected in LF and HF classical bands [27, 125, 126, 127]. Then, the PDM with the highest power in the LF band (discarding the one selected as parasympathetic) was chosen as the PDM that represents the sympathetic activity and its power in the LF band was computed ($PDMsymp$). These two components reflect the dynamics of the two ANS branches [14]. This process is illustrated in Figure 5.2.
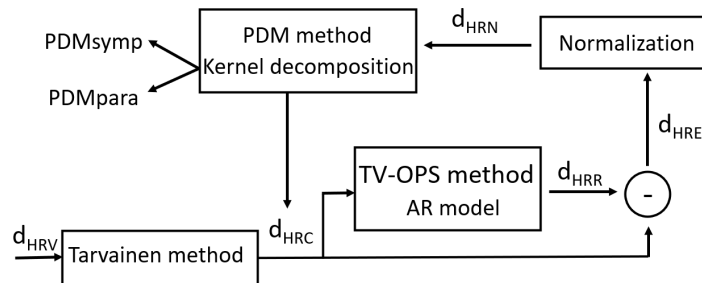
Figure 5.2: Diagram of PDM method.

5.3.6 Analysis of HRV using Orthogonal Subspace Projection

OSP is a method based on decomposing the HRV signal into two different components: one respiratory component, describing all linearly-related variations associated with respiration, and one residual component, describing all dynamics modulated by other mechanisms different from respiration. In fact, the residual component describes dynamics modulated by the sympathetic nervous system, and other (possible) vagal modulators unrelated to respiration [79, 130].

To apply this method, the respiratory signal, (d_R), and the HRV signal, d_{HRV}, are needed, together with the assumption that the respiratory signal drives changes in the HRV signal [136]. In this work, respiratory signals were obtained from the ECG using QRS slopes and R-wave angle as described in Section 5.3.4. However, this method could not be applied in the second dataset (CD), because only RR series were available, not the complete recorded ECG signal, therefore OSP was analyzed only for the HC and UD datasets.

In order to extract all dynamics of the heart rate that are linearly related to respiration, d_{HRV} can be projected onto a subspace $\mathbb{V}$ defined by all variations in respiratory signal. This subspace is constructed using the respiratory signal, d_R, and its delayed versions, going from 1 to m samples [137]. In other words, a matrix V spanning the subspace $\mathbb{V}$ is constructed as: $V = [R(0), R(1), ..., R(m)]$, with $R(d) = [d_R(d+1), d_R(d+2), ..., d_R(N-m+d)]^T$, $d = 0, ..., m$ and N as the length of the respiratory signal. In this study, the value of m (model order) is defined as the minimum amount of delays obtained using both the Minimum Description Length (MDL) principle and the Akaike Information Criterion (AIC), with a maximum delay of 10 s.

After creating the matrix V, the HRV signal can be projected onto the respiratory subspace $\mathbb{V}$ by means of:

$$d_{HRV_R} = P \cdot d_{HRV}, \tag{5.16}$$

where P is a projection matrix defined as:

$$P = V \cdot (V^T \cdot V)^{-1} \cdot V^T. \tag{5.17}$$

As a result, all dynamics of HRV linearly related to respiration are described in the respiratory component d_{HRV_R}. Furthermore, an orthogonal component (residual component), which is related to other heart rate modulators, was computed as $d_{HRV_\perp} = d_{HRV} - d_{HRV_R}$. This process is illustrated in Figure 5.3.

The relative power of each component (P_R for respiratory component and $P_\perp$ for the residual component) can be calculated as:

$$P_R = \frac{d'_{HRV_R} \cdot d_{HRV_R}}{d'_{HRV} \cdot d_{HRV}}, \quad P_\perp = \frac{d'_{HRV_\perp} \cdot d_{HRV_\perp}}{d'_{HRV} \cdot d_{HRV}}. \tag{5.18}$$
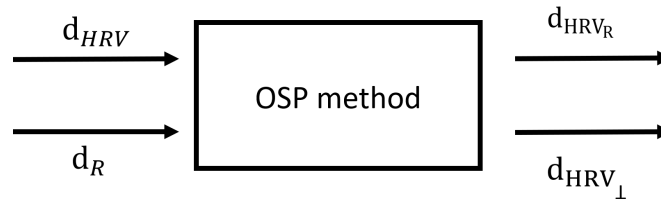
Figure 5.3: Diagram of OSP method.

These powers indicate how much information is shared between respiration and heart rate. For instance, when $P_R >> P_\perp$, most of the variations in the heart rate can be described by changes in the respiration and vice versa. P_R can also be used as a marker for RSA assessment, and due to the relationship between RSA and the vagal tone, P_R can be interpreted as a parasympathetic marker. In addition, the power of the residual component in the LF band ($P_{LF\perp}$) could be interpreted as a marker of the sympathetic system, and the power of the residual component in the HF band ($P_{HF\perp}$) as a marker of the parasympathetic system.

5.3.7   Statistical analysis

First, a statistical analysis was applied to each time domain, frequency domain, OSP and PDM parameter to determine the presence of significant differences between the five stages of the HC dataset. Thus, a Shapiro-Wilk test was applied to check the normal distribution of the parameter, with Student's t-test being applied to every pair of stages if the distribution was normal and the Wilcoxon paired test if not. Then, the correlation of each parameter extracted from 5 and 3 minutes recordings together with a paired sample Student's t-test was performed to study the similarity between these recordings.

Finally, statistical analyses were performed to compare the baseline versus immersion stages in the three hyperbaric datasets and to compare normal versus simulated scuba mask breathing. A Shapiro-Wilk test was applied to verify the normal distribution of the data, and as these distributions were no-normal, the Wilcoxon paired

test was applied. Also, another statistical analysis was made to compare the three baseline stages. In this case, as they were three independent groups with a non-normal distribution, the Kruskall-Wallis test was applied. Three different p-values, 0.05, 0.01 and 0.001, defined the significance.

5.4   Results

ECG recording of one subject stopped in the middle of the HC test, therefore there were 28 subjects for S1D, S3D and S5 stages and only 27 for S3A and S1A stages.

5.4.1   Respiratory rate in HC dataset

Table 5.2 shows the respiratory rate in the HC dataset with 5 and 3 minutes recordings. No significant differences were found among stages and between the same stage with different duration. It should be noted that 4 subjects in S1D, 5 in S3D, 4 in S5, 2 in S3A and 3 in S1A had a respiratory rate lower than 0.15 Hz.

Table 5.2: Mean ± std of the estimated respiratory rate in the HC dataset.

	Duration	S1D	S3D	S5	S3A	S1A
$F_R(Hz)$	5 min	0.22±0.09	0.22±0.09	0.22±0.07	0.24±0.08	0.23±0.09
	3 min	0.21±0.07	0.21±0.06	0.21±0.06	0.23±0.06	0.22±0.07

5.4.2   PSD vs. PDM and OSP methods

Table 5.3 shows the total power of the respiratory and the residual component of the OSP for the HC dataset for 5 and 3 minutes recordings. No significant differences were found between 5 and 3 minutes powers. $P_\perp$ was significantly higher than P_R in all stages.

Figure 5.4 shows the time domain, the classic frequency domain, the PDM and the residual OSP parameters for the HC dataset. It should be noted that for the classic frequency domain parameters, subjects with a respiratory rate lower than 0.15 Hz were discarded, thus leaving 24 subjects in S1D and S5, 23 in S3D, 26 in

Table 5.3: Mean $\pm$ std of the total power of the respiratory component and the residual component in the HC dataset. Significant differences between P_R and $P_\perp$ are highlighted with a dagger ($p-$value$\leq$0.05).

	5 min		3 min	
	P_R	$P_\perp$	P_R	$P_\perp$
S1D	0.037$\pm$0.056	1.262$\pm$0.671 †	0.043$\pm$0.068	1.353$\pm$0.772 †
S3D	0.049$\pm$0.058	1.581$\pm$1.001 †	0.054$\pm$0.071	1.672$\pm$1.054 †
S5	0.049$\pm$0.067	1.914$\pm$1.063 †	0.081$\pm$0.097	1.946$\pm$1.162 †
S3A	0.032$\pm$0.049	1.212$\pm$0.719 †	0.043$\pm$0.071	1.236$\pm$0.857 †
S1A	0.021$\pm$0.022	1.099$\pm$0.662 †	0.036$\pm$0.042	1.152$\pm$0.729 †

S3A and 25 in S1A. For the comparisons between stages there were 20 subjects in S1D vs. S3D, S1D vs. S1A, S5 vs. S1A; 21 in S1D vs. S3A, S3D vs. S5, S3D vs. S1A, S5 vs. S3A; 22 in S1D vs. S5, S3D vs. S3A; and 23 in S3A vs. S1A. As shown in Figure 5.4, mHR decreased and $RMSSD$ increased with each stage, whereas $SDNN$ and $pNN50$ reached a maximum value at stage S5 and S3A respectively. For the frequency domain results, P_{LF} and P_{HF} increased their value during the descent, reaching a maximum at the deepest stage S5 and then decreasing in value during the ascent. P_{LFn} and $R_{LF/HF}$ did not follow a clear trend, but they had their maximum in the S5 stage and their minimum in the S3A stage. Finally, $PDMsymp$, $PDMpara$, $P_{LF\perp}$ and $P_{HF\perp}$ followed the same trend, increasing their value until the S5 stage and then decreasing it until the last stage. The only exception of this path occurred with $PDMpara$, between stages S1D and S3D.

5.4.3 5 minutes vs. 3 minutes recordings

Figure 5.5 shows the time domain, the classic frequency domain, the PDM and the residual OSP parameters extracted from 5 minutes recordings and 3 minutes recordings in the HC dataset. The 3 minutes recordings were the first 3 minutes of the 5 minutes recordings. Correlation between parameters extracted with 5 minutes and with 3 minutes was greater than 90% in all parameters except in two stages of P_{LF}, in one stage of $P_{LF\perp}$ and for $PDMsymp$ and $PDMpara$ (from 0.55 to 0.89 in these last two parameters). The paired t-test did not show significant differences between the two recordings.
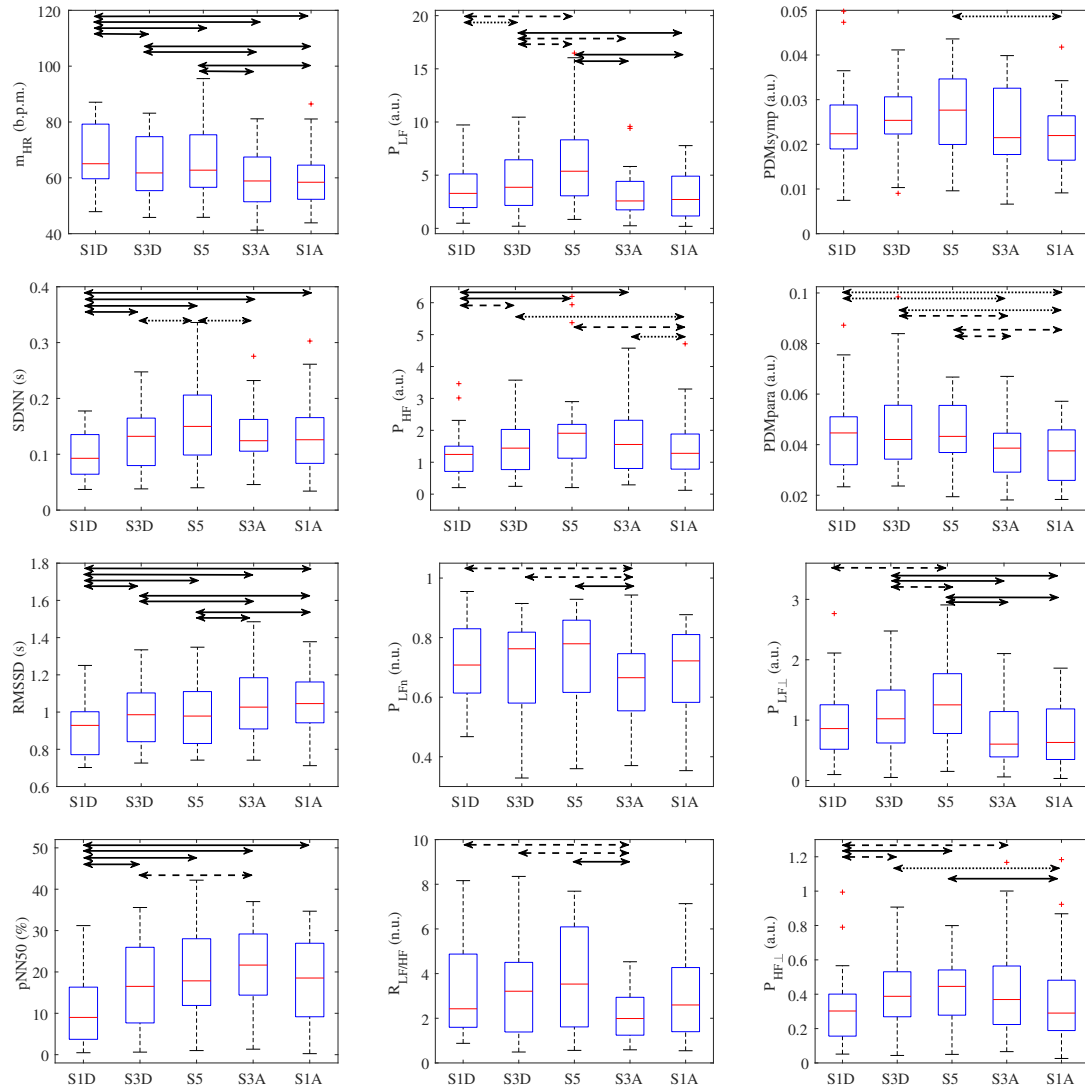
Figure 5.4: Boxplots of the time domain (first column), the classic frequency domain (second column), the PDM and the residual OSP (third column) parameters in the HC dataset. Significant differences between stages of the same dataset are represented by a double arrow (dotted if p−value≤0.05, dashed if p−value≤0.01 and solid if p−value≤0.001).
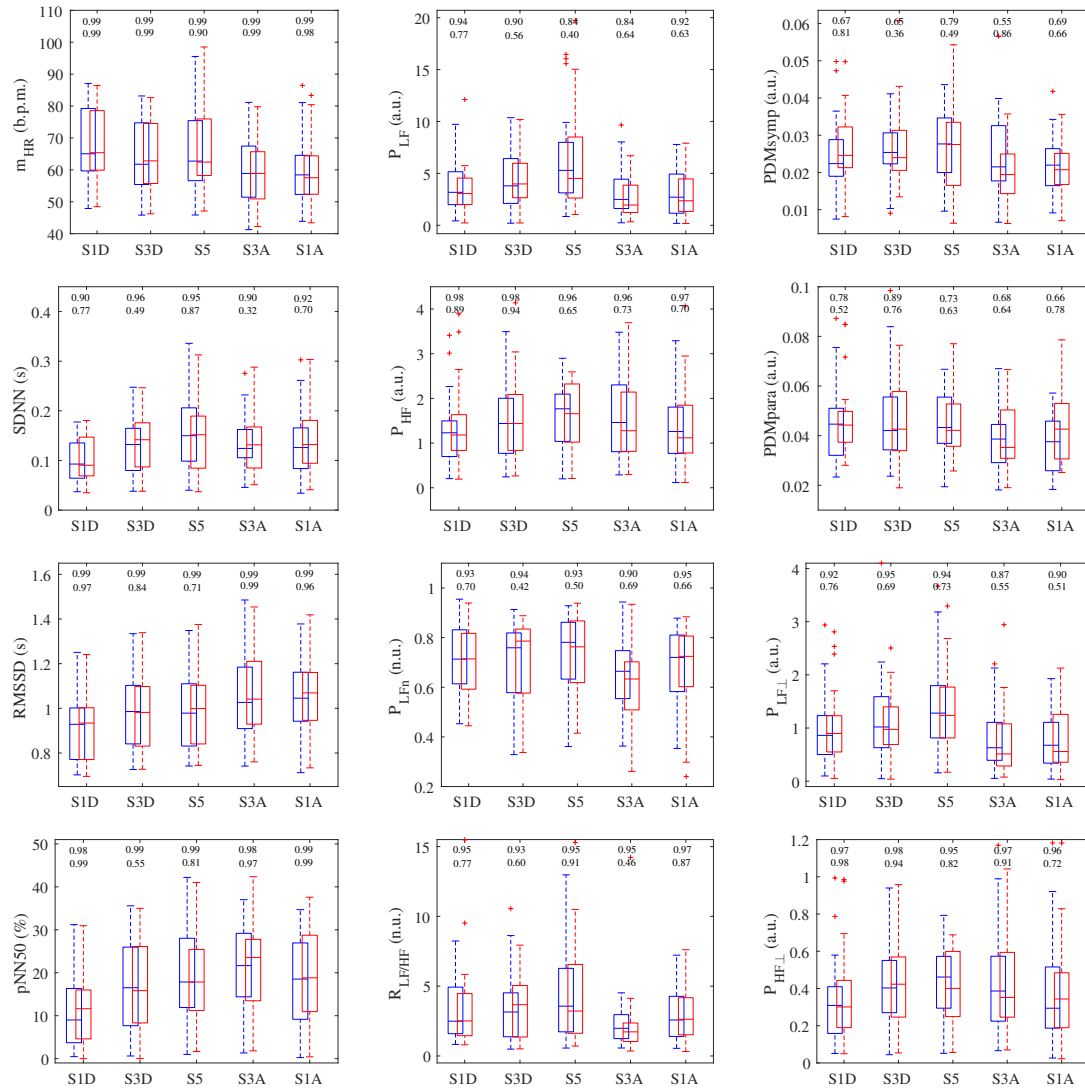
Figure 5.5: Boxplots of the time domain (first column), classic frequency domain (second column), the PDM and the residual OSP (third column) parameters of 5 minutes recordings (in blue) and 3 minutes recordings (in red) in the HC dataset. The correlation (first row) and the paired t-test (second row) between 5 and 3 minutes measurements are showed on the top.

5.4.4 Hyperbaric environments comparison

Figure 5.6 shows the time domain, the PDM and the residual OSP parameters from baseline and immersion stages in the HC, CD and UD datasets. About the time domain parameters, mHR significantly decreased from baseline to immersion in HC and CD while the rest of the time domain parameters increased. However, this behavior is the opposite in UD, where mHR significantly increased and $SDNN$, $RMSSD$ and $pNN50$ decreased. The comparison between the baseline stages of the three datasets found that mHR was significantly higher in CD with respect to the other two baseline stages while the rest of the time parameters were lower in CD. PDM parameters showed that $PDMsymp$ was significantly higher during immersion in the CD and UD datasets while $PDMpara$ was only significantly higher in UD. Table 5.4 shows the total power of the respiratory and the residual components of OSP for the HC and UD datasets. $P_\perp$ was significantly higher than P_R in both stages and in both datasets. As shown in Figure 5.6, power of the residual OSP component (calculated only in HC and UD datasets because of the lack of respiratory signal in CD) showed a significant increase in $P_{LF\perp}$ (only in UD) and in $P_{HF\perp}$ (in both datasets) during immersion.

Table 5.4: Mean $\pm$ std of the total power of the respiratory and the residual components of OSP for the HC and UD datasets. Significant differences between P_R and $P_\perp$ are highlighted with a dagger ($p-$value$\leq$0.05).

	Baseline		Immersion	
	P_R	$P_\perp$	P_R	$P_\perp$
HC	0.048±0.064	1.201±0.695 †	0.063±0.087	1.590±1.068 †
UD	0.104±0.124	1.238±0.788 †	0.089±0.110	2.836±2.035 †

5.4.5 Spontaneous vs. simulated scuba mask breathings

Figure 5.7 shows the differences between time domain, the PDM and the residual OSP parameters during spontaneous breathing and simulated scuba mask breathing. mHR significantly increased from spontaneous to simulated scuba mask breathing, $SDNN$ also increased but not significantly, $RMSSD$ significantly decreased and
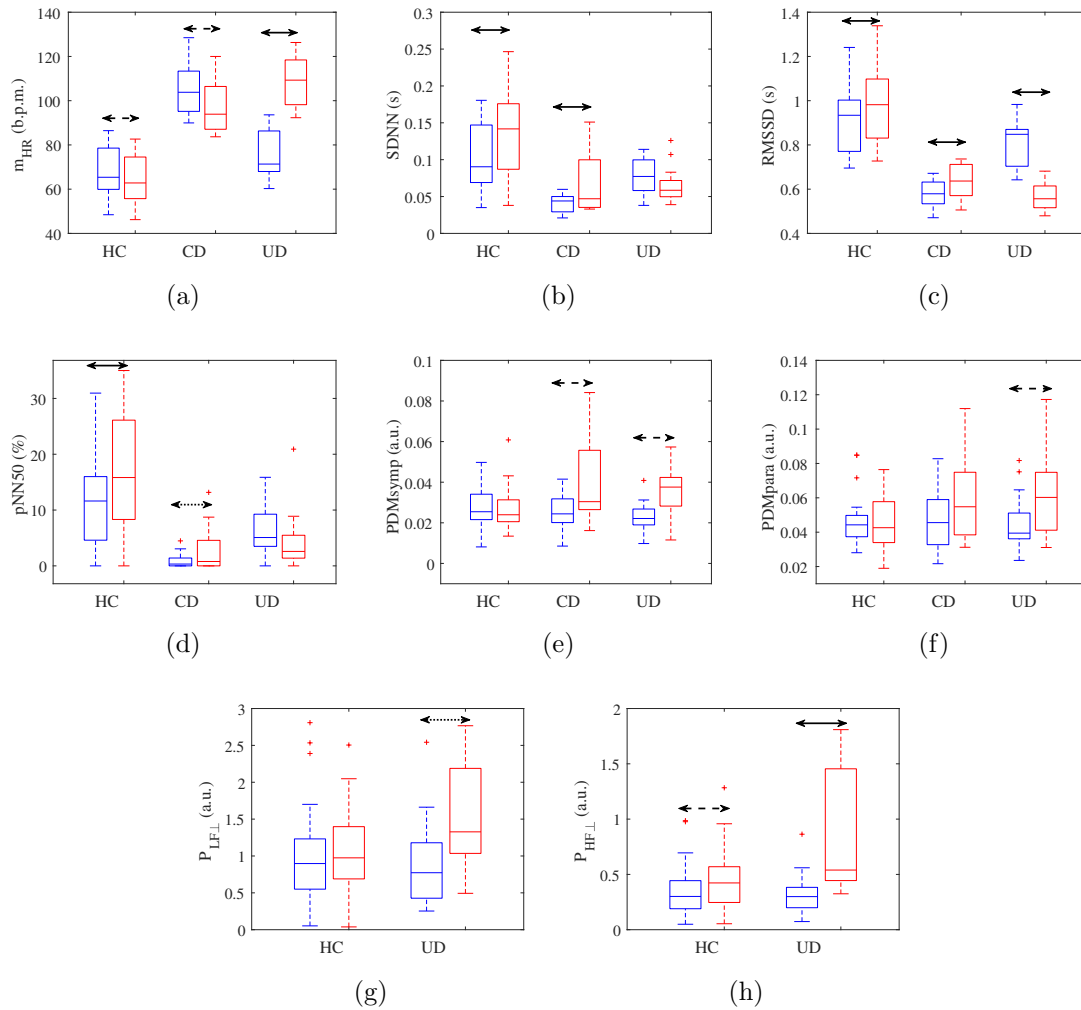
Figure 5.6: Boxplots of the time domain (a-d), the PDM (e,f) and the residual OSP (g,h) parameters of baseline (in blue) and immersion (in red) stages in the HC, CD and UD datasets. Significant differences between stages of the same dataset are represented by a double arrow (dotted if p−value≤0.05, dashed if p−value≤0.01 and solid if p−value≤0.001).

$pNN50$ did not change. $PDMsymp$ did not show differences between stages but $PDMpara$ presented a significant increase from spontaneous to simulated scuba mask breathing stage. Regarding OSP parameters, Table 5.5 shows the total power of the respiratory and the residual components of OSP for spontaneous vs. simulated scuba mask breathing. $P_\perp$ was significantly higher than P_R in both stages. For OSP residual parameters in Figure 5.7, $P_{HF\perp}$ increased when subjects were breathing through their mouths.
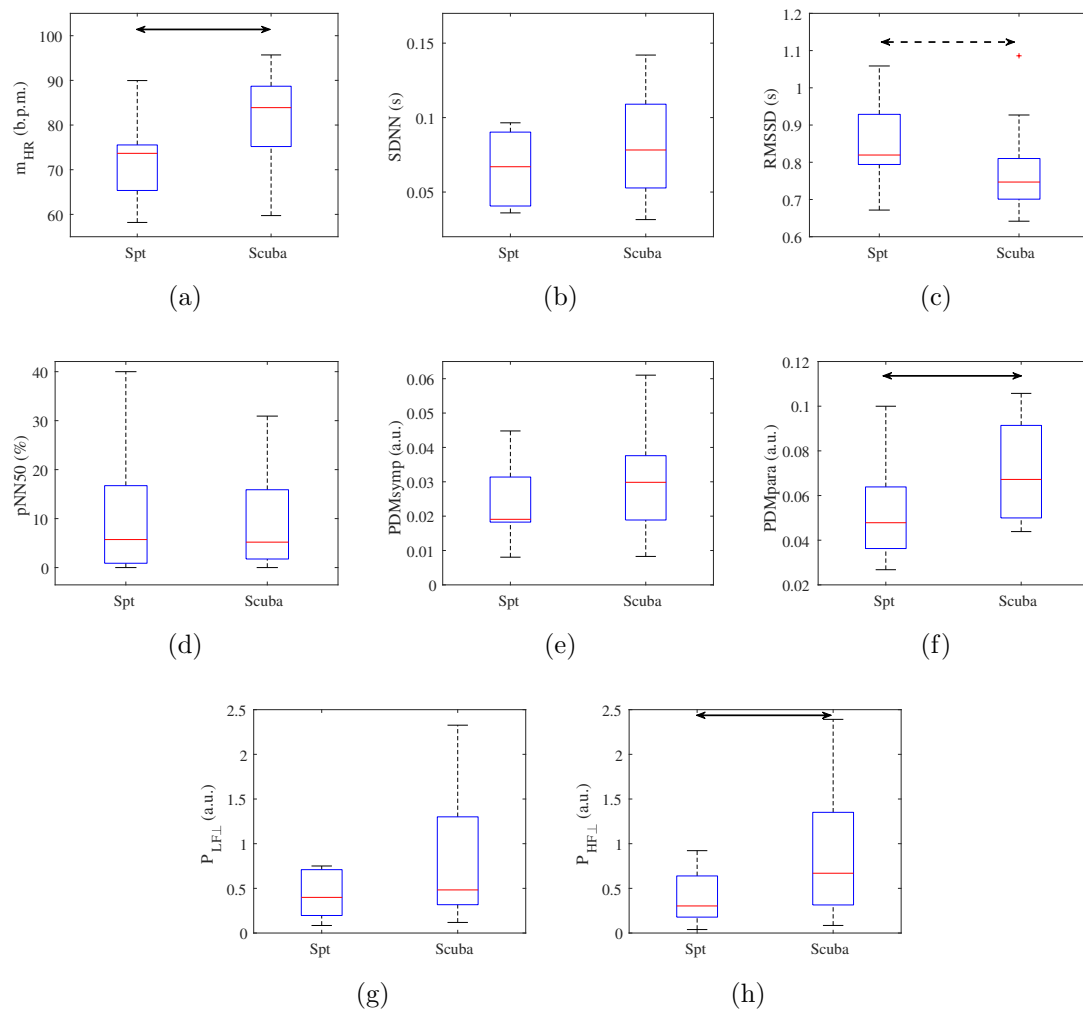
Figure 5.7: Boxplots of the time domain (a-d), the PDM (e,f) and residual OSP (g,h) parameters during spontaneous (Spt) and simulated scuba mask (scuba) breathing. Significant differences between stages are represented by a double arrow (dotted if $p-$value$\leq$0.05, dashed if $p-$value$\leq$0.01 and solid if $p-$value$\leq$0.001).

Table 5.5: Mean ± std of the total power of the respiratory and the residual components of OSP for spontaneous vs. simulated scuba mask breathing (Resp). Significant differences between P_R and $P_\perp$ are highlighted with a dagger ($p-$value$\leq$0.05).

	Spontaneous		Scuba mask	
	P_R	$P_\perp$	P_R	$P_\perp$
Resp	0.024±0.030	1.140±1.094 †	0.021±0.024	2.185±2.115 †

5.5   Discussion

The main goal of this Chapter is the study of the ANS response in three different hyperbaric environments: inside a hyperbaric chamber, where only the pressure varied; during a controlled dive in the sea, where the pressure changed but the effects of other factors were minimized; and during an uncontrolled dive in a reservoir, where more factors differed from baseline to immersion stage, such as the low visibility environment, the physical activity, the position of the diver and breathing through a scuba mask. A comparison of the HRV features between the two stages (baseline and immersion) in each dataset was carried out to study how these factors related to scuba diving activity affect the ANS response. To do this comparison, instead of the classic PSD methods, the PDM and the OSP methods were used to account for linear and non-linear interactions and to deal with the respiratory component that could affect the ANS response, respectively.

One important fact to be highlighted in this Chapter is the use of the ECG instead of the PPG signal, when in the three previous Chapters this last signal has been used. While in the HC dataset, both signals were registered, in the other two datasets only the ECG signal was recorded. In the UD dataset PPG was not recorded because the Nautilus device was attached in the diver's arm inside of the dry suit, and if the PPG sensor was located in the finger or in the forehead it could break the seal, making that the water entered inside the suit. In fact, the use of a dry suit in both immersions made that ECG could be properly recorded, since water did not enter inside the suit and therefore it can not alter or took of the electrodes located in the diver's chest. That is the reason why in this Chapter the ANS response was studied with the ECG signal.

Figure 5.4 presents the comparison of PSD, PDM and OSP methods for the HC dataset. Although PSD methods are widely spread in the literature, one of their main limitations occurs when the respiratory rate falls into the LF band (a frequent condition in experiments with scuba divers), since respiration is linked with the parasympathetic branch. It has been shown that changes in respiratory patterns alter the spectral content of HRV [75] and, consequently, the interpretation of sympathetic or vagal activations [76, 77, 78]. In fact, in Chapter 2 and in this Chapter, data from subjects with a respiratory rate below 0.15 Hz were discarded when PSD methods were used to avoid misinterpretations of the ANS response. In this Chapter, data from up to 5 subjects were discarded in some stages leading to comparisons among stages that used 20 subjects instead of 28 (the 71.43% of the total population). To avoid this limitation due to the respiratory rate, the OSP method [79, 130] is used in this work, since it is able to separate respiratory influences from the heart rate. Another limitation of the PSD methods is its incapability to account for the non-linear dynamics of HRV. That is the reason to use the PDM method, described in [14], since it is able to extract and separate the linear and non-linear sympathetic and parasympathetic dynamics of the ANS [34]. Coming back to the results in Figure 5.4, it can be seen that parasympathetic activity follows the same trend with the three different methods (P_{HF} with PSD, $PDMpara$ with PDM and $P_{HF\perp}$ with OSP), increasing their value until stage S5, and then decreasing until the end of the protocol. Also, sympathetic activity has similar behaviour with the three methods (P_{LFn} and $R_{LF/HF}$ with PSD, $PDMsymp$ with PDM and $P_{LF\perp}$ with OSP) increasing their value from the beginning to the S5 stage, and then suddenly decreasing their value until a minimum in the two last stages. Therefore, HRV analysis with OSP and PDM methods allows to properly characterize the ANS response inside the hyperbaric chamber, circumventing the respiratory rate limitation that would have forced us to eliminate some data and also allowing to analyze the linear and non-linear dynamics of the ANS response.

Next, a comparison among parameters extracted from 5 minutes recordings and from 3 minutes recordings was performed. This comparison was done because some recent works suggest that less than 5 minutes recordings may not be sufficient to assess HRV parameters accurately [131, 132], although the Task Force said that 2

minutes would be time enough for frequency domain parameters [27]. This 3 minutes temporal slot was chosen for comparison among the three datasets, since subjects remained below 15 m for only 3 minutes in the uncontrolled dive in the reservoir. Time domain parameters did not show differences due to the time slot duration, with a correlation higher than 90% in $SDNN$ and higher than 98% in the other three parameters (see Figure 5.5). The same trend among 5 and 3 minutes recordings was found in the classic frequency domain parameters extracted from PSD methods, with a correlation higher than 90% in all stages and for the four parameters, except in stages S5 and S3A in P_{LF}, with a correlation of 84%. PDM parameters showed the lowest correlation (from 55% to 89%) between 5 and 3 minutes parameters. This could be due to in 3 minutes there were not enough samples in HC dataset for a reliable measure. Although there is not a standard minimum number of samples for a reliable measure with non-linear parameters [138], in other works that used this PDM technique at least 300 samples were used [14, 34]. This 300 samples were not reached in 3 minutes recordings, but they were reached in 5 minutes recordings of HC dataset. Despite these worse correlation results, the paired t-test did not show significant differences among 5 and 3 minutes recordings in HC dataset and the trend of $PDMpara$ and $PDMsymp$ among stages was not affected, decreasing or increasing their value in both parameters at the same time. OSP parameters also did not show differences due to the time slot duration, with a correlation higher than 90% in all stages for the two parameters, except in the S3A stage in $P_{LF\perp}$, with a correlation of 87%.

Another difference between this Chapter and other hyperbaric studies is the selection of the temporal window for analyses. While other works has used a middle-to-final time range windows to compare different stages, to account for the adaptation of the diver's body to the hyperbaric conditions [12, 14, 15, 17], in our case we have selected the first 3 minutes. This temporal window allowed to study how quickly the body adapted to the hyperbaric environment. In [14], a continuous study of a 30 minutes immersion at 66 ft was performed and significant differences with respect to baseline stage were already found in the first 5 minutes, so the selection of the first 3 minutes should not imply a limitation of this study.

One of the main results of this Chapter is the lower power in the OSP respiratory component with respect to the residual OSP component, as Table 5.4 shows. This suggests that cardio-respiratory coupling is reduced in these hyperbaric scenarios, so most of the variations in the heart rate cannot be described by changes in the respiration, but they can be explained by changes in other factors. Therefore, a careful description of each stage in the dataset, with a description of all the changes related to important factors that may affect the ANS response, is needed. The three different analyzed datasets have a similar protocol: one stage of baseline and another stage of immersion, with a pressure around 3 atm. In the two stages of the hyperbaric chamber dataset, subjects remained seated comfortably without talking and the chamber was ventilated to avoid big temperature differences. The only difference between the two stages was the pressure, so its effect on the ANS response can be measured with this dataset. During the controlled dive in the sea, both stages were very similar also: divers remained in horizontal, with all the equipment and breathing through their scuba masks. The only difference was their location: in the baseline stage they were on the water surface, with their heads out of the water, and in the immersion stage they were at a depth of 20 m. It must be highlighted how different this baseline stage was from the hyperbaric chamber baseline stage: both baseline stages were so different between them because the main aim in these two datasets was to maintain baseline and immersion stages as similar as possible, to study only the pressure differences in the ANS response. However, the possible effects of cold water and currents in the immersion stage in the controlled dive in the sea has to be taken into account. Finally, the uncontrolled dive in the reservoir presents more differences between its two stages. In baseline, subjects remained sitting comfortably, outside the water, without diving equipment and breathing spontaneously, as this stage is similar to the HC baseline but very different to the CD baseline. During reservoir immersion, subjects performed a physical activity in pairs, under the water, with low visibility, with all their equipment, and breathing through scuba masks. Therefore, in our opinion, in this dataset not only the effect of the pressure, but also the effect of an environment with low visibility, physical activity, body position and scuba mask breathing could be analyzed.

Although pressure changes occurred in all three experiments, it is only in the first two where the effect of pressure can be isolated, to learn how pressure changes affects ANS response. In both datasets, there is a significant decrease in mHR and a significant increase in the rest of time domain parameters from the baseline to the immersion stage. The heart rate decrease has been reported previously in hyperbaric chamber studies [1, 15, 16, 17] and in immersion data [10, 12, 13, 14]. The possible reason for this bradycardia could be the effect of the diving reflex and the effect of the pressure [122, 139]. The significant increase in the rest of the temporal parameters (especially in $RMSSD$), together with the decrease in the mHR, seems to point out an increase in the parasympathetic activity or a decrease in the sympathetic one. However, PDM results do not show any significant change during the immersion in the parasympathetic activity ($PDMpara$) in HC and CD. The lack of parasympathetic activity due to the pressure in the hyperbaric chamber is in agreement with results in Section 2.4, where no differences were found between the first two stages. One possible factor that may affect this measure is the descent speed. In the HC protocol, it took from 5-7 minutes to transition from 1 atm to 3 atm, although this time was significantly shorter in real immersions (less than 2 minutes for an experimented diver). This slow descent could be less demanding for the subject to adapt to, and this could be a reason why no significant difference in parasympathetic activity was found in the HC data. The descent duration were not reported in the other studies. In CD, there was an increase in $PDMpara$ during immersion, but it was not statistically significant ($p-$value $= 0.1$). Concerning the sympathetic activity, a decrease in $PDMsymp$ was found in HC, that could explain the trends in the time domain parameters. In contrast, an increase in $PDMsymp$ was observed in CD. This increase could be explained by the fact that diving in deeper and colder water with greater current strength will cause substantial stress on even the most experienced divers, so this increase in the sympathetic activity possibly is not related to the pressure changes. On the other hand, the OSP method shows a lower power in the respiratory component with respect to the residual component for HC data, which indicates that most of the variations in the heart rate are not produced by changes in the respiration. Therefore, the study of the power in the LF and HF bands of the residual component could give some information about the two

branches of the ANS. There is an increase in $P_{HF\perp}$ that points to an activation of the parasympathetic activity, and this may be due to the effect of pressure as previous studies suggests [1, 15, 16, 17]. In sum, pressure changes have an impact on time domain parameters, with a decrease in mHR and an increase in $SDNN$, $RMSSD$ and $pNN50$, but the effect of pressure changes is not so clear in the frequency domain parameters: while $P_{HF\perp}$ from the OSP method could reflect a significant increase in the parasympathetic activity during immersion, $PDMpara$ from the PDM method does not show this change; however, a decrease in $PDMsymp$ is found in HC, and this sympathetic decrease could explain the results of the time domain parameters.

Finally, results from the uncontrolled reservoir dive show the opposite trend in temporal parameters than those from the hyperbaric chamber and the controlled sea dive. In UD results, a significant increase in mHR and a decrease in the other three time domain parameters (significant in $RMSSD$) are shown. This suggests an activation of the sympathetic system, as the increases in $PDMsymp$ and $P_{LF\perp}$ confirm. This activation could be explained by different factors: one could be the predominance of the physical activity and the stress of the challenging environment during the immersion. In fact, it has been proved that physical activity during immersion increase the sympathetic tone [140]. Another factor is the stress related to the immersion: some studies have pointed out that an immersion performing a stressful task could increase the heart rate and the sympathetic activity [11]. Therefore, physical activity and stress during the immersion, together with the low visibility environment, that could increase even more the stress of the immersion, and the effect of cold water, that also increases the heart rate [20, 141], contribute to the predominance of the sympathetic activity. There is also an increase in the parasympathetic activity in the UD data. UD is the only dataset with significant differences between stages in $PDMpara$ and in $P_{HF\perp}$ ($p-$value $< 10^{-5}$). This could imply that other factors, apart from the pressure, have some effect over the vagal tone. In fact, there was a last factor that affects the UD dataset: the difference in the way of breathing, spontaneous in the baseline stage versus through a scuba mask in the immersion stage. It must be highlighted that UD is the only dataset where this difference in the way of breathing between its stages exists, since in the CD dataset subjects were breathing through the scuba mask for both stages. To our understanding, there is no

previous works studying the difference between these two types of breathing. This is why we recorded a small dataset of 12 subjects, first breathing spontaneously and then inhaling and exhaling deeply and slightly more rapidly through the mouth, as if they were wearing a scuba mask and breathing through a regulator. As Figure 5.7 shows, there was an activation of the parasympathetic activity. $PDMpara$ increases from spontaneous breathing to simulated scuba mask breathing in all the subjects, so this factor could explain, together with the effect of pressure, the increase of the parasympathetic activity in the UD dataset. However, time and frequency domain parameters in the breathing dataset seem to be contradictory. It must be noticed that these results for the way of breathing (increase in mHR and $PDMpara$ and decrease in $RMSSD$) have the same trend as the results of the uncontrolled dive, so may be this factor has more significance in the ANS response than expected. Therefore, the factor of how the divers are breathing during the different stages of a diving protocol should be taken into account for future studies.

In spite of the differences in the datasets, a comparison of the baseline stages were performed. The baseline stage in the HC data was similar to that in the UD, but both were different with respect to the baseline stage in the CD data. Differences of body position (sitting vs. supine position), environment (on land vs. in cold water) and breathing (spontaneous vs. through a scuba mask) were analyzed in this baseline comparison. An increase in the mHR and a decrease in the rest of the time domain parameters, comparing the first stage of CD with respect to HC and UD, is shown in Figure 5.6. According to the literature, there is no significant change in heart rate between sitting and supine position [142] and between being outside the water or immersed with the head out [10]. However, the effect of cold water and the effect of breathing through the scuba mask increases the heart rate, as we have discussed before. Therefore, the effect of breathing through the scuba mask seems to be again an important factor when comparing the baseline stages of the three datasets.

Finally, as a limitation of this study, the number of scuba divers in both immersions (11 and 15) has to be highlighted. Nevertheless, the difficulty of recruiting experienced scuba divers has to be taken into account. In fact, in other hyperbaric studies this problem is recurrent: 10 subjects or less in [1, 12, 13, 16, 17]. Another

possible limitation is the fact that divers in the uncontrolled immersion spent only a limited time below 15 m, and because of this, the length of the selected segment for the analysis was restricted. As future studies, the recording of more scuba divers, the recording of a new immersion dataset with more time to be analyzed and the recording of deeper immersions, recording the PPG signal in all of them, should be done.

5.6 Conclusion

The main outcome of this Chapter is the comparison of three different hyperbaric environments, taking into account the effect of pressure, cold water and physical activity during the immersion among other variables. To do that, OSP and PDM methods were used to overcome the limitations of classic PSD frequency domain parameters when the respiratory rate fell in the LF band and in the account of linear and non-linear properties. Results show that the respiratory component does not have a great impact on the heart rate variability, so the effect of other factors could explain the differences between the responses of the two branches of the ANS. The effect of pressure can cause an increase in the parasympathetic activity, although this trend is not always found and differences between stages are not always significant. On the other hand, the effect of cold water, together with an environment with low visibility and physical activity during the immersion, may cause an increase in sympathetic activity. Finally, the effect of breathing through a scuba mask may cause an increase in the heart rate, but also an increase in the parasympathetic activity.

Chapter 6

Conclusions and future work

6.1 Summary and conclusions

The main aim of this dissertation is the non-invasive assessment of ANS activity and the response of the cardio-respiratory system in hyperbaric environments. For this purpose, this thesis was divided in four different parts. In the first one, a study to corroborate that PRV signal is a surrogate measurement of HRV signal in a hyperbaric chamber was performed. In the second one, the capability of extracting the respiratory rate from the PPG signal was tested, in order to evaluate the possibility of only use this signal to evaluate the ANS response. In Chapter 4, a new algorithm capable to extract parameters related to PPG morphology that are able to distinguish changes in its waveform, at least in hyperbaric environments, was presented. Finally, a study of the ANS response in three different hyperbaric environments, one in a hyperbaric chamber and two in real immersions, where some factors, as the pressure, the physical activity or the way of breathing varied, was performed with two different methods that allow us to overcome the limitations of the classic frequency domain analysis.

For the first purpose, ECG and PPG signals were recorded in subjects inside a hyperbaric chamber with five different stages where the pressure varied (from 1 atm increasing to 3 and 5 atm and then decreasing to 3 and 1 atm). The main goal of Chapter 2 was to corroborate if PRV signal extracted from the PPG provided the same information as the HRV signal extracted from the ECG, in terms of ANS

response. To that end, an analysis of time and frequency domain parameters obtained from the HRV and PRV signals was performed. Respiratory information was included in the frequency domain parameters combining the estimations of respiratory rate extracted from ECG and PPG signals. The correlation and statistical measurements of parameters extracted from both signals showed that PRV signal could be used as a surrogate measurement of HRV signal in hyperbaric environments. This, together with the fact that PPG sensor is an cheaper device which is easier to locate in any part of the body and with PPG providing some useful information as the oxygen saturation that ECG does not, made PPG a suitable tool to extract ANS information only by itself. Apart from this, also a characterization of how the ANS reacted to pressure changes and the time spent in the hyperbaric environment was done with this dataset. The principal conclusion of the ANS response was that P_{HF}, which is related with the parasympathetic activity, increased in those stages when the atmospheric pressure was high, and the heart rate and the sympathetic markers (P_{LFn} and $R_{LF/HF}$) decreased as more time was spent inside the chamber.

Respiratory information could alter the spectral content of the frequency domain parameters, therefore it is important to include the respiratory information in the study of the ANS response. In Chapter 2, this information was included combining algorithms that extracted respiratory rate from ECG and PPG signals. If only the PPG signal wants to be used, since the main conclusion of Chapter 2 was that PRV can be used to evaluate ANS response, a study of how reliable is the respiratory information extracted from the PPG is needed. This is the reason why, in Chapter 3, an evaluation of how the location of the PPG sensor affects the respiratory rate estimation and which PDR signals are more appropriated to this purpose was performed. PPG signals were recorded on finger and forehead from subjects breathing spontaneously and at different controlled respiratory rates. 4 PDR signals (PRV, PAV, PWV and RIIV) were extracted from both locations of the PPG signals, obtaining one respiratory rate estimation per PDR signal and also from all the possible combinations of them. The estimations were compared with the respiratory rate estimated from chest-band, which was taken as reference. The respiratory estimation were considered accurate if it differ less than 0.05 Hz (0.3 bpm) from the reference, based on the errors reported in previous works [73]. The success rate and the relative

error of the estimated respiratory rate from both locations were presented, as well as a confusion matrix for each PDR signal to evaluate their performance, and the power distribution of the respiratory information in the averaged spectrum. A better performance in the low frequencies was observed, in particular when the sensor was located in the finger. Therefore, one of the main conclusions of this Chapter was that finger is a best place to locate the PPG sensor than forehead, although the global results was not as good as we thought. Talking about each individual PDR signal, RIIV showed a poor performance and it affected negatively to the accuracy of the estimation when it was combined with other PDR signals; PRV in finger obtained good results in lower frequencies; PAV in finger also obtained good results at lower frequencies and the best results at higher frequencies; PWV was the one with less differences between finger and forehead. Therefore, another conclusion of this Chapter was to discard RIIV as a proper PDR signal to obtain respiratory rate estimations and to analyze the inclusion of the rest of PDR signals in the fusion algorithm depending on the final application, considering both the subject population and the breathing pattern.

In Chapter 2, the main conclusion was that PRV is a surrogate measurement of HRV signal to measure ANS activity, but not only PRV contains information about the ANS response. Also, PPG morphology can provide a great amount of information about vascular assessment or arterial compliance, since pulse pressure propagation in arteries causes alterations in blood volume and therefore changes in the PPG pulse shape. Therefore, in Chapter 4, changes in PPG morphology due to the pressure were analyzed using the hyperbaric chamber dataset. In fact, to obtain these parameters related to the PPG morphology, a new methodology to decompose the PPG pulse into two waves related with the systolic and the diastolic peaks was presented. The first wave was obtained concatenating the up-slope from the beginning to the first maximum with itself flipped horizontally. The second wave was modelled by a lognormal curve, adjusting its maximum to the diastolic peak (this happened only if the temporal location of the maximum is higher than the 35% of the pulse wave duration) and varying μ and σ in order to minimize the difference between the lognormal wave and the resulting pulse waveform. From these two waves, the amplitude, the time of their maximum, the width and the area

under these curves were calculated, together with some ratios and other parameters extracted from the literature as the large artery stiffness index, to find out if there were changes in these parameters due to the pressure. Results of the time and width of the wave related with the systolic peak pointed out to a vasoconstriction when the pressure increased and results of the time and width of the wave related with the diastolic peak reflected the vasoconstriction but also a dependency with the pulse-to-pulse interval. Therefore this methodology offers an alternative to extract parameters related to PPG morphology that are able to distinguish changes in its waveform, at least in hyperbaric environments.

In Chapter 2, the ANS response inside a hyperbaric chamber, where only the pressure changed, was analyzed. However, in a real immersion more factors as the physical activity, the cold water or the way of breathing, could alter the ANS response. Therefore, in Chapter 5 a study of the ANS response in three different hyperbaric datasets was analyzed: inside the hyperbaric chamber, where only the pressure varied; during a controlled dive in the sea, where the pressure changed but the effects of other factors were minimized; and during an uncontrolled dive in a reservoir, where more factors differed from baseline to immersion stage, such as the low visibility environment, the physical activity, the position of the diver and breathing through a scuba mask. Another issue with results in Chapter 2 were the limitations of classic PSD frequency domain parameters: i) PSD is a linear technique, so it fails to account for non-linear properties of HRV; ii) PSD depends on the respiration, overestimating the power in LF band when respiratory rate falls into this band. Therefore two new methods were presented in Chapter 5 to overcome the limitations of PSD methods: i) PDM method, which is able to extract and separate sympathetic and parasympathetic dynamics and handles linear and non-linear relationships; ii) OSP method, which is able to separate the linearly related respiratory influences from the HRV. With the use of these methods, it was concluded that the respiratory component did not have a great impact on the heart rate variability, so the effect of other factors could explain the differences between the responses of the two branches of the ANS. Coming back to the study of the three hyperbaric datasets, the effect of different factors that alter the ANS response were considered. For example, the effect of pressure caused an increase in the parasympathetic activ-

ity, although this trend was not always found and differences between stages were not always significant. On the other hand, the effect of cold water, together with an environment with low visibility and physical activity during the immersion, may caused an increase in sympathetic activity. Finally, the effect of breathing through a scuba mask may caused an increase in the heart rate, but also an increase in the parasympathetic activity.

6.2   Future work

- Create and validate a new PPG sensor compatible with the dive, capable of recording good quality signal without breaking the seal of the scuba diving dry suit.

- Corroborate if results in a humid hyperbaric chamber differ from the ones obtained in a dry hyperbaric chamber. The main difference among these two types of chambers lies in the fact that the humid one is filled with water, simulating a real immersion. With the humid chamber, the effect of the water, apart from the pressure, can be characterized. Factors as the hydrostatic pressure that shifts the body circulation, the fact of having the face immersed in the water, and the water temperature could modify the ANS response.

- Increase the number of subjects during an uncontrolled diving, increasing also the time spent in the maximum depth. If we want to analyze the ANS response properly, the more subjects we have, the better this response could be analyzed. Apart from increasing the number of subjects, it would be necessary to increase the time spent in the maximum depth, since not all the responses the body creates to maintain the homeostasis are instantaneous, some of them could need some time to appear and modify the ANS response.

- Characterize the safety ranges of all the possible parameters analyzed during an exposure to hyperbaric environments. If we are able to characterize the normal ANS response maybe we could find the ranges of the parameters that indicates how secure is the diving activity and therefore increase the divers safety by continuous monitoring.

- Be able of extract physiological and morphological parameters from the ECG and/or the PPG in real time during the exposure to hyperbaric environments. This part, together with the characterization of the safety ranges during the diving, could inform the divers in real time about the security of their activity, increasing the safety of the dive.

Scientific contributions

Journal publications

- **A. Hernando**, M.D. Peláez-Coca, M.T. Lozano, M. Aiger, David Izquierdo, A. Sánchez, M.I. López-Jurado, I. Moura, J. Fidalgo, J. Lázaro and E. Gil, "Autonomic nervous system measurement in hyperbaric environments using ECG and PPG signals", *IEEE Journal of Biomedical and Health Informatics*, vol. 23, n. 1, pp. 132-142, 2019. DOI: 10.1109/JBHI.2018.2797982.

- M.D. Peláez-Coca, M.T. Lozano, **A. Hernando**, M. Aiger and E. Gil, "Photoplethysmographic Waveform Versus Heart Rate Variability to Identify Low Stress States. Attention Test", *IEEE Journal of Biomedical and Health Informatics*, vol. 23, n. 5, pp. 1940-1951, 2019. DOI: 10.1109/JBHI.2018.2882142.

- C. Varon, J. Lázaro, J. Bolea, **A. Hernando**, J. Aguiló, E. Gil, S. Van Huffel and R. Bailón, "Unconstrained Estimation of HRV Indices after Removing Respiratory Influences from Heart Rate", *IEEE Journal of Biomedical and Health Informatics*, vol. 23, n. 6, pp. 2386-2397, 2019. DOI: 10.1109/JBHI.2018.2884644.

- **A. Hernando**, M.D. Peláez-Coca, M.T. Lozano, J. Lázaro and E. Gil, "Finger and forehead PPG signal comparison for respiratory rate estimation", *Physiological Measurement*, vol. 40, n. 9, pp. 095007, 2019. DOI: 10.1088/1361-6579/ab3be0.

- M.D. Peláez-Coca, **A. Hernando**, M.T. Lozano, C. Sánchez, D. Izquierdo and E. Gil, "Photoplethysmographic Waveform and Pulse Rate Variability

Analysis in Hyperbaric Environments", *IEEE Journal of Biomedical and Health Informatics*, 2020. DOI: 10.1109/JBHI.2020.3020743.

- **A. Hernando**, M.D. Peláez-Coca and E. Gil, "Photoplethysmogram waveform decomposition into systolic and diastolic waves for Autonomic Nervous System characterization in hyperbaric environments", *IEEE Transactions on Biomedical Engineering, Under Review.*

- **A. Hernando**, H. Posada-Quintero, M.D. Peláez-Coca, E. Gil and K.H. Chon, "Respiratory component and non-linear analysis of Heart Rate Variability for Autonomic Nervous System characterization in hyperbaric environments", *Computer Methods and Programs in Biomedicine, Under review.*

Conference publications

- **A. Hernando**, M.D. Peláez-Coca, M.T. Lozano, M. Aiger, E. Gil and J. Lázaro, "Finger and Forehead PPG Signal Comparison for Respiratory Rate Estimation Based on Pulse Amplitude Variability", *25th European Signal Processing Conference (EUSIPCO)*, Kos, Greece, pp. 2130-2134, 2017. DOI: 10.23919/EUSIPCO.2017.8081575

- C. Varon, J. Lázaro, **A. Hernando**, A. Caicedo, S. Van Huffel and R. Bailón, "Removal of Respiratory Influences from Heart Rate During Emotional Stress", *Proceedings of the XLIV International Conference on Computing in Cardiology (CinC)*, Rennes, France, 2017. DOI: 10.22489/CinC.2017.264-160.

- M.D. Peláez-Coca, M.T. Lozano, M. Aiger, **A. Hernando** and E. Gil, "Significant Physiological Features to Identify High Performance States", *Proceedings of the XLIV International Conference on Computing in Cardiology (CinC)*, Rennes, France, 2017. DOI: 10.22489/CinC.2017.280-141.

- C. Sánchez, M.D. Peláez-Coca, M.T. Lozano, M. Aiger, **A. Hernando** and E. Gil, "Autonomic Nervous System Non-stationary Response to Controlled Changes in Barometric Pressure", *Proceedings of the XLIV International Conference on Computing in Cardiology*, Rennes, France, 2017. DOI: 10.22489/ CinC.2017.281-333.

- C. Pérez, M.D. Peláez-Coca, **A. Hernando**, E. Gil and C. Sánchez, "Multivariable Relationships between Autonomic Nervous System Related Indices in Hyperbaric Environments", *41st Annual International Conference of the IEEE Engineering in Medicine & Biology Society (EMBC)*, Berlín, Germany, pp. 6789-6793, 2019. DOI: 10.1109/EMBC.2019.8856374.

- M.D. Peláez-Coca, **A. Hernando**, C. Sánchez, M.T. Lozano, D. Izquierdo and E. Gil, "Photoplethysmographic Waveform in Hyperbaric Environment", *41st Annual International Conference of the IEEE Engineering in Medicine & Biology Society (EMBC)*, Berlín, Germany, pp. 3490-3493, 2019. DOI: 10.1109/EMBC.2019.8856400.

- **A. Hernando**, M.D. Peláez-Coca, C. Sánchez, J. Bolea, D. Izquierdo, M.T. Lozano and E. Gil, "Autonomic Nervous System Response During Scuba Diving Activity", *Proceedings of the XLVII International Conference on Computing in Cardiology (CinC)*, Rimini, Italy, 2020. DOI: 10.22489/CinC.2020.308.

- C. Sánchez, **A. Hernando**, J. Bolea, D. Izquierdo, M.T. Lozano and M.D. Peláez-Coca, "Safety Ranges for Heart Rate Variability Parameters in Hyperbaric Environments", *Proceedings of the XLVII International Conference on Computing in Cardiology (CinC)*, Rimini, Italy, 2020. DOI: 10.22489/CinC. 2020.094.

Journal publications non related with the thesis

- **A. Hernando**, J. Lázaro, E. Gil, A. Arza, J.M. Garzón, R. López-Antón, C. de la Cámara, P. Laguna, J. Aguiló and R. Bailón, "Inclusion of respiratory frequency information in heart rate variability analysis for stress assessment", *IEEE Journal of Biomedical and Health Informatics*, vol. 20, n. 4, pp. 1016-1025, 2016. DOI: 10.1109/JBHI.2016.2553578.

- D. Hernando, **A. Hernando**, J.A. Casajús, P. Laguna, N. Garatachea and R. Bailón, "Methodological Framework for Heart Rate Variability Analysis During Exercise: Application to Running and Cycling Stress Testing", *Medical & Biological Engineering & Computing*, vol. 56, pp. 781-794, 2018. DOI: 10.1007/s11517-017-1724-9.

- M.D. Peláez-Coca, **A. Hernando**, J. Lázaro and E. Gil, "Impact of the PPG sampling rate in the pulse rate variability indices evaluating several fiducial points in different pulse waveforms", *IEEE Journal of Biomedical and Health Informatics, Under Review.*

List of Acronyms

scuba self-contained underwater breathing apparatus

ANS Autonomic Nervous System

HRV Heart Rate Variability

ECG electrocardiogram

PPG pulse-photoplethysmography

PRV Pulse Rate Variability

DCS decompression sickness

IPFM integral pulse frequency modulation

TVIPFM time-varying integral pulse frequency modulation

VLF very low frequency

LF low frequency

HF high frequency

PDM Principal Dynamic Mode

RSA respiratory sinus arrhythmia

OSP Orthogonal Subspace Projection

BP Blood pressure

PTT pulse transit time

RI Reflection Index

SI large artery stiffness

FM Frequency modulation

AM Amplitude modulation

BM Baseline modulation

EDR ECG derived respiratory

PDR PPG derived respiratory

PAV Pulse Amplitude Variability

PWV Pulse Width Variability

RIIV respiratory-induced intensity variability

RIFV respiratory-induced frequency variation

RIAV respiratory-induced amplitude variation

FIR finite impulse response

PSD Power Spectral Distribution

SD standard deviation

PDA Pulse Decomposition Analysis

HC Hyperbaric Chamber

CD Controlled Dive

UD Uncontrolled Dive

TV-OPS Time Variant-Optimal Parameter Search

FFT   Fast Fourier Transform

AR   autoregressive

List of Figures

List of Tables

Bibliography

[1] V Lund, E Kentala, H Scheinin, J Klossner, K Sariola-Heinonen, and J Jalonen. Hyperbaric oxygen increases parasympathetic activity in professional divers. *Acta Physiologica Scandinavica*, 170(1):39–44, 2000.

[2] D Z Levett and I L Millar. Bubble trouble: a review of diving physiology and disease. *Postgraduate Medical Journal*, 84:571–578, 2008.

[3] A E Draghici and J A Taylor. The physiological basis and measurement of heart rate variability in humans. *Journal of Physiological Anthropology*, 35(22), 2016.

[4] S Lu, H Zhao, K Ju, K Shin, M Lee, K Shelley, and K H Chon. Can photoplethysmography variability serve as an alternative approach to obtain heart rate variability information? *Journal of Clinical Monitoring and Computing*, 22:23–29, 2008.

[5] N Selvaraj, A K Jaryal, J Santhosh, K K Deepak, and S Anand. Assessment of heart rate variability derived from finger-tip photoplethysmography as compared to electrocardiography. *Journal of Medical Engineering and Technology*, 32:479–484, 2008.

[6] K Charlot, J Cornolo, J V Brugniaux, J P Richalet, and A Pichon. Interchangeability between heart rate and photoplethysmography variabilities during sympathetic stimulations. *Physiological Measurement*, 30:1357–1369, 2009.

[7] E Gil, M Orini, R Bailón, J M Vergara, L Mainardi, and P Laguna. Photoplethysmography pulse rate variability as a surrogate measurement of heart rate variability during non-stationary conditions. *Physiological Measurement*, 31:1271–1290, 2010.

[8] I Constant, D Laude, I Murat, and J L Elghozi. Pulse rate variability is not a surrogate for heart rate variability. *Clinical Science*, 97:391–397, 1999.

[9] Y Li, H Yan, Z Xu, M Wei, B Zhang, and Z Shi. Analysis of the changes in photoplethysmogram induced by exercise stress. *Journal of Medical Imaging and Health Informatics*, 33(3):347–355, 2013.

[10] J D Schipke and M Pelzer. Effect of immersion, submersion, and scuba diving on heart rate variability. *British Journal of Sports Medicine*, 35:174–180, 2001.

[11] A D Flouris and J M Scott. Heart rate variability responses to a psychologically challenging scuba dive. *Journal of Sports Medicine and Physical Fitness*, 49(4):382–386, 2009.

[12] F Chouchou, V Pichot, M Garet, J C Barthelemy, and F Roche. Dominance in cardiac parasympathetic activity during real recreational scuba diving. *European Journal of Applied Physiology*, 106:345–352, 2009.

[13] N T Berry, L Wideman, C K Rhea, J D Labban, K H Chon, B Shykoff, F J Haran, and J P Florian. Effects of prolonged and repeated immersions on heart rate variability and complexity in military divers. *Undersea and Hyperbaric Medicine*, 44:560–589, 2017.

[14] Y Noh, H Posada-Quintero, Y Bai, J White, J P Florian, P R Brink, and K H Chon. Effect of shallow and deep scuba dives on heart rate variability. *Frontiers in Physiology*, 9:110, 2018.

[15] E Barbosa, J M García-Manso, J M Martín-González, S Sarmiento, F J Calderón, and M E Da Silva-Grigoletto. Effect of hyperbaric pressure during scuba diving on autonomic modulation of the cardiac response:application of the continuous wavelet transform to the analysis of heart rate variability. *Military Medicine*, 175(1):61–64, 2010.

[16] V Lund, E Kentala, H Scheinin, J Klossner, H Helenius, K Sariola-Heinonen, and J Jalonen. Heart rate variability in healthy volunteers during normobaric and hyperbaric hyperoxia. *Acta Physiologica Scandinavica*, 167:29–35, 1999.

[17] V Lund, J Laine, T Laitio, E Kentala, J Jalonen, and H Scheinin. Instantaneous beat-to-beat variability reflects vagal tone during hyperbaric hyperoxia. *Undersea and hyperbaric medicine*, 30:29–36, 2003.

[18] K Yamauchi, Y Tsutsui, Y Endo, S Sagawa, F Yamazaki, and K Shiraki. Sympathetic nervous and hemodynamic responses to lower body negative pressure in hyperbaria in men. *American Journal of Physiology Regulatory, Integrative and Comparative Physiology*, 282:R38–R45, 2002.

[19] T Mano, S Iwase, Y Yamazaki, and M Saito. Sympathetic nervous adjustments in man to simulated weightlessness induced by water immersion. *Journal of UOEH*, 7:215–227, 1985.

[20] P Šrámek, M Šimečková, L Janský, J Šavlíková, and S Vybíral. Human physiological responses to immersion into water of different temperatures. *European Journal of Applied Physiology*, 81(5):436–442, 2000.

[21] E Gempp and P Louge. Inner ear decompression sickness in scuba divers: a review of 115 cases. *European Archives of Oto-Rhino-Laryngology*, 270:1831–1837, 2013.

[22] R W Smerz. A descriptive epidemiological analysis of isolated inner ear decompression illness in recreational divers in hawaii. *Diving and Hyperbaric Medicine*, 37:2–9, 2007.

[23] A C Guyton and J E Hall. *Textbook of medical physiology*. Elsevier Inc., 2006.

[24] L McCorry. Physiology of the autonomic nervous system. *American Journal of Pharmaceutical Education*, 71(4):78, 2007.

[25] R Hainsworth. *Heart rate variability, chapter 1: The control and physiological importance of heart rate*. Futura Publishing Company, Inc, 1995.

[26] L Sörnmo and P Laguna. *Bioelectrical Signal Processing in Cardiac and Neurological Applications*. Elsevier, 2005.

[27] Task Force of the European Society of Cardiology, the North American Society of Pacing, and Electrophysiology. Heart rate variability: Standards of measurement, physiological interpretation, and clinical use. *European Heart Journal*, 17:354–381, 1996.

[28] E J Bayly. Spectral analysis of pulse frequency modulation in the nervous systems. *IEEE Transactions on Biomedical Engineering*, 15:257–265, 1968.

[29] J Mateo and P Laguna. Improved heart rate variability signal analysis from the beat occurrence times according to the ipfm model. *IEEE Transactions on Biomedical Engineering*, 47(8):985–996, 2000.

[30] R Bailón, G Laouini, C Grao, M Orini, P Laguna, and O Meste. The integral pulse frequency modulation with time-varying threshold: Application to heart rate variability analysis during exercise stress testing. *IEEE Transactions on Biomedical Engineering*, 58(3):642–652, 2011.

[31] N Aimie-Salleh, M Balakrishnan, and A Whittaker. Stress response index for adverse childhood experience based on fusion of biomarkers. In *Proceedings of IEEE-EMBS Conference on Biomedical Engineering and Sciences (IECBES)*, 2018.

[32] S Akselrod and D Gorodon. Power spectrum analysis of heart rate fluctuation: A quantitative probe of beat-to-beat cardiovascular control. *Science*, 213:220–222, 1981.

[33] A Malliani. The pattern of sympathovagal balance explored in the frequency domain. *Physiology*, 14(3):111–117, 1999.

[34] Y Zhong, H Wang, K H Ju, K Jan, and K H Chon. Nonlinear analysis of the separate contributions of autonomic nervous systems to heart rate variability using principal dynamic modes. *IEEE Transactions on Biomedical Engineering*, 51(2):255–262, 2004.

[35] A B Hertzman and C Spielman. Observations on the finger volume pulse recorded photoelectrically. *American Journal of Physiology*, 119:334–335, 1937.

[36] A V Challoner. *Non-Invasive Physiological Measurements*. Academic Press, 1979.

[37] I Yoshiya, Y Shimada, and K Tanaka. Spectrophotometric monitoring of arterial oxygen saturation in the fingertip. *Medical and Biological Engineering and Computing*, 18:27–32, 1980.

[38] V Hartmann, H Liu, F Chen, Q Qiu, S Hughes, and D Zhenq. Quantitative comparison of photoplethysmographic waveform characteristics: Effect of measurement site. *Frontiers in Physiology*, 10:198–205, 2019.

[39] J Allen. Photoplethysmography and its application in clinical physiological measurement. *Physiological Measurement*, 28(3):R1–R39, 2007.

[40] K Takazawa, N Tanaka, M Fujita, O Matsuoka, T Saiki, M Aikawa, S Tamura, and C Ibukiyama. Assessment of vasoactive agents and vascular ageing by the second derivative of photoplethysmogram waveform. *Hypertension*, 32(2):365–370, 1998.

[41] G Slapničar, N Mlakar, and M Luštrek. Blood pressure estimation from photoplethysmogram using a spectro-temporal deep neural network. *Sensors*, 19(15):3420, 2019.

[42] R C Block, M Yavarimanesh, K Natarajan, A Carek, A Mousavi, A Chandrasekhar, C S Kim, J Zhu, G Schifitto, L K Mestha, O T Inan, J O Hahn, and R Mukkamala. Conventional pulse transit times as markers of blood pressure changes in humans. *Scientific Reports*, 10:16373, 2020.

[43] Y Kurylyak, F Lamonaca, and D Grimaldi. A neural network-based method for continuous blood pressure estimation from a ppg signal. In *IEEE International Instrumentation and Measurement Technology Conference, I2MTC*, 2013.

[44] A Gaurav, M Maheedhar, V N Tiwari, and R Narayanan. Cuff-less ppg based continuous blood pressure monitoring—a smartphone based approach. In *Proceedings of the 38st Annual International Conference of the IEEE Engineering in Medicine and Biology Society, EMBC*, 2016.

[45] L A Jensen, J E Onyskiw, and N G N Prasad. Meta-analysis of arterial oxygen saturation monitoring by pulse oximetry in adults. *Heart and Lung: The Journal of Acute and Critical Care*, 27(6):387–408, 1998.

[46] J Lázaro, E Gil, J M Vergara, and P Laguna. Pulse rate variability analysis for discrimination of sleep-apnea-related decreases in the amplitude fluctuations of ppg signal in children. *IEEE Journal of Biomedical and Health Informatics*, 18(1):240–246, 2014.

[47] E Peralta, J Lázaro, R Bailón, V Marozas, and E Gil. Optimal fiducial points for pulse rate variability analysis from forehead and finger ppg signals. *Physiological Measurement*, 40:025007 (15pp), 2019.

[48] J Yao, X Sun, and Y Wan. A pilot study on using derivatives of photoplethysmographic signals as a biometric identifier. In *Proceedings of the 29st Annual International Conference of the IEEE Engineering in Medicine and Biology Society, EMBC*, 2007.

[49] Y C Chiu, P W Arand, S G Shroff, T Feldman, and J D Carroll. Determination of pulse wave velocities with computerized algorithms. *American Heart Journal*, 121(5):1460–1470, 1991.

[50] K H Shelley. Photoplethysmography: beyond the calculation of arterial oxygen saturation and heart rate. *Anesthesia and Analgesia*, 105(6):S31–S36, 2007.

[51] M Elgendi. On the analysis of fingertip photoplethysmogram signals. *Current Cardiology Reviews*, 8(1):14–25, 2012.

[52] C C Y Poon, X F Teng, Y M Wong, C Zhang, and Y T Zhang. Changes in the photoplethysmogram waveform after exercise. In *2nd IEEE/EMBS International Summer School on Medical Devices and Biosensors*, 2004.

[53] J M Padilla, E J Berjano, J Sáiz, L Fácila, P Díaz, and S Mercé. Assessment of relationships between blood pressure, pulse wave velocity and digital volume pulse. In *Computers in Cardiology*, 2006.

[54] S C Millasseau, R P Kelly, J M Ritter, and P J Chowienczyk. Determination of age-related increases in large artery stiffness by digital pulse contour analysis. *Clinical Science*, 103(4):371–377, 2002.

[55] L Wang, E Pickwell-MacPherson, Y P Liang, and Y T Zhang. Non-invasive cardiac output estimation using a novel photoplethysmogram index. In *Proceedings of the 31st Annual International Conference of the IEEE Engineering in Medicine and Biology Society: Engineering the Future of Biomedicine, EMBC*, 2009.

[56] A A Awad, A S Haddadin, H Tantawy, T M Badr, R G Stout, D G Silverman, and K H Shelley. The relationship between the photoplethysmographic waveform and systemic vascular resistance. *Journal of Clinical Monitoring and Computing*, 21(6):365–372, 2007.

[57] D U Silverthorn. *Human physiology: an integrated approach.* Pearson/Benjamin Cummings, 2010.

[58] P H Charlton, T Bonnici, L Tarassenko, D A Clifton, R Beale, and P J Watkinson. An assessment of algorithms to estimate respiratory rate from the electrocardiogram and photoplethysmogram. *Physiological Measurement*, 37:610, 2016.

[59] D J Meredith, D Clifton, P Charlton, J Brooks, C W Pugh, and L Tarassenko. Photoplethysmographic derivation of respiratory rate: a review of relevant physiology. *Journal of Medical Engineering and Technology*, 36(1):1–7, 2012.

[60] W Karlen, S Raman, J M Ansermino, and G A Dumont. Multiparameter respiratory rate estimation from the photoplethysmogram. *IEEE Transactions on Biomedical Engineering*, 60(7):1946–1953, 2013.

[61] P Grossman, K H L Janssen, and D Vaitl. *Cardiorespiratory and Cardiosomatic Psychophysiology.* NATO ASI Series, 1986.

[62] A J Buda, M R Pinsky, N B Ingels, G T Daughters, E B Stinson, and E L Alderman. Effect of intrathoracic pressure on left ventricular performance. *New England Journal of Medicine*, 301(49):453–459, 1979.

[63] L Nilsson, A Johansson, and S Kalman. Monitoring of respiratory rate in postoperative care using a new photoplethysmographic technique. *Journal of Clinical Monitoring and Computing*, 16:309–315, 2000.

[64] L Nilsson, A Johansson, and S Kalman. Respiration can be monitored by photoplethysmography with high sensitivity and specificity regardless of anaesthesia and ventilatory mode. *Acta Anaesthesiologica Scandinavica*, 49:1157–1162, 2005.

[65] P S Addison, J N Watson, M L Mestek, J P Ochs, A A Uribe, and S D Bergese. Pulse oximetry-derived respiratory rate in general care floor patients. *Journal of Clinical Monitoring and Computing*, 29(1):113–120, 2015.

[66] G Clifford, F Azuaje, and P E McSharry. *Advanced methods and tools for ECG data analysis*. Artech House, 2006.

[67] J Lázaro, A Alcaine, D Romero, E Gil, P Laguna, E Pueyo, and R Bailón. Electrocardiogram derived respiratory rate from qrs slopes and r-wave angle. *Annals Biomedical Engineering*, 40(10):2072–2083, 2014.

[68] K H Chon, S Dash, and K Ju. Estimation of respiratory rate from photoplethysmogram data using time-frequency spectral estimation. *IEEE Transactions on Biomedical Engineering*, 56(8):2054–2063, 2009.

[69] Y D Lin, H Y Ho, C C Tsai, S F Wang, K P Lin, and H H Chang. Simultaneous heartbeat and respiration monitoring using ppg and riiv on a smartphone device. *Biomedical Engineering: Applications, Basis and Communications*, 25(4):135–141, 2013.

[70] P Leonard, N R Grubb, P S Addison, D Clifton, and J N Watson. An algorithm for the detection of individual breaths from the pulse oximeter waveform. *Journal of Clinical Monitoring and Computing*, 18(5):309–312, 2004.

[71] K H Shelley, A A Awad, R G Stout, and D G Silverman. The use of joint time frequency analysis to quantify the effect of ventilation on the pulse oximeter waveform. *Journal of Clinical Monitoring and Computing*, 20(2):81–87, 2006.

[72] D Clifton, J Douglas, P Addison, and J Watson. Measurement of respiratory rate from the photoplethysmogram in chest clinic patients. *Journal of Clinical Monitoring and Computing*, 21:55–61, 2007.

[73] J Lázaro, E Gil, R Bailón, A Mincholé, and P Laguna. Deriving respiration from photoplethysmographic pulse width. *Medical and Biological Engineering and Computing*, 51:233–242, 2013.

[74] A Johansson. Neural network for photoplethysmographic respiratory rate monitoring. *Medical and Biological Engineering and Computing*, 41(3):242–248, 2003.

[75] P Z Zhang, W N Tapp, S S Reisman, and B H Natelson. Respiration response curve analysis of heart rate variability. *IEEE Transactions on Biomedical Engineering*, 44(4):321–325, 1997.

[76] R Bailón, L Mainardi, M Orini, L Sörnmo, and P Laguna. Analysis of heart rate variability during exercise stress testing using respiratory information. *Biomedical Signal Processing and Control*, 5:299–310, 2010.

[77] X Long, P Fonseca, R Haakma, R M Aarts, and J Foussier. Spectral boundary adaptation on heart rate variability for sleep and wake classification. *International Journal on Artificial Intelligence Tools*, 23:1–20, 2014.

[78] A Hernando, J Lázaro, E Gil, A Arza, J M Garzón, R López-Antón, C de la Cámara, P Laguna, J Aguiló, and R. Bailón. Inclusion of respiratory frequency information in heart rate variability analysis for stress assessment. *IEEE Journal of Biomedical and Health Informatics*, 20(4):1016–1025, 2016.

[79] C Varon, J Lázaro, J Bolea, A Hernando, J Aguiló, E Gil, S Van Huffel, and R Bailón. Unconstrained estimation of hrv indices after removing respiratory influences from heart rate. *IEEE Journal of Biomedical and Health Informatics*, 23(6):2386–2397, 2019.

[80] D Sokas, M Gailius, and V Marozas. Diver physiology monitor and its graphical user interface. In *Proceedings of International Scientific-Practical Conference, Virtual Instruments in Biomedicine*, 2016.

[81] J P Martínez, R Almeida, S Olmos, A P Rocha, and P Laguna. A wavelet-based ecg delineator: evaluation on standard databases. *IEEE Transactions on Biomedical Engineering*, 51(4):570–581, 2004.

[82] J Mateo and P Laguna. Analysis of heart rate variability in the presence of ectopic beats using the heart timing signal. *IEEE Transactions on Biomedical Engineering*, 50(3):334–343, 2003.

[83] E Gil, J M Vergara, and P Laguna. Detection of decreases in the amplitude fluctuation of pulse photoplethysmography signal as indication of obstructive sleep apnea syndrome in children. *Biomedical Signal Processing and Control*, 3(3):267–277, 2008.

[84] J Y A Foo and C S Lim. Pulse transit time as an indirect marker for variations in cardiovascular related reactivity. *Technology and Health Care*, 14:97–108, 2006.

[85] E Pueyo, L Sörnmo, and P Laguna. Qrs slopes for detection and characterization of myocardial ischemia. *IEEE Transactions on Biomedical Engineering*, 55(2):468–477, 2008.

[86] D Romero, M Ringborn, P Laguna, and E Pueyo. Detection and quantification of acute myocardial ischemia by morphologic evaluation of qrs changes by an angle-based method. *Journal of Electrocardiology*, 46:204–214, 2013.

[87] P H Charlton, D A Birrenkott, T Bonnici, M A F Pimentel, A E W Johnson, J Alastruey, L Tarassenko, P J Watkinson, R Beale, and D A Clifton. Breathing rate estimation from the electrocardiogram and photoplethysmogram: a review. *IEEE Reviews in Biomedical Engineering*, 99:1–17, 2017.

[88] R Bailón, L Sörnmo, and P Laguna. A robust method for ecg-based estimation of the respiratory frequency during stress testing. *IEEE Transactions on Biomedical Engineering*, 53(7):1273–1285, 2006.

[89] K Nakajima, T Tamura, and H Miike. Monitoring of heart and respiratory rates by photoplethysmography using a digital filtering technique. *Medical Engineering and Physics*, 18(5):365–372, 1996.

[90] S Fleming and L Tarassenko. A comparison of signal processing techniques for the extraction of breathing rate from the photoplethysmogram. *International Journal of Biological and Medical Research*, 2(4):232–236, 2007.

[91] W S Johnston and Y Mendelson. Extracting breathing rate information from a wearable reflectance pulse oximeter sensor. In *Proceedings of the 26st Annual International Conference of the IEEE Engineering in Medicine and Biology Society: Linkages for Innovation in Biomedicine*, 2004.

[92] P H Charlton, T Bonnici, L Tarassenko, J Alastruey, D A Clifton, R Beale, and P J Watkinson. Extraction of respiratory signals from the electrocardiogram and photoplethysmogram: technical and physiological determinants. *Physiological Measurement*, 38(5):669–690, 2017.

[93] L Nilsson, T Goscinski, S Kalman, L G Lindberg, and A Johansson. Combined photoplethysmographic monitoring of respiration rate and pulse: a comparison between different measurement sites in spontaneously breathing subjects. *Acta Anaesthesiologica Scandinavica*, 51:1250–1257, 2007.

[94] J M Garzón-Rey, J Lázaro, J Milagro, E Gil, J Aguiló, and R Bailón. Respiration-guided analysis of pulse and heart rate variabilities for acute emotional stress assessment. In *Proceedings of the XLIV International Conference on Computing in Cardiology*, 2017.

[95] S Dash, K H Shelley, D G Silverman, and K H Chon. Estimation of respiratory rate from ecg, photoplethysmogram, and piezo-electric pulse transducer signals: a comparative study of time–frequency methods. *IEEE Transactions on Biomedical Engineering*, 57(5):1099–1107, 2010.

[96] J Lázaro, Y Nam, E Gil, P Laguna, and K H Chon. Respiratory rate derived from smartphone-camera-acquired pulse photoplethysmographic signals. *Physiological Measurement*, 36:2317–2333, 2015.

[97] J A Hirsch and B Bishop. Respiratory sinus arrhythmia in humans: how breathing pattern modulates heart rate. *American Journal of Physiology*, 241(4):H620–H629, 1981.

[98] P Grossman and E W Taylor. Toward understanding respiratory sinus arrhythmia: relations to cardiac vagal tone, evolution and biobehavioral functions. *Biological Psychology*, 74(2):263–285, 2007.

[99] C Julien. The enigma of mayer waves: Facts and models. *Cardiovascular Research*, 70(1):12–21, 2006.

[100] G Pfurtscheller, G Schwarz, and A Schwerdtfeger. Heart rate variability and impact of central pacemaker on cardiac activity. *Clinical Neurophysiology*, 129(10):2188–2190, 2018.

[101] S Sun, W H Peeters, R Bezemer, X Long, I Paulussen, R M Aarts, and G J Noordergraaf. Finger and forehead photoplethysmography-derived pulse-pressure variation and the benefits of baseline correction. *Journal of Clinical Monitoring and Computing*, 33(1):65–75, 2019.

[102] F Javed, P M Middleton, P Malouf, G S H Chan, A V Savkin, N H Lovell, E Steel, and J Mackie. Frequency spectrum analysis of finger photoplethysmographic waveform variability during haemodialysis. *Physiological Measurement*, 31(9):1203–1216, 2010.

[103] R E De Meersman. Aging as a modulator of respiratory sinus arrhythmia. *Journal of Gerontology*, 48(2):B74–B78, 1993.

[104] M D Peláez-Coca, M T Lozano, A Hernando, M. Aiger, and E. Gil. Photoplethysmographic waveform versus heart rate variability to identify low-stress states: Attention test. *IEEE Journal of Biomedical and Health Informatics*, 23(5):1940–1951, 2020.

[105] A Wang, L Yang, C Liu, J Cui, Y Li, X Yang, S Zhang, and D Zheng. Athletic differences in the characteristics of the photoplethysmographic pulse shape: Effect of maximal oxygen uptake and maximal muscular voluntary contraction. *BioMed Research International*, 752570:8, 2015.

[106] S P Linder, S M Wendelken, E Wei, and S P McGrath. Using themorphology of photoplethysmogram peaks to detect changes in posture. *Journal of Clinical Monitoring and Computing*, 20(3):151–158, 2006.

[107] M C Baruch, D E Warburton, S S Bredin, A Cote, D W Gerdt, and C M Adkins. Pulse decomposition analysis of the digital arterial pulse during hemorrhage simulation. *Nonlinear Biomedical Physics*, 5(1):1, 2011.

[108] L Wang, L Xu, S Feng, M Q H Meng, and K Wang. Multi-gaussian fitting for pulse waveform using weighted least squares and multi-criteria decision making method. *Computers in Biology and Medicine*, 43(11):1661–1672, 2013.

[109] C Liu, T Zhuang, L Zhao, F Chang, C Liu, S Wei, Q Li, and D Zheng. Modelling arterial pressure waveforms using gaussian functions and two-stage particle swarm optimizer. *BioMed Research International*, 923260:10, 2014.

[110] M Huotari, A Vehkaoja, K Määttä, and J Kostamovaara. Photoplethysmography and its detailed pulse waveform analysis for arterial stiffness. *Journal of Mechanics of Materials and Structures*, 44:345–362, 2011.

[111] D Goswami, K Chaudhuri, and J Mukherjee. A new two-pulse synthesis model for digital volume pulse signal analysis. *Cardiovascular Engineering*, 10:109–117, 2010.

[112] S C Huang, H Y Jan, G H Lin, W C Lin, and K P Lin. Decomposition analysis of digital volume pulse signal using multi-model fitting. In *XIII Mediterranean Conference on Medical and Biological Engineering and Computing*, 2013.

[113] A Sološenko, A Petrėnas, V Marozas, and L Sörnmo. Modeling of the photoplethysmogram during atrial fibrillation. *Computers in Biology and Medicine*, 81:130–138, 2017.

[114] U Rubins. Finger and ear photoplethysmogram waveform analysis by fitting with gaussians. *Medical and Biological Engineering and Computing*, 46:1271–1276, 2008.

[115] J Lázaro, E Gil, M Orini, P Laguna, and R Bailón. Baroreflex sensitivity measured by pulse photoplethysmography. *Frontiers in Neuroscience*, 13:339:1–13, 2019.

[116] S Kontaxis, E Gil, V Marozas, J Lázaro, E García, M Posadas de Miguel, S Siddi, M L Bernal, J Aguiló, J M Haro, C de la Cámara, P Laguna, and R Bailón. Photoplethysmographic waveform analysis for autonomic reactivity assessment in depression. *IEEE Transactions on Biomedical Engineering*, 68(4):1273–1281, 2021.

[117] A Hernando, M D Peláez-Coca, M T Lozano, M Aiger, D Izquierdo, A Sánchez, M I López-Jurado, I Moura, J Fidalgo, J Lázaro, and E Gil. Autonomic nervous system measurement in hyperbaric environments using ecg and ppg signals. *IEEE Journal of Biomedical and Health Informatics*, 23(1):132–142, 2019.

[118] P J Chowienczyk, R P Kelly, H MacCallum, S Millasseau, T Andersson, R Gosling, J Ritter, and E Anggard. Photoplethysmographic assessment of pulse wave reflection: blunted endothelium-dependent response to beta$_2$ adrenergic vasodilation in type ii diabetes. *Journals of the American College of Cardiology*, 34:2007–2014, 1999.

[119] Y K Qawqzeh, M B I Reaz, O Maskon, K Chellappan, and M A M Ali. Photoplethysmogram reflection index and aging. In *International Conference on Graphic and Image Processing*, 2011.

[120] M D Peláez-Coca, A Hernando, M T Lozano, C Sánchez, D Izquierdo, and E Gil. Photoplethysmographic waveform and pulse rate variability analysis in hyperbaric environments. *IEEE Journal of Biomedical and Health Informatics*, 2021.

[121] C R Mortensen. Hyperbaric oxygen therapy. *Current Anaesthesia and Critical Care*, 19(5-6):333–337, 2008.

[122] B A Gooden. Mechanism of the human diving response. *Integrative Psychological and Behavioral Science*, 29:6–16, 1994.

[123] L Mourot, M Bouhaddi, E Gandelin, S Cappelle, N U Nguyen, J P Wolf, J D Rouillon, R Hughson, and J Regnard. Conditions of autonomic reciprocal interplay versus autonomic co-activation: effects on non-linear heart rate dynamics. *Autonomic Neuroscience: Basic and Clinical*, 137:27–36, 2007.

[124] H Al-Haddad, P B Laursen, D Chollet, F Lemaitre, S Ahmaidi, and M Buch-heit. Effect of cold or thermoneutral water immersion on post-exercise heart rate recovery and heart rate variability indices. *Autonomic Neuroscience*, 156(1-2):111–116, 2010.

[125] D L Eckberg. Sympathovagal balance: a critical appraisal. *Circulation*, 96(9):3224–3232, 1997.

[126] G E Billman. The lf/hf ratio does not accurately measure cardiac sympatho-vagal balance. *Frontiers in Physiology*, 4:26, 2013.

[127] D S Quintana and A J H James. Considerations in the assessment of heart rate variability in biobehavioral research. *Frontiers in Physiology*, 5:805, 2014.

[128] Y Zhong, K Jan, K H Ju, and K H Chon. Quantifying cardiac sympathetic and parasympathetic nervous activities using principal dynamic modes analysis of heart rate variability. *American Journal of Physiology-Heart and Circulatory Physiology*, 291:H1475–H1483, 2006.

[129] L R Mujica-Parodi, M Korgaonkar, B Ravindranath, T Greenberg, D Tomasi, M Wagshul, B Ardekani, D Guilfoyle, S Khan, Y Zhong, K H Chon, and D Malaspina. Limbic dysregulation is associated with lowered heart rate vari-ability and increased trait anxiety in healthy adults. *Human Brain Mapping*, 30:47–58, 2009.

[130] D Widjaja, A Caicedo, E Vlemincx, I Van Diest, and S Van Huffel. Separation of respiratory influences from the tachogram: A methodological evaluation. *Plos One*, 9(7):e101713, 2014.

[131] N Bourdillon, L Schmitt, S Yazdani, J M Vesin, and G P Millet. Minimal win-dow duration for accurate hrv recording in athletes. *Frontiers in Neuroscience*, 11:456, 2017.

[132] L Pecchia, R Castlado, L Montesinos, and P Melillo. Are ultra-short heart rate variability features good surrogates of short-term ones? state-of-the-art review and recommendations. *Healthcare Technology Letters*, 5(3):94–100, 2018.

[133] V Z Marmarelis. Identification of nonlinear biological systems using laguerre expansions of kernels. *Annals of Biomedical Engineering*, 21(6):573–589, 1993.

[134] M P Tarvainen, P O Ranta-Aho, and P A Karjalainen. An advanced detrending method with application to hrv analysis. *IEEE Transactions on Biomedical Engineering*, 49(2):172–175, 2002.

[135] R Zou, H Wang, and K H Chon. A robust time-varying identification algorithm using basis functions. *Annals of Biomedical Engineering*, 31(7):840–853, 2003.

[136] G G Berntson, J T Cacioppo, and K S Quigley. Respiratory sinus arrhythmia: Autonomic origins, physiological mechanisms, and psychophysiological implications. *Psychophysiology*, 30(2):183–196, 1993.

[137] C Varon, A Caicedo, D Testelmans, B Buyse, and S Van Huffel. A novel algorithm for the automatic detection of sleep apnea from single-lead ecg. *IEEE Transactions on Biomedical Engineering*, 62(9):2269–2278, 2015.

[138] M G Bocci, E Gilardi, V Fiore, S Calcinaro, C Fragnoli, R Mariglia, and F Franceschi. Linear and nonlinear heart rate variability indexes in clinical practice. *Computational and Mathematical Methods in Medicine*, 2012:219080, 2012.

[139] D R Pendergast, R E Moon, J J Krasney, H E Held, and P Zamparo. Human physiology in an aquatic environment. *Comprehensive Physiology*, 5:1705–1750, 2015.

[140] D R Seals, D G Johnson, and R F Fregosi. Hyperoxia lowers sympathetic activity at rest but not during exercise in humans. *American Journal of Physiology*, 260:R873–R878, 1991.

[141] R V Lundell, A K Räisänen-Sokolowsk, T K Wuorimaa, T Ojanen, and K I Parkkola. Diving in the arctic: Cold water immersion's effects on heart rate variability in navy divers. *Frontiers in Physiology*, 10:1600, 2020.

[142] G B Nepal and B H Paudel. Effect of posture on heart rate variability in school children. *Nepal Medical College Journal*, 14(4):298–302, 2012.